DEVELOPING AN ACOUSTIC DISCHARGE MEASUREMENT TECHNIQUE FOR HYDROELECTRIC PERFORMANCE TESTING

by

Kevin D. Gawne

A Thesis
Submitted to the Faculty of Graduate Studies
in Partial Fulfillment for the Degree of

MASTER OF SCIENCE

Department of Civil Engineering
University of Manitoba
Winnipeg, Manitoba

THE UNIVERSITY OF MANITOBA

FACULTY OF GRADUATE STUDIES

*****

COPYRIGHT PERMISSION PAGE

DEVELOPING AN ACOUSTIC DISCHARGE MEASUREMENT TECHNIQUE

FOR HYDROELECTRIC PERFORMANCE TESTING

BY

KEVIN D. GAWNE

A Thesis/Practicum submitted to the Faculty of Graduate Studies of The University of Manitoba in partial fulfillment of the requirements of the degree of

MASTER OF SCIENCE

ABSTRACT

The efficient operation of hydroelectric generating plants requires an accurate definition of the performance relationships of each turbine/generator unit. Of the information obtained by performance testing, discharge is the most difficult to measure accurately. It is envisioned that acoustic transit-time velocity measurement technology can be applied at low-head plants to obtain more accurate discharge measurements over current practices. The technique proposed herein involves continuously traversing a number of acoustic paths, each providing a chordal average velocity measurement, across the turbine intake to obtain a complete integration of the complex velocity profile typical of low-head hydroelectric plant conditions. Hydraulic laboratory testing of a single acoustic cell is the focus of this study.

The acoustic cell was traversed across a laboratory intake structure to measure discharge; this measurement was compared to known laboratory flowrate to assess the accuracy and repeatability of the proposed discharge measurement technique. Various continuous sampling strategies (*i.e.*, traverse rates) and discrete sampling strategies (Gauss-Legendre positioning) are evaluated. A number of flow perturbances were also added to the intake structure to evaluate the technique in complex flow conditions.

Based on the results described herein, it is concluded that the proposed continuous traversing technique can provide efficient, accurate and repeatable discharge measurements under complex flow conditions relative to discrete sampling techniques. In disturbed flow conditions, testing revealed that discrete sampling strategies were subject to considerable systematic integration error. Further laboratory testing of a multiple cell system is recommended because of the promising results obtained from this study. Also, two key recommendations pertaining to field testing of low-head plants are made: 1) low order discrete sampling techniques should not be practiced; and 2) careful consideration should be devoted to the geometry of the acoustic paths as conflicting effects on accuracy are dependent on the acoustic pathlengths and path angles employed.

ACKNOWLEDGMENTS

The assistance and support of many people has enabled me to complete this work. I would like to express sincere thanks to Manitoba Hydro for initiating this project, and for financial support. The Natural Sciences and Engineering Research Council of Canada is also deserving of acknowledgment for research grant and scholarship support. I would like to offer particular thanks to:

Dr. Jay Doering, my advisor, for his guidance and encouragement throughout my graduate studies. Also, for his continued enthusiasm towards this project.

Ms. Halina Zbigniewicz and Mr. Marc Drouin, of Manitoba Hydro's Hydraulic Engineering and Operations Department, for providing the direction and assistance required to complete this work.

Mr. Roy Hartle, from the University of Manitoba Hydraulics Research and Testing Facility (HRTF), for his invaluable technical assistance which was essential to complete the laboratory component of this project.

Dr. Andrew Trivett and Dr. Jim Snow of Focal Technologies, Dartmouth, Nova Scotia, for their technical guidance on acoustic instrumentation.

I would also like to express my deepest thanks to my parents. Without their unwavering encouragement and support, I would not be where I am today. I would like to thank my good friends in FIDS and HRTF for their comradeship that has made my academic experience so enjoyable. Finally, I thank Jackie, my dear girlfriend, for her endless patience, encouragement and understanding that I needed to complete my graduate studies.

TABLE OF CONTENTS

LIST OF FIGURES

LIST OF TABLES

NOMENCLATURE

Symbol	Definition
A	area of metering section
a	coefficients of polynomial
a'	lower limit of integration
b'	upper limit of integration
c	speed of sound in water
c'	ordinate between limits of integration
c_{emp}	empirical estimate of speed of sound in water
CTR	continuous traverse
D	diameter of cylindrical flow obstruction
$f(x)$	transformed function to be integrated using Gauss-Legendre technique
GL	Gauss-Legendre sampling strategy
h_i	Sampling position in intake corresponding to x_i
H_l	head losses between intake and exit of hydroelectric unit
H_n	net head
H_u	head utilized by turbine runner
L	length of acoustic pathline
n	number of 'non-laned' velocity measurements
N	order of Gauss-Legendre integration
n'	vortex shedding frequency
P	acoustic path (X or Y)
P_c	total hydraulic power consumed to rotate turbine/generator unit
P_f	power consumed by mechanical friction
P_g	power generated from a hydroelectric unit
P_l	generator losses
P_t	brake power available to generator
P_T	total losses
Q_{CTR}	discharge measurement using CTR sampling strategy
Q_e	effective flow acting on the turbine runner
Q_{GL}	discharge measurement using GL sampling strategy
Q_l	leakage past the turbine runner
$Q_{measured}$	measured discharge using either CTR or GL
Q_{mraw}	raw (not calibrated) MAG flowmeter measurement
Q_{ref}	reference discharge
Q_t	total flow in the passage
r^2	coefficient of determination
S	salinity
s	segment of time series
S_t	Strouhal number
T	temperature
t_d	downstream acoustic pulse transit-time
t_u	upstream acoustic pulse transit-time

Symbol	Definition
$v(x \text{ or } h)$	function describing the true velocity profile
V_n	normal water velocity measurement
$\overline{V}_n$	average normal velocity measured using acoustic scintillation flow measurement
$\overline{V}_{n,s}$	mean normal velocity for segment s
V_p	pathline water velocity
VP_d	acoustic pulse velocity traveling downstream
VP_u	acoustic pulse velocity traveling upstream
W	number of windows used to calculate discharge for CTR traverse
W'	intake width
w_i	Gauss-Legendre weight
X	X acoustic path
x_i	Gauss-Legendre ordinates
Y	Y acoustic path
z	depth of speed of sound measurement
θ	acoustic pathline angle relative to assumed flow direction
γ	specific weight of water
η	turbine/generator unit absolute efficiency
η_g	efficiency of generator
η_h	hydraulic efficiency of turbine
η_m	mechanical efficiency of turbine
Δt	lag time of acoustic scintillation flow measurement
η_t	total efficiency of turbine
η_v	volumetric efficiency of turbine
Δx	acoustic path separation of acoustic scintillation flow measurement

CHAPTER 1
INTRODUCTION

In order to efficiently operate hydroelectric generating plants the performance characteristics of the hydroelectric turbine/generator units must be accurately known. Field performance testing is used to obtain the necessary head, power, gate setting and discharge information required to develop efficiency relationships for each unit. Inaccurate testing yields efficiency relationships that incorrectly identify the best operating point of the hydroelectric unit; this can result in significant loss of generation revenues. Performance tests are also carried out for acceptance testing of new hydroelectric units or components thereof and to identify a need for unit service. In addition, discharge relationships developed through performance testing are used for accurate management of the water resource on the scale of the river system.

Of the measurements required for a performance test, accurate discharge data is typically the most difficult to obtain. Numerous discharge measurement techniques have been developed for performance testing, however the majority of these methods are not conducive to the physical characteristics of low-head plants. Low-head plants typically have short conduit systems that limit flow metering to the intake area, where velocity profiles are quite complex. Many utilities operating low-head plants use the current-meter approach to measure discharge. This technique involves traversing an array of propeller-type flow meters, mounted on a space truce, across the turbine intake to obtain a grid of velocity measurements. A summation technique is then applied to the products of velocity and the respective areas to obtain a discharge measurement. There are a number of problems associated with this approach, *viz.* the ability of the numerical summation of a limited number of velocity measurements to accurately determine discharge.

It is anticipated that acoustic technology can be used to develop an improved method of metering flow through low-head units. Unlike propeller-type flow meters, which provide a point measurement of velocity, acoustic instrumentation can provide chordal average

velocity estimates by measuring the transit-time of acoustic pulses traveling through the flowing water. It is proposed that acoustic instrumentation be continuously traversed across the turbine intake to essentially sample the entire velocity profile. Complete integration of the complex velocity profile should result in an accurate discharge measurement. With improved discharge measurement data, the best operating point of the hydroelectric unit can be better defined, thus improving the efficiency of generating hydroelectricity.

The goal of this research is to develop an acoustic discharge measurement (ADM) technique through hydraulic laboratory testing. The performance of a single, large scale 'acoustic cell' was assessed by comparing discharge measurements in an intake with known laboratory discharge values. The cell was tested in uniform flow conditions using continuous and discrete level traverses to assess the repeatability and relative accuracy of these sampling strategies. To assess the performance of the ADM technique and the various sampling strategies under complex flow conditions, a number of disturbances were added to the flow.

Chapter 2 provides a background discussion of hydraulic performance testing and an overview of established discharge measurement techniques. Also included in this chapter is an explanation of the difficulties of flow measurement at low-head plants and a detailed explanation of the current-meter method typically applied to these conditions. Chapter 3 provides detailed background and review of literature on the practice of acoustic flow measurement. The proposed technique of acoustic discharge measurement is explained in Chapter 4 along with an overview of the testing program and apparatus used to evaluate this technique. Chapter 5 explains the data processing required for the laboratory reference discharge and the acoustic discharge measurements. The laboratory test results and subsequent analysis and discussion is presented in Chapter 6. The performance of the acoustic discharge measurement system under both uniform and disturbed flow conditions is the focus of Chapter 6. A discussion of errors is then presented at the end of the chapter. The final chapter, Chapter 7, presents a summary of the results obtained

from the analysis, followed by recommendations for future studies of the proposed technique in both the laboratory and field environments.

CHAPTER 2
BACKGROUND: PERFORMANCE TESTING OF HYDROELECTRIC TURBINES

2.1 FIELD PERFORMANCE TESTING OF HYDROELECTRIC TURBINES

The economic and efficient operation of a hydroelectric generating station requires an accurate description of the head-power-discharge, head-gate-discharge and head-power-efficiency relationships for each turbine/generator unit. Figure 2.1 illustrates a typical set of curves describing these relationships. The principle objective of field performance testing is to obtain the necessary information to develop such curves that are in turn used to determine the optimum setting of the turbine wicket gates corresponding to peak absolute efficiency, commonly referred to as 'best gate.' Substantial economic loss can result from the inaccurate definition of this operating curve. For one of Manitoba Hydro's low-head plants, a 1 percent error in the definition of best gate can translate to a loss of tens of thousands of dollars in generation revenues per year for each unit. When considering the entire hydroelectric generating utility, this impact could be substantial.

Performance testing is also used for: acceptance testing of new hydroelectric units or components thereof; identifying the need for upgrade or maintenance works, for example turbine runner replacements or trash removal; and accurate management of the water resource on the scale of the river system.

Although the performance of hydroelectric turbines is typically model tested in a laboratory environment, it is necessary to undertake prototype testing in the field since complete similitude of all properties is not possible. Some disagreement between model and prototype geometry is likely, and factors such as approach flow conditions, intake and trash-rack head losses and the effect of operating adjacent units are typically not modeled (Arndt and Gulliver, 1991). Furthermore, the more direct approach of assessing the need for refurbishment or upgrades is to perform field testing.

2.2 COMPONENTS OF PERFORMANCE TESTS

The main objective of performance testing is to determine the absolute efficiency of the hydroelectric unit. That is, what is the proportion of power generated to the power consumed, which can be expressed as

$$\eta = \frac{P_g}{P_c} = \frac{P_c - P_T}{P_c}, \tag{2.1}$$

where η = turbine/generator unit absolute efficiency,

P_g = power generated (available for transmission),

P_c = total hydraulic power consumed to rotate turbine/generator unit, and

P_T = total losses.

Unit absolute efficiency can be subdivided into four component efficiencies, three of which are related to the turbine. First, the hydraulic efficiency of a turbine accounts for the head losses between the intake and exit of the unit, as defined by

$$\eta_h = \frac{H_u}{H_n} = \frac{H_n - H_l}{H_n}, \tag{2.2}$$

where η_h = hydraulic efficiency of turbine,

H_u = head utilized by the turbine runner,

H_n = net head, and

H_l = head losses between the intake and exit of the unit.

The net head is defined as the difference between the total head at the turbine intake less the remaining hydraulic head at the draft tube. The second component of absolute unit efficiency is the volumetric efficiency, which is given by

$$\eta_v = \frac{Q_e}{Q_t} = \frac{Q_t - Q_l}{Q_t}, \tag{2.3}$$

where η_v = volumetric efficiency of turbine,

Q_e = effective flow acting on the turbine runner,

Q_t = total flow in the passage, and

Q_l = leakage past turbine runner.

Water not acting on the turbine runner, rather leaking between the runner and the housing, does not produce work. The ability of the machine to transmit power from the turbine runner to the generator is defined by the mechanical efficiency,

$$\eta_m = \frac{P_t}{P_t + P_f}, \tag{2.4}$$

where η_m = mechanical efficiency of the turbine,

P_t = brake power available at the shaft which is transferred to the generator, and

P_f = power consumed by mechanical friction.

Mechanical losses include mechanical friction, for example, bearing losses and viscous losses between the runner shaft and casing.

The efficiency of the turbine, η_t, is defined as

$$\eta_t = \eta_h \eta_v \eta_m . \tag{2.5}$$

The fourth, and final, component of unit absolute efficiency is the generator efficiency, defined by

$$\eta_g = \frac{P_g}{P_g + P_l}, \tag{2.6}$$

where η_g = generator efficiency,

P_g = power output of generator, and

P_l = generator losses (*e.g.*, resistive, inductive and frictional losses).

This represents the ability of the generator to convert the rotational power from the turbine shaft to electrical power for transmission. The overall unit efficiency is defined as

$$\eta = \eta_h \eta_v \eta_m \eta_g = \eta_t \eta_g, \tag{2.7}$$

The total electrical power generated from the unit is defined by

$$P_g = \eta \gamma Q_t H_n, \tag{2.8}$$

where γ = specific weight of water.

Equation (2.8) is used to determine the absolute unit efficiency by measuring the generation output, head conditions and the unit discharge. If generator efficiency is known, equation (2.7) may also be used to determine the turbine efficiency.

Generation output is typically measured via a watt-hour meter installed on each unit. Headwater and tailwater level measurements are obtained using water level instrumentation, for example acoustic echo level sensors. Wicket gate settings are typically measured indirectly using a linear variable differential transducer (LVDT) mounted on the servo-piston that rotates the gates. The relationship between servo-stroke and wicket gate angle is then used to determine the setting of the gates. Of all the information required for performance testing, unit discharge is usually the most difficult to obtain. As such, considerable effort has been devoted to measure unit discharge accurately; this has lead to the development of a number of discharge measurement techniques.

2.3 ESTABLISHED TECHNIQUES OF FLOW MEASUREMENT FOR PERFORMANCE TESTING

There are a number of methods that have been developed and code accepted (ASME, 1992; IEC, 1991) to measure the flow through a turbine. The applicability of a given method depends on the characteristics of the intake, conduit, turbine, magnitude of discharge and operation specific conditions such as the ability to completely shut down or de-water a unit. To provide some background, the more popular methods are outlined below. The current-meter and acoustic transit-time methods are of particular relevance to this thesis, as such Sections 2.4 and 3.3 provide detailed background information on these techniques, respectively.

Gibson Pressure-Time

The Gibson pressure-time method, also known as the gravimetric method, involves measuring the change in pressure required to decelerate a mass of fluid between two well-spaced pressure taps to estimate discharge. The integral of differential pressure from initiation of the test to the completion of the gate closure is proportional to discharge. Although this method has produced accurate results, it is best suited to high-head plants that have long penstock systems (Levesque, 1994). An additional limitation of this method is load rejection is required (*i.e.*, a full shut down of the turbine by closure of the gates).

Tracer-Dilution

The tracer-dilution method is based on the mass balance of a conservative dye that is pumped at a constant rate into the intake passage and sampled at the draft tube outlet. Total discharge is determined as the ratio of the initial tracer concentration to the final mixed concentration times the injected flow rate. The literature has shown that accurate, precise absolute efficiency may be obtained from this method (Nystrom, 1991). However, an inherent weakness of this method is the difficulty of obtaining thorough mixing, particularly for short conduit systems (Winstone, 1989).

Allen Salt Velocity

The Allen salt velocity method, also known as the transit-time method, uses two well-spaced electrode stations to determine the transit-time of the center of a salt cloud by generating a conductance chronograph. Although this method has been considered accurate enough to define reference discharges for comparison studies, it is disruptive to plant operations as considerable down time is required to install and remove the special test equipment from the intake and draft tube passages (Spencer, 1986). To obtain accurate discharge measurements, long transit-times are required. As such, the technique is best suited to units with long penstock systems.

Differential Pressure

The differential pressure method is based on the well-known fact that discharge can be related to differential pressure in a conduit of varying cross-sectional area. Typically, differential pressure is measured across the 'Winter-Kennedy' taps in the turbine scroll case. A calibration of the proportional relationship may be obtained by modeling, however similitude error limits the accuracy of the discharge estimates for the prototype. The differential pressure method is primarily used to test relative performance of a hydroelectric units to identify, for example, the reduction of turbine efficiency due to runner wear.

Current-Meter

The current-meter method is a well-established technique for metering low-head plants. A number of 'point velocity' measurements are obtained within the flow area using propeller-type flow meters. An appropriate summation of the grid of velocity measurements yields an estimate of discharge.

Acoustic Transit-Time

Transit-time acoustic discharge measurement, commonly referred to as acoustic discharge measurement (ADM) is a popular technique for flow metering within uniform conduits. The method operates on the principle that the velocity of an acoustic signal in water is influenced when a component of the water velocity is parallel to the direction of acoustic propagation (Schuster, 1975). The average water velocity along a path between a pair of acoustic transducers is proportional to the difference between the acoustic transit-times of each direction. A discrete number of average chordal velocities are obtained from acoustic transducer pairs installed at fixed levels within the conduit and then integrated across the flow area using numerical integration techniques.

2.4 DISCHARGE MEASUREMENT FOR PERFORMANCE TESTING AT LOW-HEAD PLANTS

Performance testing is generally more difficult at low-head plants than at high-head plants. Figure 2.2 illustrates a typical cross section of a low-head unit. The characteristically short, non-uniform conduit system of low-head plants precludes accurate absolute discharge measurement by the majority of established techniques. For example, tracer-dilution tests are best suited to long conduit systems because adequate mixing of the concentrate is required. The Allen salt velocity method is not applicable to low-head plants because long transit-times are required.

The current-meter method is typically employed for testing low-head plants. A finite number of point velocity samples are obtained at specified locations within the turbine intake using a propeller type velocity meter, or 'Ott' meter, as shown in Figure 2.3. The meters are either installed on a frame fixed inside the intake, which requires de-watering of the unit, or by traversing an array of meters mounted on a carriage down the stop-log guides (Figure 2.2) and sampling velocities at specified levels. Figure 2.4 illustrates such a carriage used for Ott meters. Point velocities are sampled at each level for a defined

duration; hydraulic testing codes recommend a duration of two minutes or more (ASME, 1992; IEC 1991). An appropriate summation of the grid of velocity measurements times the respective areas yields an estimate of discharge. Various positioning and summation strategies are specified in performance testing codes. It has been estimated that the uncertainty of the current-meter technique is approximately 2 % (*e.g.*, Mikhail, 1994; IEC, 1991).

A significant difficulty associated with any velocity measurement method being applied at low-head plants is the ability of the technique to adequately sample the complex velocity profiles within the intake. Figure 2.5 illustrates a typical profile observed at a low-head plant from a current-meter test. The intersections of the gridlines represent single velocity measurements. Two features of this figure are worth highlighting: 1) the water velocity is not measured between the grid intersections; and 2) the profile is not uniform. A number of factors contribute to the complexity of the velocity profile:

1) the close proximity of the metering plane to the bulkhead and pier structures;
2) disturbance from major elements of the trash-racks shortly upstream of the metering plane;
3) blockage of the trash rack;
4) flow reversals;
5) operation of adjacent units; and
6) non-uniform, converging intake geometry.

Among the several advantages of the current-meter method of discharge measurement are its relatively low initial cost and minimal disruption to normal plant operations when the traversing approach is employed. As opposed to the majority of the aforementioned methods that require considerable down time, de-watering and installation of special equipment within the water passages, traversing the intake with propeller meters does not significantly disrupt plant operation. Discrete sampling of velocities provides useful information about the spatial variation of velocity across the metering plane for the

assessment of intake and trash-rack performance. In addition, individual velocity measurements can be used to more accurately calculate the kinetic energy at the intake. There are, however, definite shortcomings of the current-meter method, including:

1) the inability of the finite sampling strategy to accurately represent a complex flow profile;
2) each meter requires unique periodic calibration;
3) the difficulty in accurately measuring flow reversals; and
4) the disruption of the flow field by the traversing apparatus.

Employing acoustic technology at low-head plants will potentially improve the accuracy and efficiency of discharge measurements over the current-meter method. Acoustic discharge measurement is the focus of this thesis, as such, the following chapter provides detailed background on this field.

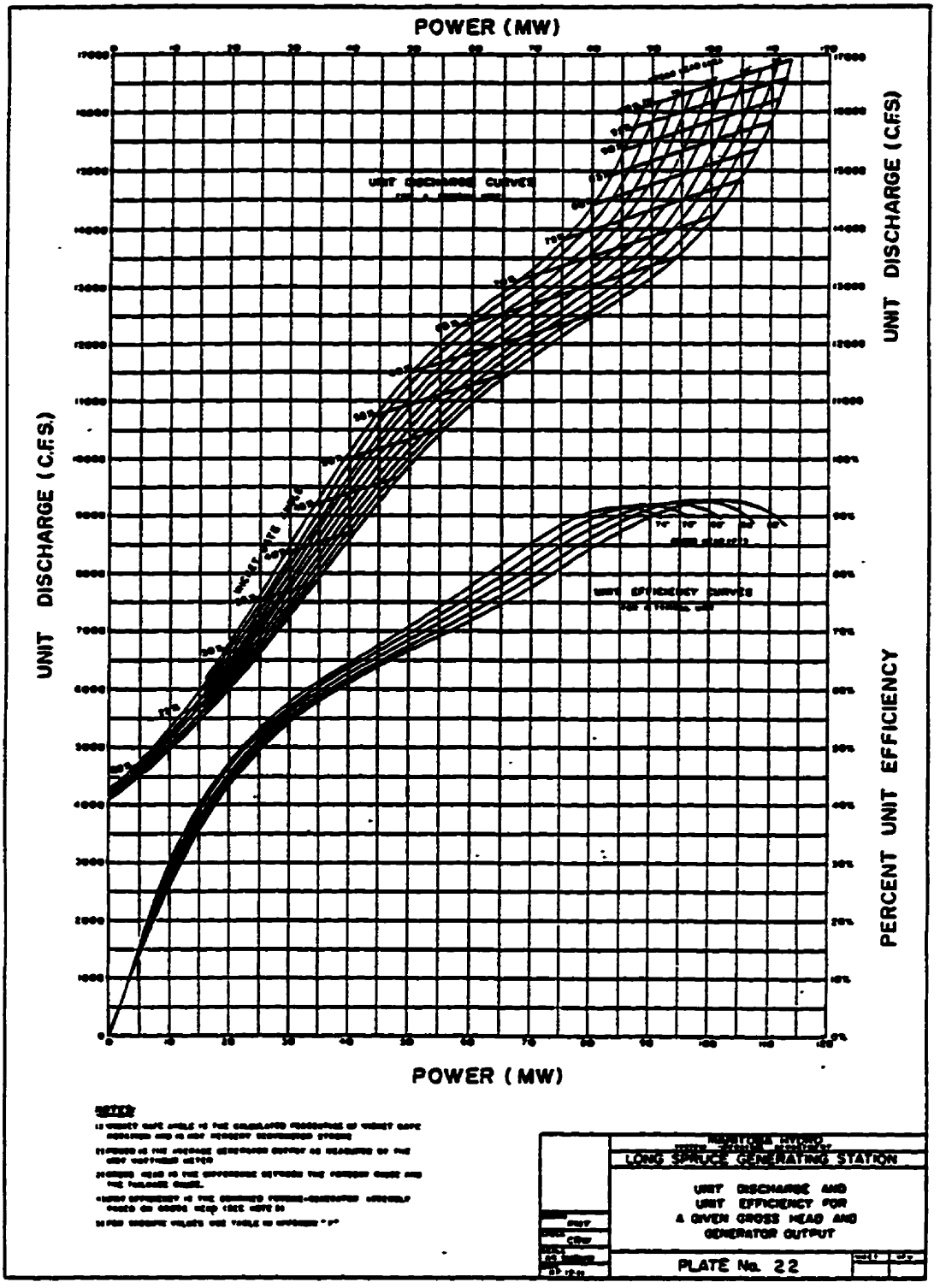

Figure 2.1 Typical performance curves for a low-head hydroelectric plant.

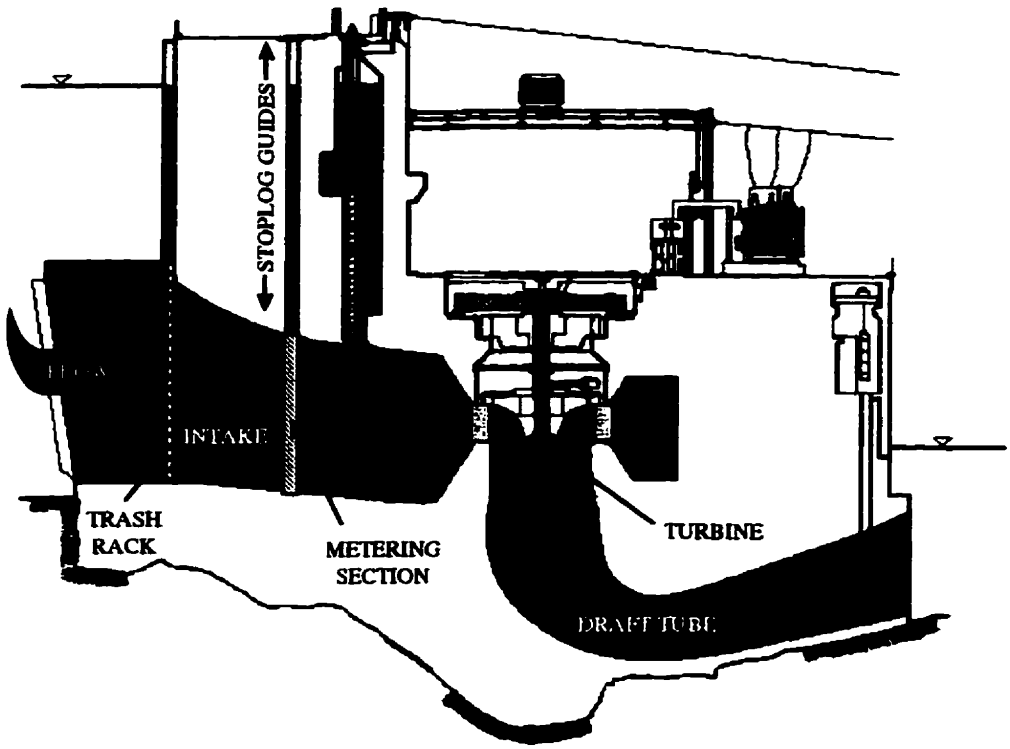

Figure 2.2 Cross-section of a low-head hydroelectric unit.

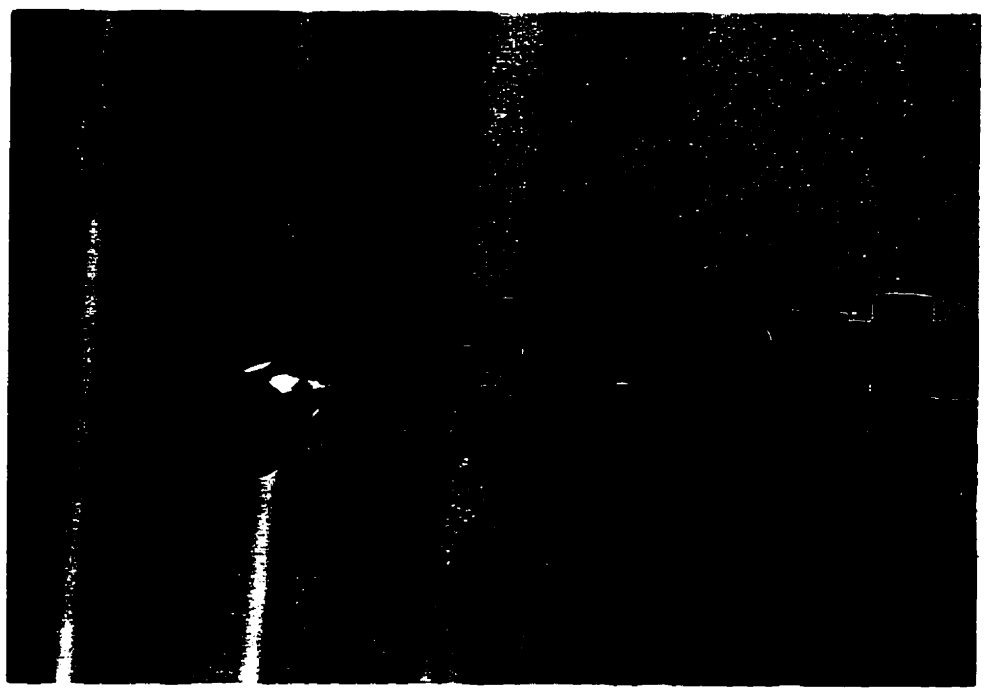

Figure 2.3 Ott meter.

Figure 2.4 Carriage for Ott meters.

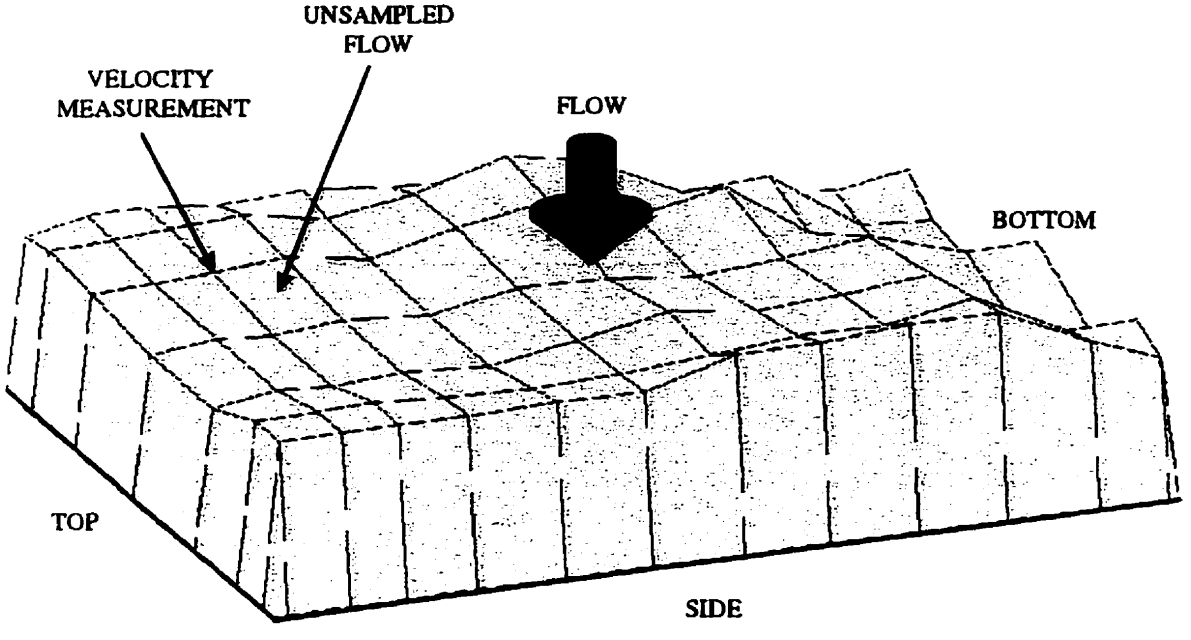

Figure 2.5 Velocity profile obtained from current-meter method.

CHAPTER 3
LITERATURE REVIEW:
DISCHARGE MEASUREMENT USING ACOUSTICS

3.1 DOPPLER VELOCIMETRY

Doppler velocity measurement is based on Doppler shift theory where frequency shifts of acoustic echoes, or back-scatter, are directly proportional to the component of flow along the acoustic beam axis. Acoustic signals that echo off suspended sediments or air bubbles are time-gated to define the location of the velocity sample and analyzed to determine the frequency shift of the pulse. Three or more beams are used to fully resolve the resultant velocity.

Acoustic Doppler theory was first applied in the marine environment to develop speed and position detecting instrumentation for submarine vessels. Since then, technology employing the Doppler principle has become well-established in marine research. With respect to discharge measurement, acoustic Doppler current profiling methods (ADCP) are widely used for oceanographic flow measurements. More recently, ADCP has been applied to shallow water discharge measurement, for example in rivers and estuaries. Since 1967, the U.S. Geological Survey has developed and encouraged development of acoustic Doppler technology and methods to measure river discharge from a moving vessel to eliminate problems associated with the existing practice of shallow water profiling (Simpson and Oltmann, 1993).

For shallow water ADCP, the transducer instrumentation is typically fixed alongside a vessel that is steered using a gyrocompass and triangulation positioning technology. Eliminating the vessel velocity component from the traverse, yields a number of velocity estimates for various depths in the waterway which are integrated to yield a discharge measurement. Simpson and Oltmann (1993) applied ADCP on the Sacramento River, California. After correcting for systematic error, they estimated the uncertainty bounds to

be approximately ±1.5 %, which is similar to conventional current-meter discharge measurements, however the method is much more efficient. It is important to note that these uncertainty levels are largely dependent on the specific conditions of the test and location, for example the number of sampling stations and the geometry of the metering section (in this case, the riverbed).

ADCP is not yet established in the hydroelectric field. In one application, Birch and Lemon (1993) used a similar instrument as Simpson and Oltmann (1993) to sample a three dimensional grid of forebay velocities for comparison to a physical model of the Rocky Reach hydroelectric dam located on the Columbia River in Washington State. The authors highlighted the efficiency and non-intrusive qualities of the method, however it was apparent that were definite limitations in applying the technique to discharge measurement through plant intakes. First, attempting to profile close to a turbine intake resulted in reflections off the powerhouse face and returned corrupted echoes. In addition, it was difficult to obtain velocity samples at bottom boundaries because of echo returns from side lobes not aligned with the primary beams of the instrument. Also, the uppermost level of the profile was not sampled because a 'quiet time' was required for the transducers to stop ringing before returns could be listened for. Despite these shortcomings, with appropriate beam geometry, it is possible that ADCP will attain a presence in hydroelectric turbine performance testing.

3.2 ACOUSTIC SCINTILLATION

Acoustic scintillation velocity measurement is a correlation sonar technique that has been used to measure flows by analyzing the time record of scintillations between two acoustic paths separated by a known distance. Scintillations are the random fluctuations of the amplitude and phase of a wave caused by variations in the refractive index of the medium, which results from turbulence in the flow. Numerous applications of this theory have been documented, such as wind velocity measurements (Lawrence *et al.*, 1972) and tidal turbulence and velocity measurements (Clifford and Farmer, 1983). The

applicability of acoustic scintillation discharge measurement to hydroelectric plants is currently under study (Bell and Lemon, 1996; Birch and Lemon, 1995; Lemon, 1995; Birch and Lemon 1993).

Figure 3.1 is a simplified illustration of the principle of scintillation velocity measurement. Statistical correlation of the received acoustic signals is used to trace the advection of a random disturbance across the two paths of closely spaced transducer pairs. By calculating the average advection time and knowing the separation between the paths, the lateral average velocity can be calculated, *i.e.*,

$$\overline{V}_n = \frac{\Delta x}{\Delta t}, \tag{3.1}$$

where $\overline{V}_n$ = average normal velocity,

Δx = path separation, and

Δt = lag time.

Integrating lateral average velocities, either by continuous traversing, traversing and stopping to sample, or by sampling from numerous transducer pairs fixed at different levels in an intake, yields an estimate of discharge. Bell and Lemon (1996) recommended mounting numerous transducer pairs to a rigid frame that can be positioned in the intake gate slots.

Bell and Lemon (1996) discussed sources of error, both systematic and random, of the scintillation technique for flow measurement. The systematic uncertainties were classified as: 1) bypass flow; 2) integration error; and 3) lateral average velocity measurement error. Bypass was defined as flow outside of the metering area not captured by the acoustic paths. To integrate the velocity profile, the researchers applied an adaptive Romberg integration algorithm, with a cubic spline interpolation in the integrand between the measured points. The authors explained that the error of this integration technique was similar to that of the Gauss-Quadrature method which is explained in Section 3.3.2. The systematic uncertainty of the lateral average velocity measurements

resulted from the combination of the uncertainties in the measurement of transducer spacing, array orientations and of timing by the instrument electronics.

Bell and Lemon (1996) identified a number of possible sources of random uncertainty: 1) laterally averaged velocity; 2) the variability of the discharge and flow distribution with time; 3) uncertainty of the angle of the flow introduced by off-axis components; 4) movement of the frame in the gate slot; and 5) electronic uncertainties. The latter two sources were not considered to be significant relative to the first three. The most significant contribution to the first source of uncertainty was defining the exact location of the peak of the 'cross-correlation' curve when calculating the advection time. The second random uncertainty, temporal variability of discharge and flow distribution, is significant to any technique that does not employ simultaneous velocity sampling and continuous discharge measurement. The authors cautioned that this variability must be evaluated carefully as velocity variation recorded at one location in the flow may be compensated by variations at other locations. The cosine response of the instrumentation was investigated in laboratory tow-tank tests. It was determined that the random uncertainty of the horizontal velocity component increased from 0.4 to 0.5 % after rotating the transducer arrays by 45 degrees.

Acoustic scintillation flow measurement has strong potential to develop within the field of hydraulic performance testing. It is particularly well-suited to low-head plants, where the characteristics of the intake and conduit system preclude the use of other established non-intrusive discharge measurement techniques.

3.3 TRANSIT-TIME ACOUSTIC DISCHARGE MEASUREMENT

Transit-time ADM is, by far, the most widely accepted acoustic technique for discharge measurement in the field of hydroelectric performance testing. ADM is the focus of this research, thus the practice is reviewed thoroughly in the following sections.

3.3.1 Principle

ADM operates on the principle that the velocity of an acoustic signal is influenced by the velocity component of the flowing medium parallel to the direction of acoustic propagation, as illustrated in Figure 3.2. Sound pulses traveling upstream are impeded by the flow resulting in increased transit-times, conversely, downstream transit-times are reduced. The average water velocity along a path between a pair of acoustic transducers is proportional to the difference between the upstream and downstream transit-times.

Equations (3.2) and (3.3) explain how the chordal average normal velocity of flow can be calculated from acoustic transit-time measurements. Referring to Figure 3.2, the velocity of upstream and downstream traveling acoustic pulses can be calculated as

$$VP_u = c - V_p = \frac{L}{t_u}, \text{ and} \tag{3.2}$$

$$VP_d = c + V_p = \frac{L}{t_d},$$

where VP_u = acoustic pulse velocity traveling upstream,

VP_d = acoustic pulse velocity traveling downstream,

c = speed of sound in water,

V_p = water velocity in the direction of the acoustic path,

L = length of acoustic pathline,

t_u = upstream acoustic pulse transit-time, and

t_d = downstream acoustic pulse transit-time.

Solving for the pathline water velocity results in equation (3.3).

$$V_p = \frac{(c^2 + V_p^2)}{2L}(t_u - t_d) \tag{3.3}$$

Dividing the pathline average water velocity by the cosine of the path angle (θ), yields the chordal average normal velocity

$$V_n = \frac{V_p}{\cos\theta}. \tag{3.4}$$

3.3.2 Integration of the Velocity Profile Using Discrete Level Sampling: Gauss-Quadrature Integration

A powerful numerical method of approximating integrals, generally referred to as Gaussian or Gauss-Quadrature (GQ) integration, is traditionally used for ADM. The technique requires that the function to be integrated be evaluated at specified ordinates, x_i which correspond to the zeros of orthogonal polynomials (*e.g.*, Legendre, Laguerre, Hermite). For rectangular conduits, Legendre ordinates are used (IEC, 1991). Clearly, the real function describing the velocity profile, $v(x)$, is never truly known. However, sampling the velocity at specified levels in the intake, corresponding to x_i, provides the functional evaluation, $v(x_i)$. It can be shown that an N level GQ integration can exactly evaluate the integral of a $(2N\text{-}1)^{th}$ or lower-order polynomial (Nielsen, 1964). Appendix A provides a detailed explanation of Gauss-Legendre integration. The following is an illustration of the technique.

A transformation of the integration interval, over the vertical distance of the intake $[h_0, h_1]$ to a standard interval $[x_0, x_1]$ is first applied,

$$I = \int_{h_0}^{h_1} v(h)dh = \frac{(h_1 - h_0)}{2} \int_{-1}^{1} v\left(\frac{(h_1 - h_0)x + (h_1 + h_0)}{2}\right)dh = \int_{-1}^{1} f(x)dx, \tag{3.5}$$

where $f(x)$ is the transformed function.

The integral is then evaluated using the Quadrature rule,

$$I \cong \sum_{i=1}^{N} w_i f(x_i), \tag{3.6}$$

where w_i = integration weights,

x_i = ordinates of the integration (zeros of a Legendre polynomial), and

N = the number of functional evaluations used (sampling levels).

As an illustration, consider the hypothetical velocity profile illustrated in Figure 3.3 and assume a unit width. This profile was generated by plotting the 7th order polynomial given by

$$\begin{aligned} v(h) = 22.2349 + 71.7290h - 50.4293h^2 + 14.6997h^3 \\ - 2.1408h^4 + 0.1644h^5 - 0.0064h^6 + 0.0001h^7, \end{aligned} \tag{3.7}$$

where $v(h)$ is velocity in cm/s. For clarity, only 4 decimal places are shown, however a higher accuracy was maintained through the following calculation. To exactly evaluate the integral of this polynomial, a 4 level Gauss-Legendre integration is used. From equations (3.5) and (3.6), the transformed integral is evaluated as

$$\int_{h=0}^{h=15} v(h)dh = 7.5\sum_{i=1}^{4} w_i v(7.5x_i + 7.5). \tag{3.8}$$

Figure 3.3 includes the 4 evaluations of the function $v(h_i)$ that correspond to the x_i ordinates. Table 3.1 summarizes the ordinates, weights and functional values required to evaluate equation (3.8).

Table 3.1 Gauss-Legendre w_i, x_i and functional evaluations for 7th order polynomial integration.

i	w_i	x_i	$v(7.5x_i + 7.5)$ [cm/s]	$w_i v(7.5x_i + 7.5)$ [cm/s]
1	0.3478548451	-0.8611363116	56.6340	19.7004
2	0.6521451549	-0.3399810436	41.3908	26.9929
3	0.6521451549	0.3399810436	41.5518	27.0982
4	0.3478548451	0.8611363116	47.2384	16.4330
$Q_{GL} = 7.5\sum_{i=1}^{4} w_i v(7.5x_i + 7.5)$ $[\frac{m^3}{s}]$				6.7668

Using calculus, the integral is given in equation (3.9).

$$\int_0^{15} v(h)dh = \left(\begin{matrix} 22.3489h + \frac{1}{2}71.7290h^2 - \frac{1}{3}50.4293h^3 + \frac{1}{4}14.6997h^4 - \frac{1}{5}2.1408h^5 \\ + \frac{1}{6}0.1644h^6 - \frac{1}{7}0.0064h^7 + \frac{1}{8}0.0001h^8 \end{matrix}\right)\Bigg|_0^{15} \quad (3.9)$$

$$= 6.7668 \frac{m^3}{s}$$

The calculated error was less than 10^{-5} %; a result of the precision of defining x_i and w_i.

3.3.3 Initial Development of ADM

The major drive towards acoustic flow measurement began in 1957, when the California Department of Water Resources, the U.S. Geological Survey and the U.S. Corps of Engineers teamed with a U.S. manufacturing company to develop an acoustic velocity flow meter (Lanning and Ehrhart, 1977). This effort was prompted by the possibility of applying submarine sonic equipment to measuring large flows of water at an accuracy previously thought to be unattainable. This initial phase produced a limited degree of success, primarily due to the non-optimal placing of acoustic paths and the use of inadequate transducer technology; hydrophones were originally used, as opposed to piezoelectric crystals that are used today.

The California Department of Water Resources and another company undertook the design and fabrication of one pipe flow meter and two canal flow meters at key control locations along the California Aqueduct. All of the installations were single path, crystal transducer configurations; the canal transducers were mounted on rails to facilitate metering at varying depths. These installations were problematic because the transducers were susceptible to damage due to vibrations and the canal traversing mechanism tended to breakdown. In order to overcome the problems associated with traversing the canal and to improve the accuracy of the canal meter in unstable flow, a stationary 4 level Gauss sampling strategy was employed (Lanning and Ehrhart, 1977). Laboratory testing of Gauss sampling for canal and pipeline flow rates confirmed the capability for highly accurate flow measurement, even under unstable flow conditions. Since this initial development, transit-time acoustic velocimetry has been extensively tested and applied to a number of fields, such as petroleum, hydroelectric, thermoelectric, water resources and wastewater.

3.3.4 Application of ADM to Performance Testing

The potential for highly accurate, non-intrusive discharge measurement has resulted in the extensive growth of ADM in the field of hydroelectric performance testing. Acoustic installations are best suited to high-head hydroelectric plants that characteristically have long penstock systems. Given these conditions, transducers may be installed well downstream of a disturbance, for example a bend, convergence or intake structure, where a fully-developed symmetrical velocity profile exists. Extensive inter-comparison field testing of ADM has been undertaken (*e.g.*, Grego, 1996; Sugishita *et al.*, 1996; Missimer *et al.*, 1986) have illustrated the usefulness of this technique for high-head applications. Through laboratory testing and numerical modeling, it has been shown that discharge may be measured with uncertainties of considerably less than 1 percent (Lowell and Hirschfeld, 1979; Lanning and Ehrhart, 1977).

Lowell and Hirschfeld (1979) identified three sources of error in acoustic flow-meters: 1) 'as built' dimensional uncertainties; 2) integration errors which result from uncertainties in the velocity profile; and 3) errors which are due to upstream conditions. Typical dimensional uncertainties were estimated to result in flow rate errors of ±0.2 to ±0.3 %. The authors stated that, "Assuming good geometry and upstream conditions, integration error of four-path meters has shown to be less than 0.1 %." Lowell and Hirschfeld (1979) approximated that four-path systems applied to ideal conduits would measure discharge with an uncertainty of less than ±0.5 %.

Also addressed in the literature is the susceptibility of fixed level ADM to integration error in non-ideal flow conditions. Understandably, the more complex the velocity profile is, the more difficult it is to integrate that profile to obtain a discharge measurement. It has been recommended in the literature (Walsh *et al.*, 1996; Dube, 1995; IEC, 1991) that certain measures be taken to reduce the uncertainties resulting from the integration, profile and upstream conditions; these are as follows:

1) use crossed-plane configurations;
2) orientate the planes to minimize error due to upstream perturbances; and
3) increase the number of acoustic paths to better sample complex, asymmetric velocity profiles.

For applications where the streamline direction is difficult to specify, for example when the measurement section is too close to an upstream bend, transition, or obstruction that causes asymmetrical profiles and/or converging or diverging streamlines, crossed path configurations have been recommended. Using a crossed plane configuration significantly reduces the error resulting from an assumed resultant velocity direction (θ in Figure 3.2). The accepted approach is to simply average the normal velocities derived from the two planes (IEC, 1991).

With respect to the second measure, Lowell and Hirschfeld (1979) indicated that cross-flow errors can be reduced by orienting the acoustic paths so they are perpendicular to the

plane of a bend or elbow. With this practice, cross-flow components are directed perpendicular to the acoustic paths, thus not influencing the transit times and the dependent velocity measurements.

Increasing the number of acoustic paths can improve the accuracy of the integration of non-ideal velocity profiles. As introduced in Section 3.3.2, by increasing the number of functional evaluations, the Gauss integration method can be used to evaluate more complex integrals, *i.e.*, higher order polynomials. Walsh *et al.* (1996) compared the performance of a 4 and 9 level acoustic installation at the Robert Moses Niagara Power Plant, New York. The field study addressed the integration uncertainties of stationary ADM under non-uniform, or skewed, velocity profiles. The installation was located two diameters downstream of a 48 degree elbow. Data from 60 tests at a range of gate openings revealed a systematic difference of 0.9 % between discharges obtained from the 4 and 9 level systems. The authors concluded that this disagreement was primarily due to a velocity deficit in the profile that the 4 path system "couldn't see," that the 9 path system could. This study highlighted the need for additional sampling levels to adequately estimate the integral of more complex velocity profiles.

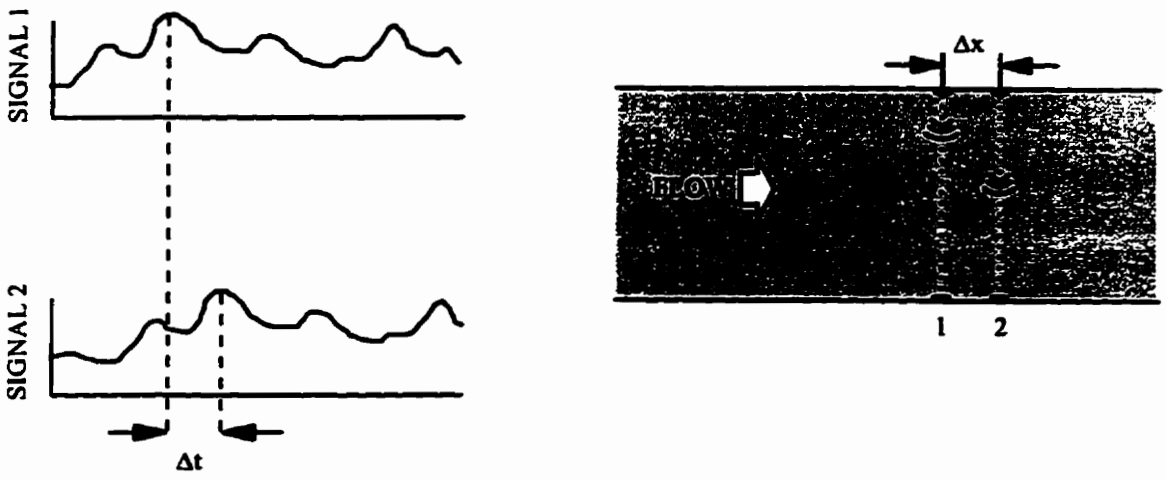

Figure 3.1 Acoustic scintillation flowmetering principle.

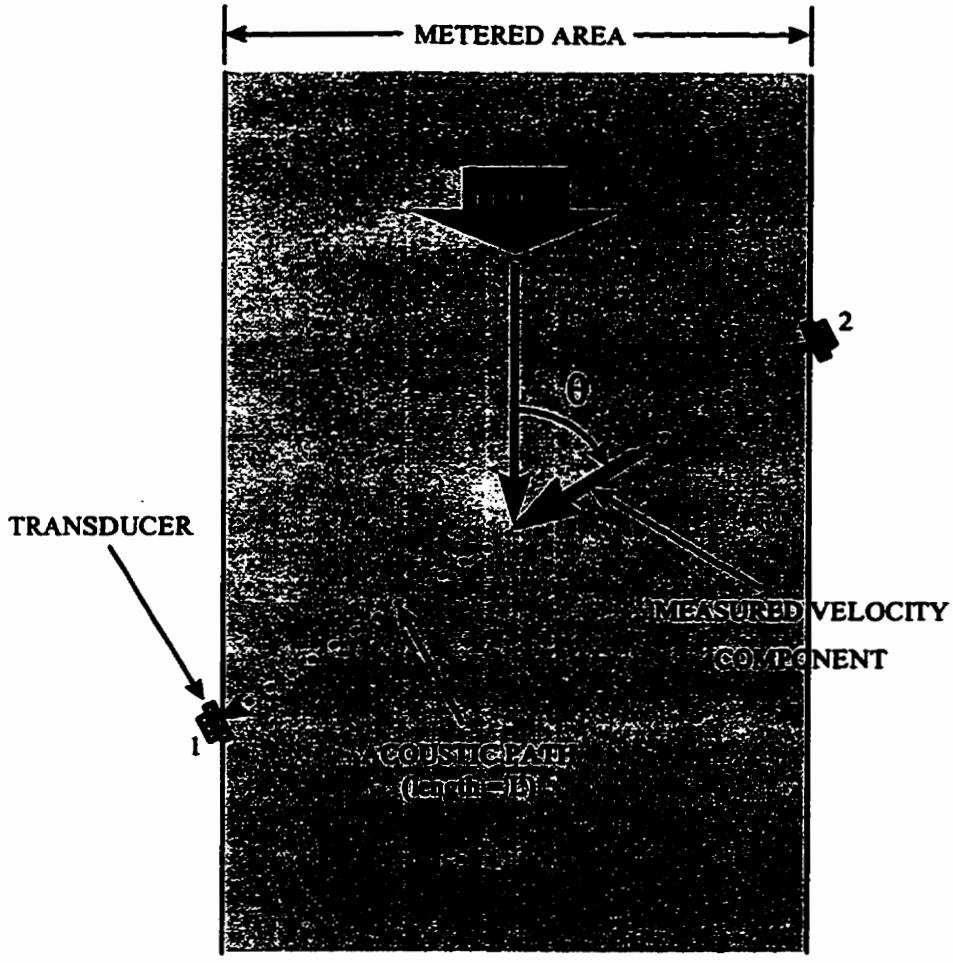

Figure 3.2 Principle of transit-time acoustic velocimetry.

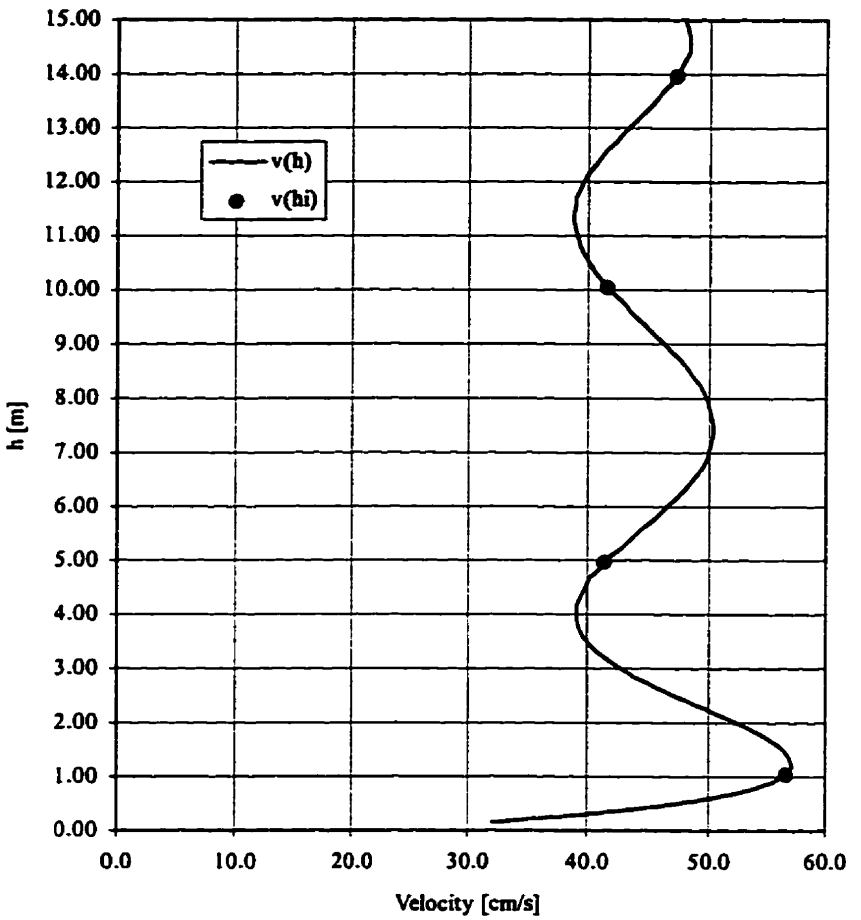

Figure 3.3 Hypothetical velocity profile represented by a 7th order polynomial.

CHAPTER 4
PROPOSED TECHNIQUE AND TESTING PROGRAM

4.1 PROPOSED ADM TECHNIQUE FOR LOW-HEAD PLANTS

It is anticipated that transit-time acoustic velocimetry can be used to provide improved estimates of discharge. The proposed technique is in essence a hybrid version of the traversing current-meter and ADM methods. An array of acoustic paths can be configured to obtain chordal averages of velocity at a high sampling rate. By traversing this array across the intake via the stop-log guides, virtually the entire flow profile can be sampled. This technique will provide a more complete integration of the velocity profile relative to discrete sampling techniques, such as the current-meter and existing ADM approaches. Improving the integration will result in a very accurate discharge estimate. Employing acoustic velocimetry will also provide information about high frequency fluctuations and accurately measure flow reversals; current-meter technology does not provide this information.

Figure 4.1 illustrates a single 'acoustic cell' consisting of two pairs of acoustic transducers in a crossed path configuration. For each transducer pair, the travel times of upstream and downstream traveling acoustic pulses are measured and an average line velocity is obtained between the transducers. A number of these acoustic cells would be mounted adjacently, as depicted in Figure 4.2. Each cell would measure chordal average normal velocity. The carriage of transducers would be continuously traversed down the stop-log guides using similar gantry and carriage equipment as used for the current-meter method, to vertically integrate the velocity profile.

4.2 TESTING PROGRAM

Preliminary evaluation of the technique was carried out by testing a single acoustic cell in the Hydraulics Research and Testing Facility (HRTF) at the University of Manitoba. A 1 m by 1 m intake was constructed to define a metering plane. A positioning system was used to traverse the four acoustic transducers across the flow area to sample average chordal velocities. The technique was evaluated primarily by comparing the discharge measurements derived from the acoustic cell with known laboratory discharge values. Specifically, a testing program was designed to determine:

1) the accuracy of the single cell system;
2) the repeatability of the single cell system;
3) an appropriate sampling strategy (*i.e.*, traversing rate, GL sampling);
4) the accuracy of the discharge measurement technique for measuring non-uniform velocity profiles; and
5) the susceptibility to error under disturbed and non-parallel flow conditions.

The accuracy of the technique was evaluated by comparing absolute discharge measurements with known laboratory flow supplying the model. An assessment of the repeatability of the technique was made by comparing subsequent measurements of the same flow.

Based on measurement accuracy and repeatability, a range of sampling strategies were evaluated. It was anticipated that traversing the intake too quickly would under sample the velocity profile, resulting in inaccurate and/or non-repeatable discharge measurements. Conversely, excessively slow traversing strategies would over sample the velocity profile without improving the quality of the discharge measurement. A range of Gauss-Legendre (GL) sampling strategies were also tested. The objective was to define the appropriate degree of sampling and the relative performance of continuous versus discrete sampling strategies in both favorable and disturbed flow conditions.

As the discharge measurement technique is to be applied at low-head plants, it was necessary to assess the technique under complex flow conditions. Flow perturbations were introduced shortly upstream of the metering plane in the intake to assess the ability of the technique to integrate non-uniform velocity profiles and to measure flows containing vortex shedding.

The typical non-prismatic intake geometry of low-head plants contributes to the complexity of velocity profiles. Since the intakes converge quite rapidly towards the turbine, non-parallel flow lines exist in the metering plane. To assess the ability of the proposed technique to resolve the normal flow component under converging flow conditions, a flow constriction was included shortly downstream of the metering plane to introduce non-parallel flow.

4.3 PHYSICAL DESCRIPTION OF LABORATORY SETUP

4.3.1 Flow Supply, Flume and Intake Structure and Acoustic Cell

Flow Supply

Hydraulic testing was carried out on the model floor of the HRTF. The flow system is a closed circuit, that is, water is re-circulated from a sump pit using two high discharge low-head pumps (75 and 60 hp) into the constant head tank, tapped off the tank to source the flume through a 350 mm PVC pipe, passes through the intake structure, out of the flume and returned to the sump pit. The capacity of the flow system is approximately 500 l/s.

Flume and Intake

A timber flume and intake structure, shown in Figure 4.3, was constructed to perform hydraulic tests on a single traversing acoustic cell. The flume was 10.60 m long by 2.48

m wide by 1.60 m deep. The walls of the flume consisted of 19 mm plywood sealed with a roller applied rubber lining (Vulkem 350).

The supply dropped vertically into the flume upstream of flow straightener. The flow straightener consisted of horizontally stacked 290 mm long by 76 mm diameter PVC tubes that were contained by 25 mm flattened expanded metal sheeting on both the upstream and downstream ends. The straightener was used to disrupt the large scale turbulence and to direct the flow towards the intake structure. To stabilize the headwater conditions and further break-up the flow, a 50 mm layer of filter media was attached to the upstream side of the flow straightener.

The leading wall of the intake structure was positioned 2.0 m downstream of the flow straightener. The flow was forced to converge laterally to a width of 1.00 m over a length of 0.90 m. The flow then converged vertically to a ceiling 1.00 m high. The intake was prismatic (1.00 m × 1.00 m) for a distance of 1.42 m. Within this length, the upstream face of the metering section was located 0.69 m from the end of the vertical convergence. At a distance of 0.10 m downstream of the metering section, the intake structure converged laterally to a width of 0.50 m. The vertical convergence shown in Figure 4.3 was added as a flow disturbance for only a portion of the testing program. A motor controlled sluice gate, located 3.0 m downstream of the intake structure, released to the exit chute which directed the water to the sump pit.

The acoustic transducers were recessed in slots in the walls of the metering section to: 1) minimize the flow disruption resulting from the transducer struts; and 2) minimize the flow leakage around the transducers. Four transducer ports cut into the ceiling of the intake provided access to the metering section for the transducers; thus, the metering section was not sealed. The area around the metering section was sealed from both the forebay and tailrace resulting in a still intermediate pool.

Figure 4.4 illustrates the exterior of the metering section. In this figure, the transducers, mounted on the end of the transducer struts (blue in color) are extracted from the

metering section and positioned just above the transducer ports. Figure 4.5 illustrates a test in progress. In this case the transducers were positioned near the bottom of the metering section with the carriage slightly submerged in the intermediate pool. Also illustrated in this figure is the still water condition of the intermediate pool.

Acoustic Cell

The acoustic cell consisted of four transducers in a crossed path configuration, as illustrated in Figure 4.6. To ensure that the transducers would transmit and receive sufficient acoustic signal strengths, an accurate alignment procedure was used. As shown in Figure 4.6 the transducers were mounted to the ends of the support struts using 'accordion-like' two-axis optical mirror mounts (Newport model #MFM-075) for alignment in the vertical and horizontal planes. Figure 4.7 illustrates the alignment procedure used. A small mirror was taped to the face of the transducer being aimed. A hand laser pointer, positioned a distance A from the opposing transducer was pointed at the center of the reflector. The optical mount on transducer 1 was adjusted such that distance A was equivalent to distance B. The adjustment was repeated for the perpendicular plane, resulting in the alignment of transducer 1. This process was repeated for each transducer. Table 4.1 includes the respective path lengths and orientations for the two paths.

Table 4.1 Acoustic cell configuration.

Acoustic Path	*Orientation to Flow (θ) [degrees]*	*Pathlength [m]*
X	57.1	1.170
Y	57.1	1.171

4.3.2 Reference Discharge Measurement

A MSR in-line Magmeter (MAG) was used to monitor and measure the reference discharge (MSR, 1992). Using electromagnetic principles, this commercially produced meter calculates discharge from water velocity measurements at a single location within the pipe. For fully developed turbulent pipe flow, over a wide range of Reynolds numbers, the average velocity occurs at a radial distance 11% of the pipe diameter inward from the wall (Flint-Petersen and Rajaratnam, 1987); the MAG meter sensor is positioned at this location within the pipe. The MAG was installed 3.30 m (10 diameters) downstream of the 90 degree elbow and 2.10 m upstream of the butterfly valve; this positioning well-exceeds the manufacturer's recommendations to ensure a symmetrical velocity profile. In addition, the MAG meter was inserted from the bottom of the 350 mm PVC line to reduce the influence of air entrainment.

4.3.3 Positioning System

Traversing Mechanism and Carriage

To traverse the discharge metering area, a rigid steel carriage and guide assembly was fabricated (as seen in Figures 4.4 and 4.5). The transducers were mounted on the ends of four HSS 33×2.5 mm steel struts projecting downward from the carriage. The 1.40×1.00×0.30 m carriage was guided by concentric collars that slide vertically around two HSS 73×4.8 mm steel columns. The columns were stabilized and aligned to the vertical using four adjustable guy wires.

The carriage was positioned by a servo-motor controlled lead-screw. The lead-screw was a 22.2 mm diameter, 2.82 mm/thread galvanized threaded rod. The maximum traverse length was 1.30 m; a distance greater than one meter was used to provide access to the transducers for installation and alignment. To reduce the required torque from the positioning motor, the carriage weight was counter-balanced using a pulley/deadweight system.

Electronic Positioning System

A computer controlled electronic positioning system was used to accurately and precisely traverse the transducers across the flow. Figure 4.8 is a schematic diagram of the positioning system. A Galil DMC-1020 two axis bus mounted controller card was installed in an AT-based PC. An analog signal between ±10 volts was transmitted to the amplifier to control the velocity, acceleration and position of the motor. An Electrocraft BDC-25L amplifier was used to power the Electrocraft E-3626 brushless servo motor which rotated the lead-screw. Coupled with the specified amplifier, the motor was rated at 17.6 kg-cm peak torque and 4.4 kg-cm continuous stall torque. A 1000 pulse per revolution (ppr) optical encoder, affixed to the top of the motor, provided feedback to the controller to monitor position and velocity. The controller system deciphers the encoder signal in quadrature, thus the resolution of the positioning system was 4000 counts per revolution of the motor shaft; with a 2.82 mm/thread lead-screw directly connected to the motor, this translated to a vertical resolution of just over 7×10^{-4} mm.

Programming of the Positioning System

ASCII text files were created to control the positioning system for the various traverses tested. The minimum that was required to command a move was rotational speed, acceleration/deceleration and relative or absolute position. Additional commands such as pausing, error limit, torque limit and tuning integrators were used to accurately execute both the continuous and GL traverses. Appendix B contains sample position controller programs.

Continuous monitoring of position and proper tuning of the amplifier and controller card ensured accurate and precise positioning of the transducers. An error limit was defined to reduce the variability in traverse rates and to safeguard against damage to the controller system resulting from possible jamming of the traversing carriage. The motion was halted and an error code was displayed if the encoder feedback indicated that the position error exceeded this limit; an error limit of 2000 counts was defined which translated to

1.41 mm of vertical traverse. Thus, as the carriage was traversing, the maximum instantaneous position error was 1.41 mm.

4.3.4 Acoustic Transducers, Electronics and Software

Transducers

1 MHz transducers were deemed to be appropriate as the pathlengths of the lab cell were approximately 1 m and the prototype pathlengths would likely be between 1 and 5 meters. Lower frequency signals are less susceptible to attenuation, however the trade-off from using higher frequency acoustics is that received signals are not as well-defined. Piezoelectric ceramic discs, 19.05 mm in diameter, were potted in custom machined stainless steel housings. The discs were composed of lead zirchonate titanate with fired on silver electrodes, aligned to radiate in the thickness direction. Figures 4.9 and 4.10 illustrate the ceramic discs and steel housings and the final potted transducer, respectively. The primary lobe of the transducer was essentially cylindrical over the pathlengths used. The company responsible for potting the transducers (Focal Technologies Inc., Dartmouth, Nova Scotia) estimated that the primary lobe diameter was approximately 2.5 cm at a distance of 1 meter from the transducer face.

Custom Electronics

Signal generation and timing electronics were adopted from the Velocity-Density-Vorticity (VDV) oceanographic sensor technology developed by Focal Technologies, Inc., Dartmouth, Nova Scotia (Trivett *et al.*, 1996; Trivett *et al.*, 1995).

Figure 4.11 illustrates a schematic of the standard VDV electronics. While the original VDV transmits a 5 MHz frequency, the setup for testing was modified to use 1 MHz transducers. The electronics were modified to ultimately be capable of making measurements from several transducer pairs to be mounted on a traversing frame, as described in Section 4.1. The current configuration samples velocity at approximately 8 Hz, and transmits the data via an RS-232 serial data link to a PC. The electronics

package, excluding the transducers, was housed in a sealed 5 cm diameter PVC pipe, 32 cm in length. A DC power supply was used to power the modified VDV electronics.

Software

The VDV package contained a Programmable Array Logic (PAL) device that performed travel time measurements. Two PIC micro-controllers acquired the PAL data in real-time. A 'TattleTale 5F' was included in the package to perform supervisory control and timing of the velocity measurements. Powered by the DC supply, the TattleTale was run on command from the data logging PC.

C++ source code, written by Focal Technologies, was run as a front-end to the system. The program calculated, displayed and logged pathline velocity and sound speed measurements for the two pairs of transducers based on specified pathlength values and transit-time data from the TattleTale.

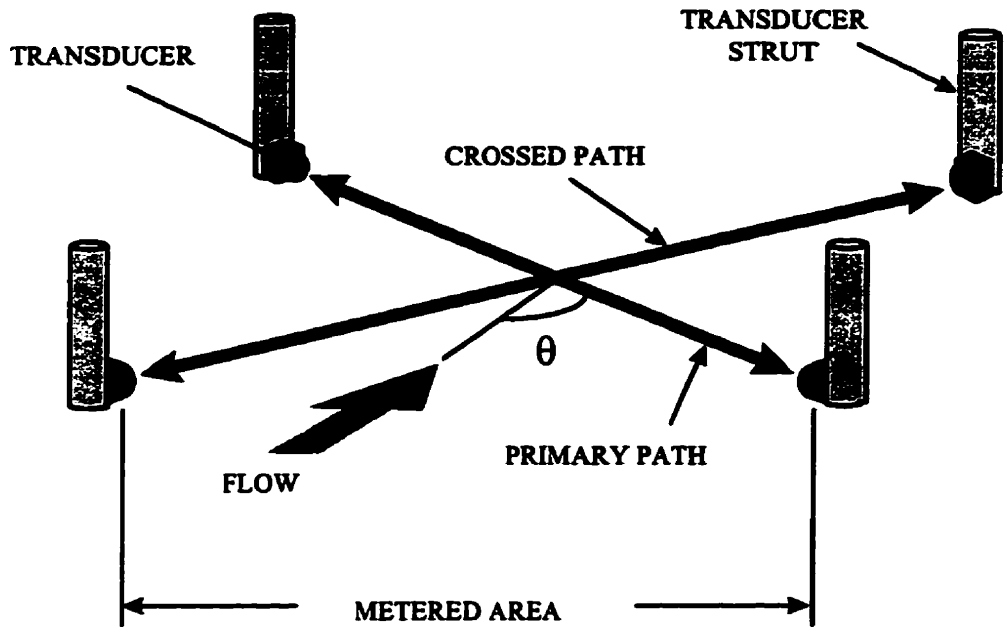

Figure 4.1 Single crossed-path acoustic cell.

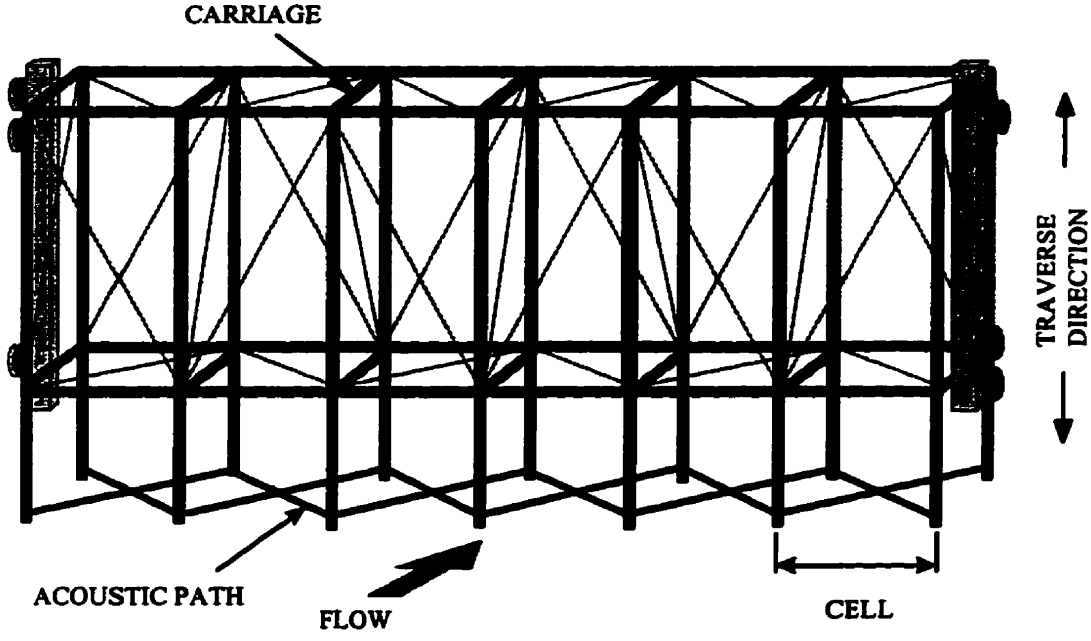

Figure 4.2 Conceptual array of acoustic cells.

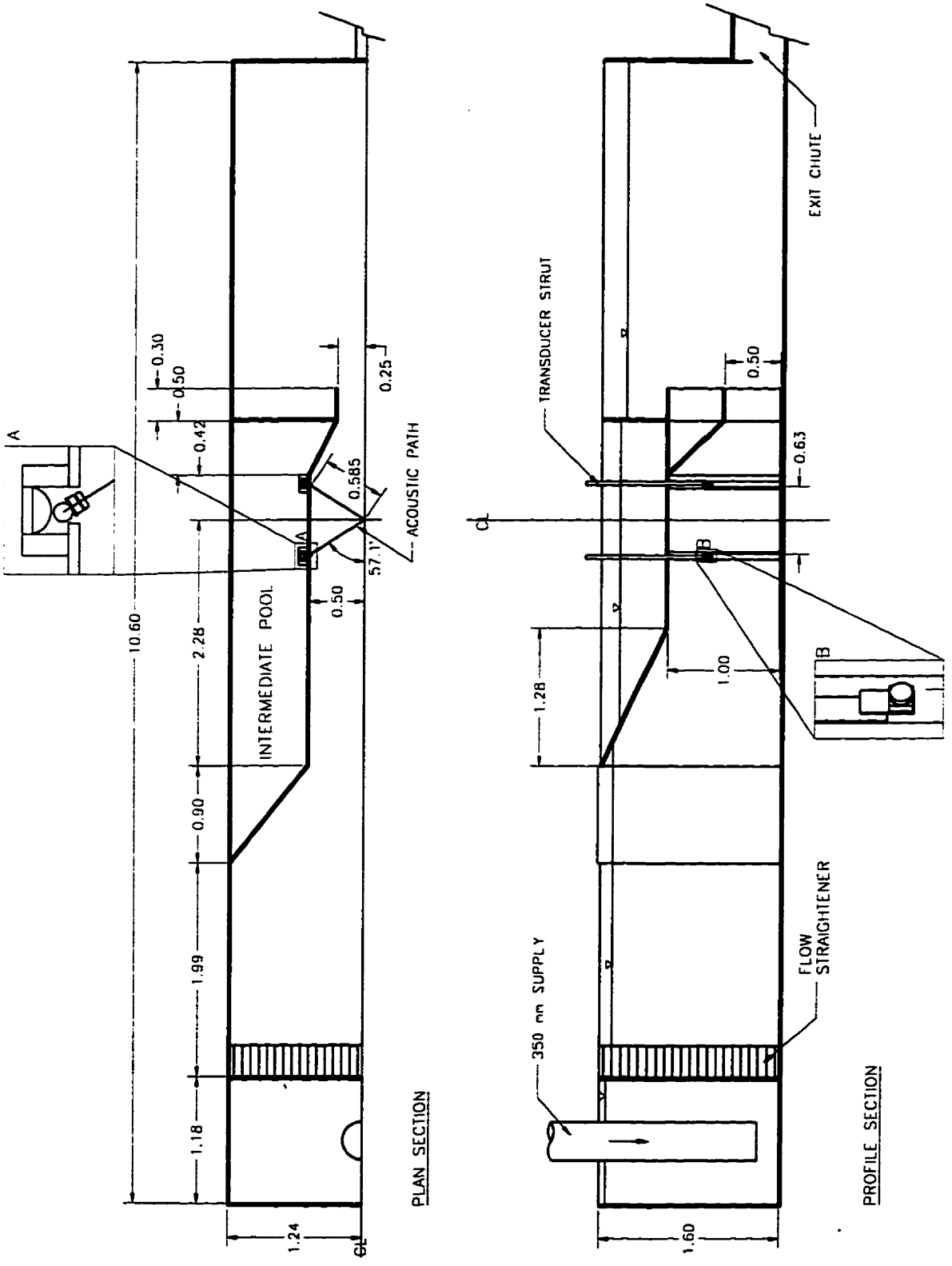

Figure 4.3 Flume and intake structures.

Figure 4.4 Exterior of metering section.

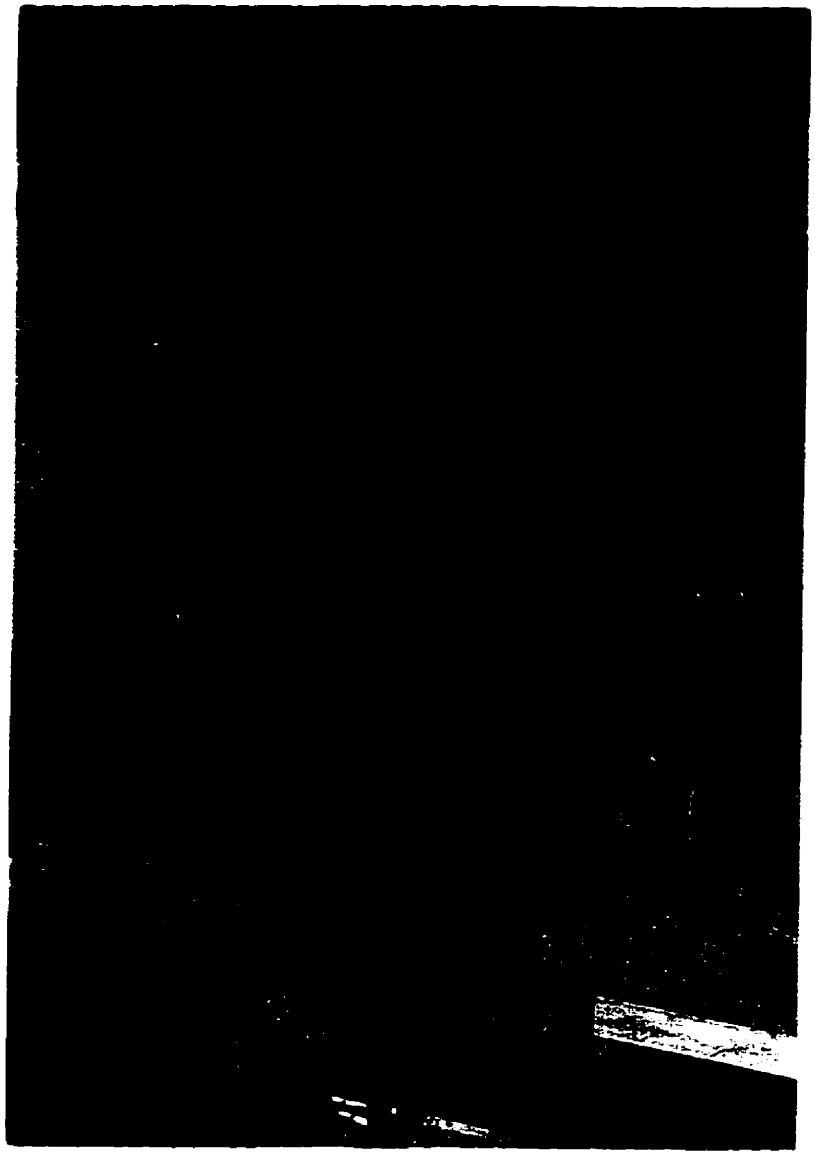

Figure 4.5 Test in progress showing intermediate pool.

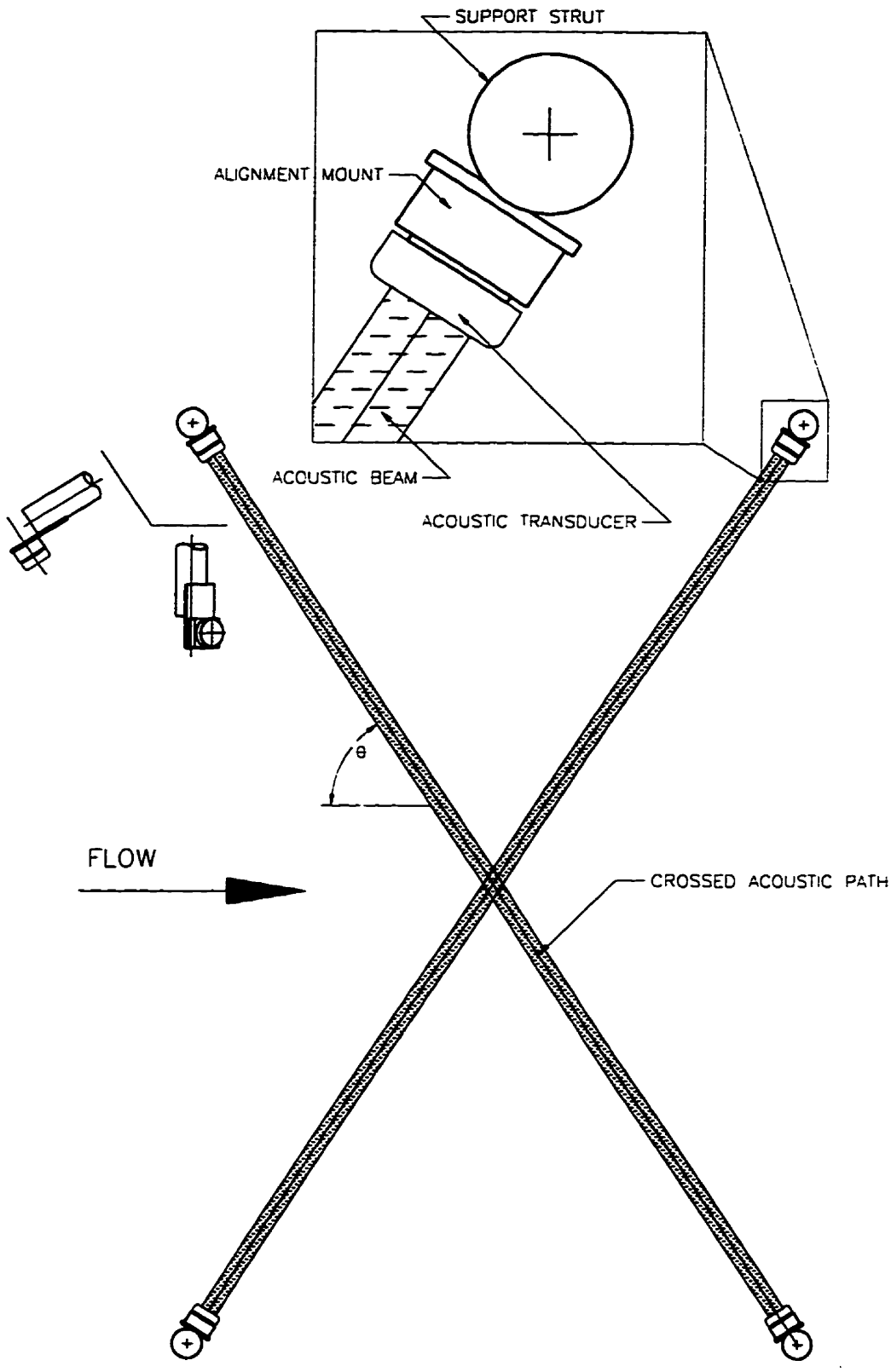

Figure 4.6 Plan view of acoustic cell.

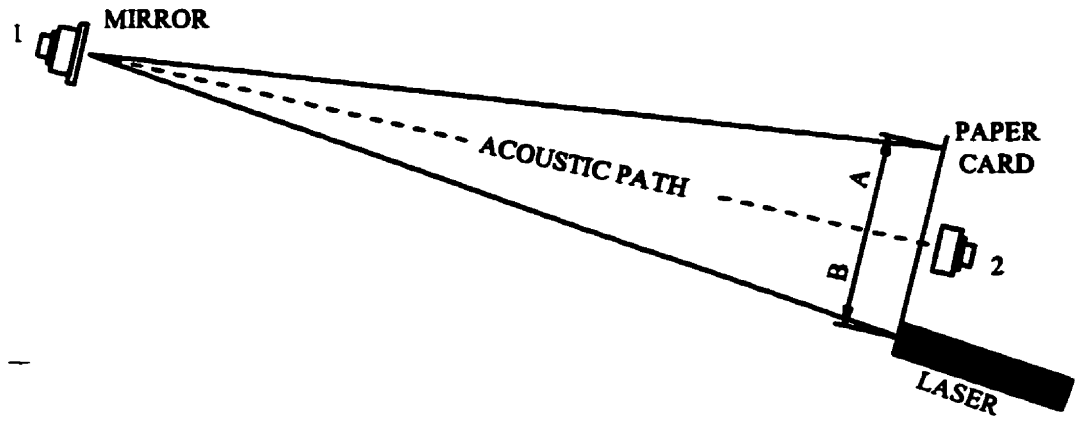

Figure 4.7 Alignment of acoustic transducers.

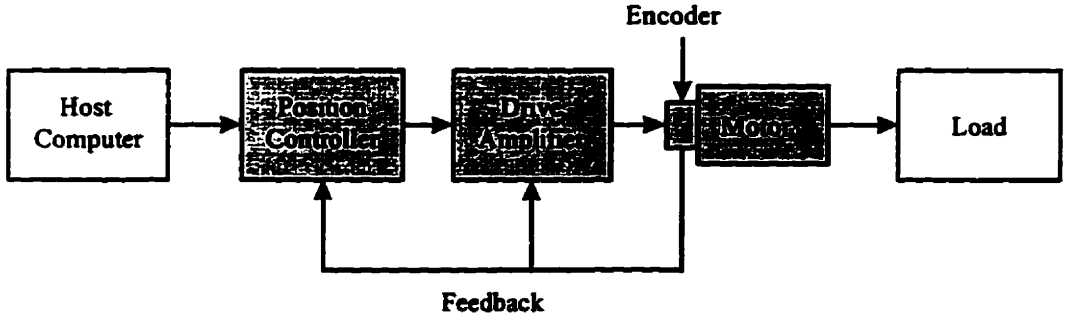

Figure 4.8 Schematic of positioning system.

Figure 4.9 Ceramic discs and transducer housings.

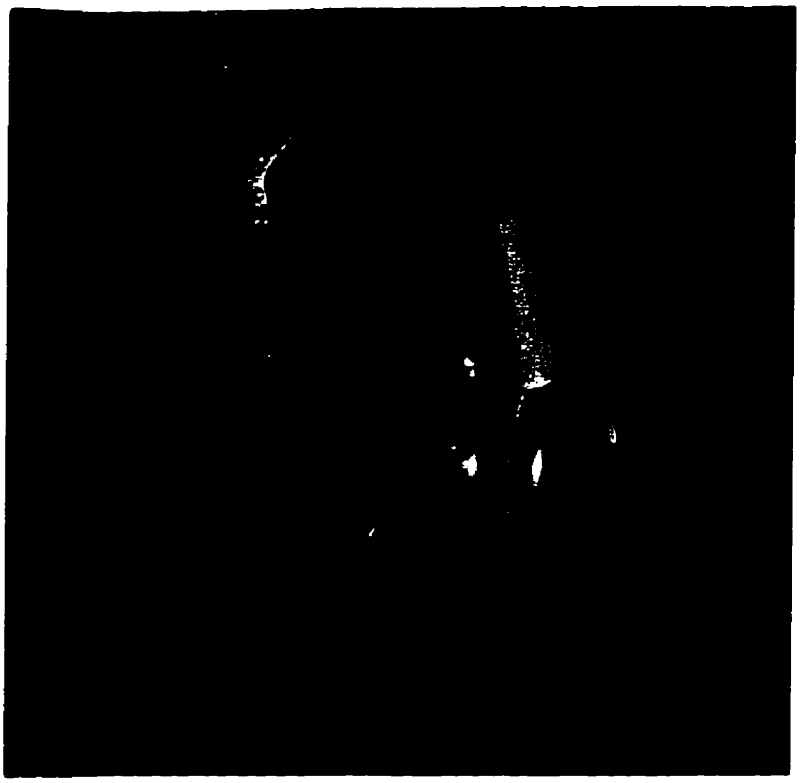

Figure 4.10 Potted transducer.

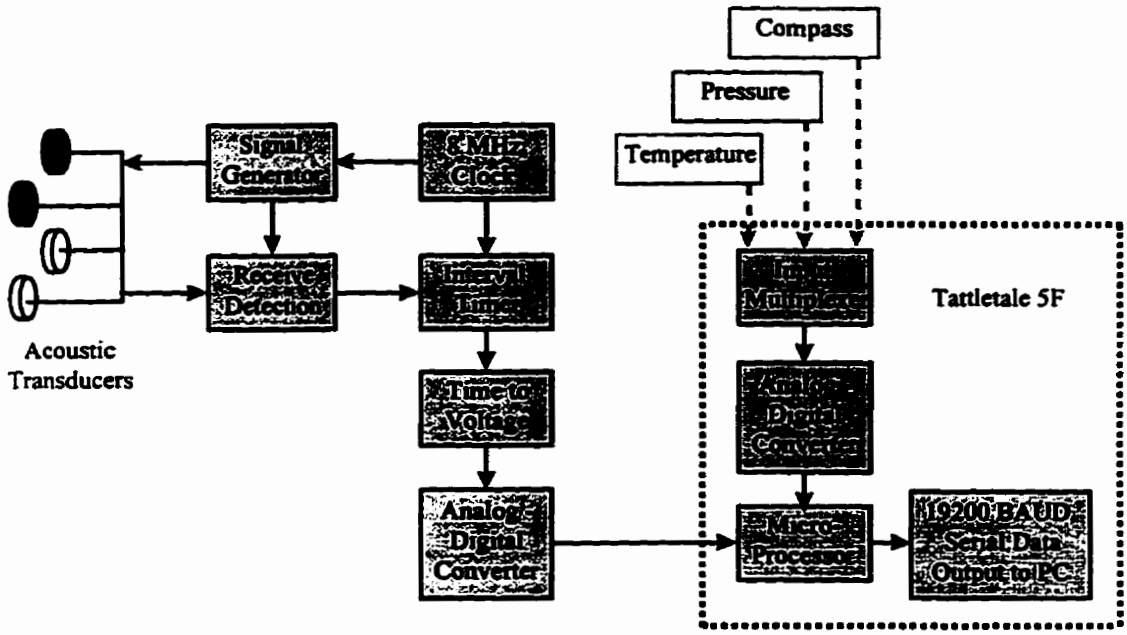

Figure 4.11 Schematic of VDV electronics (adopted from Trivett *et al.*, 1995).

CHAPTER 5
POST-PROCESSING OF DATA

Figure 5.1 illustrates the data collection components and the general data processing steps used in testing. Three independent systems were run in parallel: 1) the reference discharge measurement; 2) the acoustic velocity measurement system; and 3) the position control system. Post-processing of the reference discharge and acoustic velocity measurement systems was performed using Matlab script files. Appendix C contains representative files used for the various testing sequences.

5.1 REFERENCE DISCHARGE

The MAG flowmeter was calibrated volumetrically before testing the ADM technique (Appendix D). Therefore, the first step of processing was to apply the calibration

$$Q_{ref} = 8.694 + 1.106\, Q_{mraw}, \tag{5.1}$$

where Q_{ref} = MAG reference discharge [l/s], and
Q_{mraw} = MAG raw discharge measurement [l/s].

Figure 5.2 illustrates a typical time record of calibrated, non-filtered MAG meter output. Understandably, the variance of the data was high since the meter is designed to calculate discharge based on a single velocity measurement of the turbulent flow within the pipe. The actual variability of the true discharge was considerably less. Also evident in the figure are a few flow measurements that were much lower than the average discharge. These anomalies were likely a result of air entrainment (MSR, 1992). Air bubbles attach to the sensor head of the meter and break the conductive circuit, resulting in a corrupted velocity measurement. To minimize the influence of air entrainment: 1) the MAG meter was installed on the bottom of the supply pipe; and 2) flow returning to the sump was

redirected to reduce the turbulence and air entrainment in the proximity of the pump intakes, however occasional 'drop-outs' were still observed. To circumvent this problem, outlier measurements were removed with a simple iterative routine (Appendix C). The measurement with the greatest deviation from the mean was identified as an outlier and removed. The mean and standard deviation of the remaining data was re-calculated. This process was repeated until the revised standard deviation was lower than a pre-defined threshold value (arbitrarily defined to be 20 l/s). The reference discharge was then calculated as the mean of the remaining calibrated values. Normal operation of this meter uses a filtering routine, programmed within the MAG computer, to yield very stable discharge measurements. However, this function was bypassed in the form of post-processing.

5.2 VELOCITY AND DISCHARGE MEASUREMENT

Using Matlab script files (Appendix C), the velocity data was post-processed to: 1) segment the data with respect to the synchronized positioning of the transducers; 2) apply a revised calibration of the velocity data (outlined in Appendix D) to re-calculate the pathline velocity; 3) to resolve the chordal average normal velocity component from the pathline velocity measurements; 4) identify and remove erroneous velocity data from the data set; and 5) calculate the ADM measured discharge.

5.2.1 Synchronization of Positioning and Velocity Measurement Systems

Since the position control and acoustic instrumentation were run independently, a stopwatch was used to synchronize position and velocity measurements. The traverses were programmed to display a message to 'begin timing' (see Appendix B). A 10 second pause was programmed prior to commencing the traverse. Within this window, the logging of acoustic data was started and the timing instantaneously stopped. Knowing

the lag time between when the logging of the VDV data commenced and when the traverse began, the appropriate number of 'non-traverse' velocity measurements were removed from the record. Clearly, the direct approach would have been to simply execute the traverse and log the data at the same time, however the two systems were separated by approximately 5 m to reduce the amount of electrical interference between the systems.

Discrete velocity measurements were obtained for GL integration of the velocity profiles. The carriage was lowered to the specific location within the intake, paused for 2 minutes and then lowered to the next programmed location. Throughout the traverse, only one acoustic velocity measurement record was logged. As such, knowing the traversing time between discrete samples and the sampling rate, post-processing was used to extract the two minute blocks of data from the base record. Separate Matlab script files were created for each GL sampling strategy (*e.g.*, 10 level, 8 level, *etc.*); Appendix C contains some example script files.

5.2.2 Pathline Velocity

Pathline velocity was measured by determining the transit-times of an upstream traveling pulse (t_u) and of downstream traveling acoustic pulses (t_d). Equation 5.2, derived as equation 3.3 in Section 3.3.1, can be solved for the pathline water velocity.

$$V_p = \frac{(c^2 + V_p^2)}{2L}(t_u - t_d) \tag{5.2}$$

Eliminating the V_p^2 term results in a simpler solution for V_p, *i.e.*,

$$V_p \cong \frac{c^2}{2L}(t_u - t_d). \tag{5.3}$$

The fractional error of this simplification is on the order of V_p^2/c^2. Assuming typical values for V_p and c, this error is on the order of only 10^{-6}. The speed of sound, c, is calculated using

$$c = \frac{2L}{t_u + t_d}. \tag{5.4}$$

It is important to note that assuming a value for the speed of sound in water would have significantly compromised the accuracy of the velocity measurement as this value is squared in the calculation. The speed of sound in water is dependent on temperature, pressure and salinity. Clay and Medwin (1977) provide an empirical relationship for the speed of sound in water

$$\begin{aligned} c_{emp} &= 1449.2 + 4.6T - 0.055T^2 + 0.00029T^3 \\ &\quad + (1.34 - 0.010T)(S - 35) + 0.016z \end{aligned}, \tag{5.5}$$

where c_{emp} = empirical estimate of the speed of sound in water [m/s],
T = temperature [°C],
S = salinity [ppt], and
z = depth [m].

For laboratory testing, temperature was most influential on sound speeds with salinity, S, being zero, and the depth of water approximated as half of the total depth. Equation (5.5) was used for comparison with measured c values.

Two digital outputs were provided by the VDV package for each transducer pair, one proportional to the travel time difference for calculation of V_p, and the second proportional to the sum of travel times used to calculate c. Table 5.1 summarizes the range in digital output and typical corresponding pathline water velocities and sound speeds.

Table 5.1 Digital VDV output and velocity measurement resolution.

Data	*Range in Digital Output [counts]*	*Corresponding Range in Measurement [m/s]**	*Resolution [m/s]**
pathline velocity**	± 4096	± 7.95	0.0019
speed of sound	0 - 8190	1119.5 - 1681.4	0.08
* calculated based on pathlengths of 1.17 m ** calculated based on a sound speed of 1480 m/s			

Appendix D outlines the calibration of the VDV system. The calibration revealed that an adjustment of the instrument zero offset was required. Also, the slew rate, a time constant applied to the electronics, was re-calibrated. These two calibrations were applied to the raw VDV output to determine the measured pathline velocity.

5.2.3 Normal Velocity Component

To determine the normal velocity component of the flow from pathline velocities, the data was transformed using

$$V_{n,P}^{i} = \frac{V_{p,P}^{i}}{\cos\theta_P}, \tag{5.6}$$

where $V_{n,P}^{i}$ = i^{th} normal velocity measurement for path P,

$V_{p,P}^{i}$ = i^{th} pathline velocity measurement for path P,

θ_P = path angle to normal flow, and

P = acoustic path (either X or Y).

5.2.4 Removal of Erroneous Velocity Measurements

Following testing in the intake structure, it was evident that the acoustic system was producing some velocity measurements significantly different from the true values. Fortunately, erroneous data was easily identified as values deviated from the expected in a systematic manner. Figure 5.3 illustrates this observation, where the correct velocity

measurements are in the +15 cm/s to +30 cm/s range. Other values deviate from the expected by approximately ±45 cm/s or more, resulting in 'lanes' of erroneous velocity measurements.

After considerable consultation with Focal Technologies, two possible explanations for the 'laned' data were derived: 1) echoing off the plywood intake structure; and 2) severe signal attenuation due to entrained air or suspended solids. The high air content plywood boundaries act as an air-water interface, which is a strong reflector of acoustic energy. In the case of the erroneous data, a reflected pulse is detected by a transducer. The intake geometry consisted of linear joints separated by a consistent distance from each transducer (with depth); thus, it is reasonable to expect that echoes would result in consistent errors (*i.e.*, lanes).

A number of measures were taken to reduce the echoing problem. First, the transducer faces were repositioned further out of the slots, *i.e.*, into the main flow. This reduced the susceptibility of detecting side lobe echoes off the nearest plywood edge of the slots (refer to Figure 4.3). Secondly, 75 mm PVC pipe was cut in half longitudinally and inserted behind the transducers to remove corner reflectors; this was intended to disperse any pulses that passed by the receiving transducer. Black rubber is a good absorber of acoustic energy because of its chemical makeup. Strips of rubber were used to line the slots behind the transducers, however this measure did not result in any noticeable improvement and was later removed.

In addition to spreading loss of an acoustic pulse, the signal strength can be attenuated and distorted by silt, solids, entrained air, marine life or fouling (Lowell and Hirschfeld, 1979). This effect can be so severe that the signal is weakened to the point that the receive detector misses the desired point on the signal waveform. For the configuration tested, the resulting timing shift could be 500 nanoseconds or one half or one quarter of this, depending on the sense of the pulse. This corresponds well with the constant lane separations observed in the data. As discussed in Section 5.1, attempts were made to reduce the air entrainment, however it was not completely eliminated. The close

proximity of the metering section to the supply pipe provided little distance for the air bubbles to dissipate.

It is important to acknowledge that signal attenuation is a very real problem in underwater acoustics. For field applications, it is essential that signal recognition circuitry be incorporated into the detection system to identify missed pulses and avoid severe velocity measurement errors (IEC, 1991; Lowell and Hirschfeld, 1979).

For laboratory testing, only a simple routine was required to remove the erroneous data because these values were significantly different from reasonable velocities. Within Matlab script, a search was performed to find the indices of velocity data that fell within a pre-defined window (*e.g.*, ±20 cm/s) around an expected average normal velocity (EANV). For continuous traverses the EANV was easily calculated by dividing the reference discharge by the total intake area. A more involved procedure was used for GL sampling strategies as complicated profiles resulted in individual point velocities that varied significantly from the overall average. Indexed by location within the intake, appropriate EANVs were extracted from an ASCII text file containing 100 continuous traverse velocities. This file was created prior to processing the GL data by segmenting a continuous traverse into 100 windows of average velocity, each representing 1 cm of the traverse. Thus, for each GL ordinate, an expected velocity was referenced and the 'laned' data was removed from the record. For the various flowrates and sampling strategies tested, approximately 80 % or more of the data observed was good, the remaining 'laned' data was removed.

5.2.5 Discharge Calculation

Continuous Sampling (undisturbed flow)

Discharge calculation for continuous traverse tests was relatively simple. Of the non-laned data set, the records of normal velocities obtained from the X and Y paths were

averaged separately. These two values were then averaged to reduce the cross-flow error. Equation (5.7) summarizes the calculation of discharge for continuous traverses.

$$Q_{CTR} \cong \frac{1}{2}\left(\frac{\sum_{1}^{n_X} V_{n,X}^{i}}{n_X} + \frac{\sum_{1}^{n_Y} V_{n,Y}^{i}}{n_Y}\right) A \qquad (5.7)$$

where Q_{CTR} = discharge measurement using CTR,

$V_{n,X}^{i}$, $V_{n,Y}^{i}$ = i^{th} normal velocity components from X, Y transducer pairs,

n_X, n_Y = number of normal velocity measurements from X, Y transducer pairs, and

A = area of the metering section.

Continuous Sampling (disturbed flow)

Equation (5.7) was used for the continuous traverse discharge calculations under ideal flow conditions (*i.e.*, undisturbed). However, complicating the flow profile by introducing disturbances in the intake revealed that the occurrence of 'laned' velocity measurements was non-random. This was likely due to the higher concentration of entrained air proximal to the disturbances. Since the velocities near these disturbances were generally lower than average and laned data was removed from the data set, less low velocity measurements were included in the discharge calculation. This in turn, yielded discharge measurements that were biased slightly high (*i.e.*, 1-2 %). To circumvent this problem, the metering section was divided into a large number of 'windows', depending on the record length, and individual averages were calculated for each window. The record of window values was then averaged to calculate discharge; this calculation is described in equations (5.8) and (5.9).

$$V_{n,P}^{w} = \frac{\sum_{1}^{n_{P,w}} V_{n,P}^{i}}{n_{P,w}} \tag{5.8}$$

where $V_{n,P}^{w}$ = average normal velocity for path P in window w, and

$n_{P,w}$ = number of non-laned velocity measurements for path P in window w.

$$Q_{CTR,w} \cong \frac{1}{2W}\left(\sum_{1}^{W} V_{n,X}^{w} + \sum_{1}^{W} V_{n,Y}^{w}\right) A \tag{5.9}$$

where $Q_{CTR,w}$ = discharge measurement using CTR traverse with window values, and

W = number of windows (100-500).

Discrete Sampling (Gauss-Legendre)

Discharge calculation for the Gauss-Legendre traverses was slightly more involved. The integral of the velocity profile, *v(h)*, was approximated using the Gauss-Legendre method, as recommended in the IEC code (1991) for rectangular conduits. From Section 3.3.2 the approximation is given by

$$W' \int_{h_0}^{h_1} v(h)dh \cong W' \frac{(h_1 - h_0)}{2} \sum_{i=1}^{N} w_i v((h_1 - h_0)x_i + (h_1 - h_0)) = Q_{GL}, \tag{5.10}$$

where Q_{GL} = discharge measurement using the Gauss-Legendre traverse, and

W' = the width of the intake.

The actual dimensions of the intake structure measured to be 0.9985 m high by 1.0013 m wide, thus equation (5.10) took the form

$$Q_{GL} = 0.4999 \sum_{i=1}^{N} w_i v(0.49925 x_i + 0.49925) . \tag{5.11}$$

To evaluate $v(h_j)$, the average normal velocity over the sampling duration was determined from the normal velocities measured using the X and Y pathline velocities as described by

$$v(x_i) \cong \frac{1}{2}\left(\frac{\sum_{1}^{n_{X,i}} V^{j}_{n,X,i}}{n_{X,i}} + \frac{\sum_{1}^{n_{Y,i}} V^{j}_{n,Y,i}}{n_{Y,i}} \right) . \tag{5.12}$$

A range of GL sampling strategies from N of 2 to 12 were evaluated over the course of testing. The standardized coordinates, x_i, and corresponding weights, w_i, are tabulated in Appendix A.

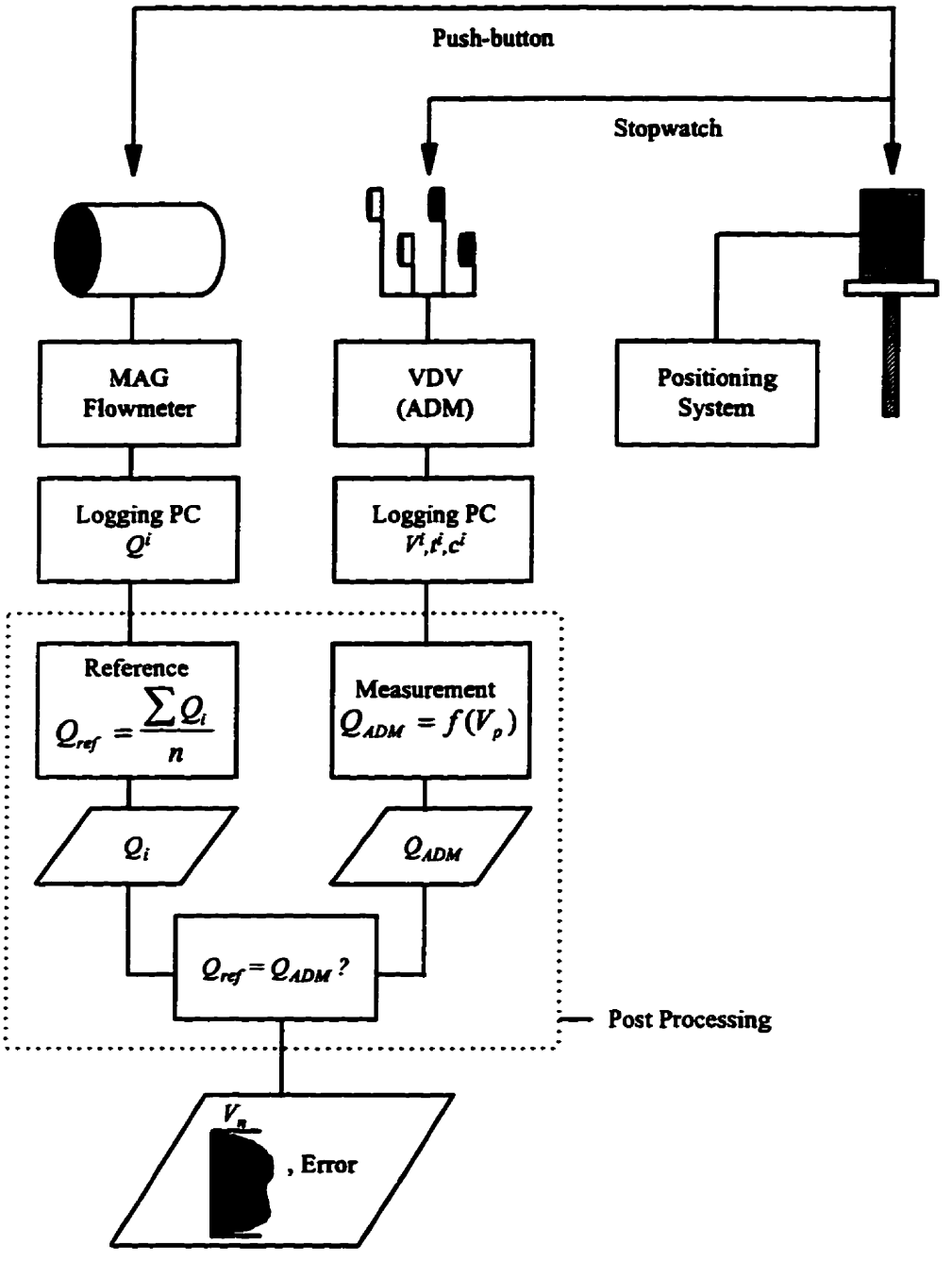

Figure 5.1 Data collection and processing.

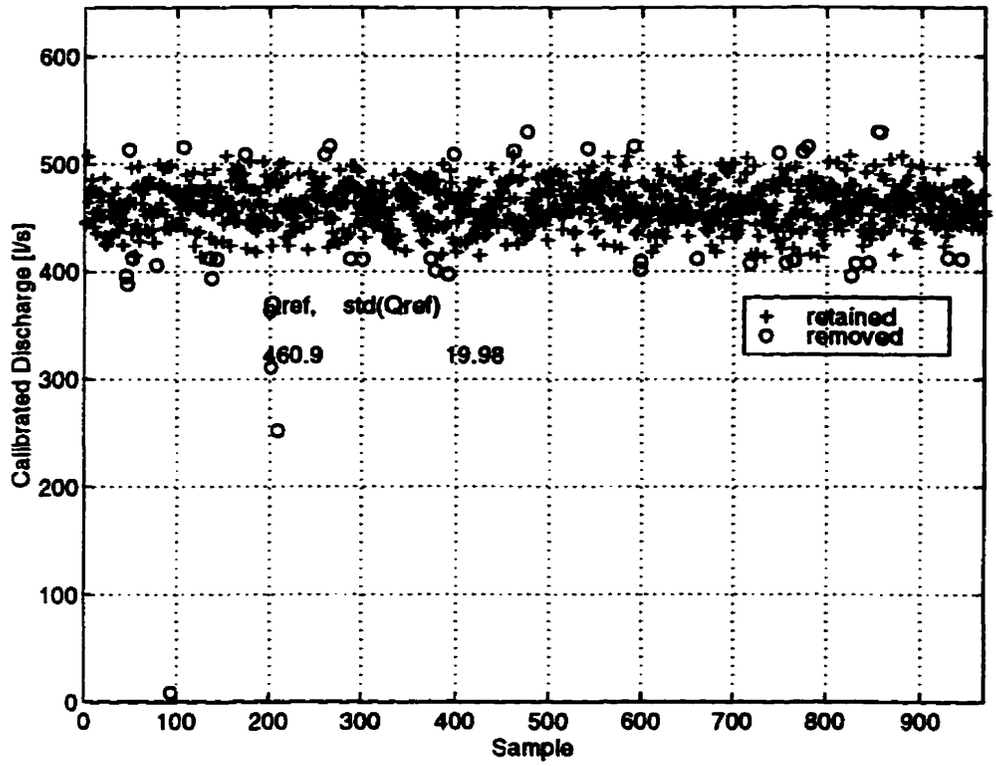

Figure 5.2 Time record of calibrated, non-filtered MAG meter output.

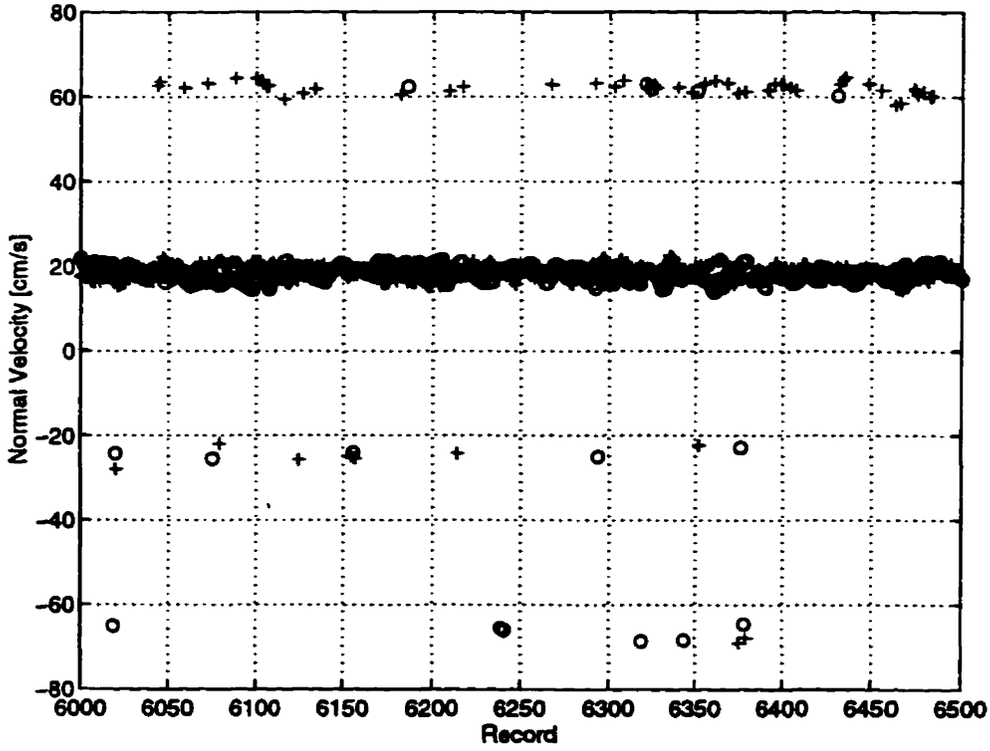

Figure 5.3 Time record of velocity measurements including 'laned' data.

CHAPTER 6
ANALYSIS AND DISCUSSION OF RESULTS

6.1 EVALUATION OF VELOCITY PROFILE STABILITY

The inherent assumption employed when traversing techniques are used is stability of the velocity profile. For example, in the case of a discrete velocity measurement strategy it is assumed that the true mean of the velocity at the measuring point is captured within the sampling duration. The extreme case of this assumption is exercised when a continuous traverse is performed as the instrumentation is not stopped to obtain an average velocity at each location; the assumption is the profile is stationary. Clearly, even under favorable conditions this ideal never exists. However, the tradeoff with a continuous traverse is more points are sampled across the profile.

Two sources of velocity profile variability exist: 1) the random turbulent fluctuations in velocity at some particular location on the profile; and 2) the overall variability of flowrate with time due to headwater fluctuations or surging of the unit. Hypothetically, if the limit of an instantaneous traverse using an infinite sampling rate was used, a true 'snap-shot' of the velocity profile would be sampled and an exact *instantaneous* discharge measurement would be obtained. However, the temporal variability of discharge would not be captured by performing such a traverse. Slower traverse rates would capture the overall variability of discharge. The optimal traverse would be just long enough to capture the variability of the discharge and adequately sample the individual velocities such that the turbulent components average to zero.

To assess the stability of the velocity profile, the acoustic transducers were positioned at a fixed location within the metering area and 15 minutes of velocity data was logged. The time series was segmented into successively smaller durations, from one complete record to 100 segments of 9 seconds of data. For each time segment the average normal velocity was calculated using equation (6.1); because both X and Y pathline velocities were

averaged, low frequency variation of the net horizontal flow direction was eliminated, *i.e.*,

$$\overline{V}_{n,s} = \frac{1}{2}\left(\frac{\sum_{1}^{n_{X,s}} V^{i}_{n,X,s}}{n_{X,s}} + \frac{\sum_{1}^{n_{Y,s}} V^{i}_{n,Y,s}}{n_{Y,s}} \right), \tag{6.1}$$

where $\overline{V}_{n,s}$ = mean normal velocity for segment s, and

s = segment of time series.

The temporal variability of the normal velocity was evaluated by calculating the difference between the maximum and minimum mean normal velocities for all segments of the same duration. Figure 6.1 illustrates the results obtained from a test run at 185.8 l/s. As expected, the difference between the maximum and minimum segment averages increased with a reduction in segment length. The deviation reached a maximum of 3.4 cm/s or 19.6 % of the mean when the record was divided into 9 second segments. From the figure it is apparent that 2 minute averages deviated by as much as 4 % of the mean. This is troubling, as in field practice two minute averages are considered sufficient to obtain representative velocity samples; performance testing codes (ASME, 1992; IEC, 1991) recommend this duration as a minimum for discrete sampling techniques. This preliminary test suggested that the velocity profile obtained in the lab was overly unstable, and was not representative of field conditions.

The variability was, for the most part, due to upstream conditions. In particular, the water supply was provided through a straight drop pipe, without a diffuser, and there was only a short flow development distance from the flow supply pipe to the discharge metering section. To improve the upstream conditions, two layers of plastic coated pig hair filter media were attached to the upstream face of the flow straightener. The filter served to back up the water and force the flow to better distribute prior to entering the straightener.

The stability of the normal velocity profile was re-evaluated using the same analysis. Figure 6.2 illustrates the results obtained at a discharge of 286.0 l/s. Clearly, the low frequency variability of the normal velocity was dramatically reduced. Segmenting the data into 9 second durations, resulted in a deviation between the maximum and minimum average of 1.8 cm/s or 6.6 % of the mean. For this record the maximum deviation between 2 minute averages was approximately 0.2 cm/s or 0.8 % of the mean; this was a dramatic improvement over the deviation of 4 % observed before the filter media was added. Recognizing that the stability of the profile is dependent on velocity, the same test was performed for a range of discharges. Figure 6.3 illustrates the results obtained from all the stability tests. Again, all tests performed after the filter media was installed revealed more stable profiles. Understandably, the lower flow (121.7 l/s) segment averages were more variable since the frequency of vortex shedding is lowered as the water velocity is reduced. Therefore, a longer sampling period is required to realize the average water velocity. The maximum deviation for 2 minute samples was between 0.8 % and 1.7 %; based on these results, a 2 minute duration was considered to be acceptable for the discrete sampling tests (*i.e.*, Gauss-Legendre sampling strategies).

6.2 ASSESSMENT OF SAMPLING STRATEGIES

To assess the accuracy and repeatability of various sampling strategies, 103 tests were performed over a range of 6 discharges (approximately 160, 250, 275, 350, 400 and 460 l/s) . Continuous traverses of 20, 12, 8, 6, 4 and 3 minutes and 12, 10, 8, 6, 4, and 2 level GL strategies were tested. The traversing rate of the continuous profiles was limited by the capacity of the positioning system. The upper limit of the range of GL strategies was limited due to the proximity of the acoustic pathlines to the flow boundaries. A disproportionately high number of 'laned' velocity measurements were observed for the first and last level of higher order GL strategies. Thus, testing was limited to a maximum of 12 sampling levels. Appendix E contains a detailed list of the results for each test.

Table 6.1 summarizes the testing program, listing the number of flowrates that were used to evaluate each strategy and the total number of tests for each strategy. Not all sampling strategies were tested to the same degree for a number of reasons: 1) as the testing progressed, the number of runs for each strategy at a given discharge was reduced because the repeatability of the results was quite good; 2) some strategies were discontinued early in the testing program due to the relatively poor accuracy levels (*e.g.*, GL2); and 3) the poor accuracy obtained from lower order GL strategies prompted testing of higher level GL strategies.

Table 6.1 Summary of tests performed for undisturbed flow conditions.

Sampling Strategy	*No. of Flowrates Tested*	*No. of tests*
CTR20	6	11
CTR12	2	4
CTR8	5	9
CTR6	6	16
CTR4	5	12
CTR3	1	3
GL12	5	10
GL10	5	10
GL8	6	11
GL6	2	4
GL4	2	6
GL2	2	7

Figure 6.4 illustrates a typical velocity profile obtained for a continuous traverse. This particular data was obtained from a 20 minute continuous traverse at a reference discharge of 388.1 l/s. For each transducer pair, 9676 velocity measurements were obtained. After removing the echoed or corrupted measurements, 8589 (89 %) and 8493 (88 %) of the data remained for the X and Y paths, respectively. It was quite clear from the figure that, with no obstructions to the flow, the profile was quite uniform. However, some 'weaving' of the X and Y velocities indicated an overall helicoidal flow existed; without a crossed path configuration, this would not have been detected and a cross-flow error would have resulted.

Figure 6.5 illustrates velocity profiles for a range of flowrates. For illustration purposes, the profiles were smoothed using 100, 1 cm window averages of twenty minute continuous traverses. It is clear from the figure that the velocity profile was quite uniform and consistent in shape over the discharges tested. Velocities at the top half of the intake slightly exceeded the velocities observed towards the floor of the structure; this is likely a result of the vertical convergence of the ceiling shortly upstream of the metering section. Also noteworthy is the fact that, although the overall smoothed profiles were quite uniform, small features (*i.e.*, peaks and troughs) were observed.

Discharge measurement error was defined as

$$Error = \frac{(Q_{measured} - Q_{ref})}{Q_{ref}} \times 100\,\%, \tag{6.2}$$

where $Q_{measured}$ is the measured discharge (using either CTR or GL sampling strategies). For each sampling strategy, across all flowrates tested, the average absolute error (AAE) was calculated to assess the relative performance of sampling strategies. It is important to recognize, however, that this measure is based on a limited sample (from 3 to 16 tests). In addition, because not all sampling strategies were tested for each discharge, the AAE values are somewhat biased to the corresponding flowrates.

Table 6.2 Summary of results for undisturbed flow conditions.

Sampling Strategy	*Average Absolute Value of Discharge Error [%]*
CTR20	1.18
CTR12	1.52
CTR8	0.68
CTR6	1.36
CTR4	1.37
CTR3	2.59
GL12	0.56
GL10	0.74
GL8	0.94
GL6	1.31
GL4	2.14
GL2	2.77

Table 6.2 provides a summary of performance of the various sampling strategies and Figure 6.6 illustrates the results for the complete set of tests performed. It is apparent from the figure, that there was considerable variability in the discharge measurement errors, especially for the CTR tests and the lower order (*i.e.*, N=2) GL tests. This variability, in combination with the fact that only a limited number of tests were performed for each sampling strategy, precludes a statistical identification of the true optimal sampling strategy. However, some comparative observations can be made. Excluding the CTR3 sampling strategy, which was subject to a very limited number of tests, the data suggested that no significant improvement was gained by using long traverses (CTR 20) relative to quicker traverses. The AAE of the CTR20 results (1.18 %) was only slightly less than that of the CTR4 results (1.37 %). In addition, the repeatability of the discharge measurements was not compromised by using faster traverse rates. This suggests that the upper limit of the traversing rate was not attained.

With regards to the GL sampling strategies, a more defined relationship was evident. The results asymptotically approach the zero error axis with increasing sampling levels, N. This is expected since the $(2N\text{-}1)^{th}$ degree Legendre polynomial better represents the

subtle detail of the true velocity profile as N increases. The AAE ranged from 0.56 % to 2.77 % for the GL12 and GL 2 sampling strategies, respectively.

An important observation regarding the repeatability of the discharge measurement error can be made from Figure 6.6. Although the variability of the results was generally quite high for each sampling strategy over all the discharges tested, the agreement between consecutive tests at the same flowrate was quite good. For example, the maximum range in error calculated for the CTR4 tests for each flowrate was 0.60 % compared to the range in errors of -1.68 % to 2.81 % over all the flows tested. Further discussion of the repeatability of measurement is possible by looking at data obtained for one flowrate (and one test day). Table 6.3 lists the testing results obtained at a flowrate of approximately 400 l/s.

Table 6.3 Test results obtained for 400 l/s flowrate (undisturbed).

Trial	*Sampling Strategy*	*Reference Discharge [l/s]*	*Measured Discharge [l/s]*	*Discharge Error [%]*	*Empirical Sound Spd. [m/s]*	*Measured Sound Spd. [m/s]*	*Sound Spd. Error [%]*
a	CTR20	388.2	396.4	2.13	1476.4	1481.3	+0.33
b	CTR20	391.1	396.3	1.33	1477.3	1481.3	+0.27
c	CTR12	389.5	396.4	1.79	1478.1	1481.3	+0.22
d	CTR12	390.3	395.7	1.40	1479.0	1480.7	+0.12
e	CTR12	392.1	394.9	0.70	1479.0	1481.1	+0.14
f	CTR6	390.7	396.4	1.45	1479.9	1481.6	+0.11
g	CTR6	390.8	395.0	1.06	1479.9	1480.8	+0.06
h	CTR6	394.4	395.5	0.27	1480.8	1481.1	+0.02
i	GL12	392.8	394.6	0.45	1481.6	1481.8	+0.01
j	GL12	392.8	395.1	0.59	1482.6	1483.6	+0.07
k	GL10	393.7	396.8	0.77	1485.0	1487.1	+0.14
l	GL10	393.9	396.6	0.70	1485.9	1488.2	+0.16
m	GL8	395.5	396.2	0.18	1486.7	1491.7	+0.34
n	GL8	395.1	396.2	0.27	1486.7	1491.4	+0.32
o	GL6	396.2	398.9	0.69	1487.5	1492.3	+0.32
p	GL6	395.5	397.9	0.61	1488.3	1492.6	+0.29
q	GL4	395.3	400.4	1.30	1488.3	1492.2	+0.26
r	GL4	398.3	401.9	0.90	1489.1	1492.3	+0.21
s	GL2	395.2	399.5	1.07	1490.0	1492.6	+0.18
t	GL2	395.7	399.1	0.86	1490.0	1491.7	+0.12
u	GL2	397.6	398.8	0.32	1490.0	1491.9	+0.13

For the duration of the entire test sequence, approximately 7 hours, the measured discharge varied between 394.6 to 401.9 l/s. The water temperature increase over this duration (approximately 4.5 °C) likely resulted in a subtle decrease of frictional losses within the flow supply system, thus increasing the system output.

Each subset of flow measurements for the specific strategy tested were very repeatable; for example the CTR20 changed by approximately 0.25 %. The deviation from the reference, however, changed from 2.13 % to 1.33 %. Similarly, the CTR6 discharge measurements were within 1.4 l/s or 0.35 % for the 3 tests performed but the reference discharge varied between 390.7 and 394.4 or 0.94%. These occurrences suggest that the repeatability of the ADM method is similar, if not better than the reference discharge measurement. The GL flow measurements were also very repeatable. In these cases, the errors were more repeatable than the CTR runs; this was likely because the longer test durations resulted in more representative reference discharge measurements.

In general, the results in Table 6.3 indicated two distinct biases: 1) all the discharge errors were positive and 2) although the speed of sound measurements were very close to the empirically calculated values, a negative error was consistent. Biasing of the results occurred for all discharges, although the sign and magnitude of the errors were not consistent and a direct relationship with discharge did not exist. Figures 6.7 and 6.8 illustrate this observation. The distinct grouping of the data also suggested that a systematic error was present within a testing sequence (*i.e.*, a single flow rate), but this error changed between sequences. All the sequences were performed on separate days excluding the 164 l/s and 255 l/s flowrates which were tested over a 9.5 hour period. The data suggests that an electronic error was biasing either the reference or the ADM systems, or both. The bias of the speed of sound values, although not significant did suggest that the VDV instrument was biased. A change in the zero offset of the VDV electronics upon restarting for each discharge sequence was suspected as the cause for this bias.

To verify calibration of the VDV instrumentation, a linear regression analysis was performed on the complete set of data obtained from the sampling strategy investigation. Figure 6.9 illustrates the resulting fit. The slope of the regression line was nearly identical to the value calculated from the calibrated results (1.0041 versus 1.0039). The high coefficient of determination (r^2 = 0.9986) confirmed that a linear response still existed.

From this series of sampling strategy tests, a number of observations can be made:

1) Increasingly accurate discharge measurements were obtained as the number of Gauss-Legendre sampling levels was increased. Gauss-Legendre tests of *N* equal 8 or more resulted in an accuracy better than all of the continuous traverses, with the exception of the 8 minute CTR. For uniform velocity profiles, high order GL sampling strategies were generally superior to continuous traversing. These results agreed with previous studies (*e.g.*, Lanning, C. and Ehrhart, R., 1977) that, under favorable flow conditions (*i.e.*, uniform velocity profiles), Gauss sampling techniques are effective and often superior to multiple level or continuous sampling methods. Uniform velocity profiles can be adequately represented by high order polynomials, thus the Gauss integration is quite accurate. Under these flow conditions, the merit of discrete long duration sampling (2 minutes) outweighs the error from not sampling the entire velocity profile.

2) Discharge measurements obtained from both continuous and GL traverses were quite repeatable when considering each flowrate separately; the average variability was only 0.16 %. This indicates that, even though there was considerable variability in the velocity profile, as indicated in Section 6.1, discharges based on 2 minute sampling durations or continuous traverses as quick as 4 minutes were very repeatable.

3) The bias of errors within each discharge measurement sequence suggested that a systematic error was occurring, but the value of this error was changing from one

flowrate to the next. This error was not directly related to discharge. It is possible that the zero offset of the VDV or MAG meter electronics changed when the systems were restarted (*i.e.*, warmed-up) prior to each discharge measurement sequence.

4) The speed of sound measurements were in excellent agreement with empirically predicted values.

5) The calibration of the VDV system, as outlined in Appendix D, was verified.

6.3 ASSESSMENT OF THE ADM TECHNIQUE UNDER NON-IDEAL FLOW CONDITIONS

The proposed ADM technique is to be applied at low-head plants where complex velocity profiles typically exist. For this reason, a range of flow disturbances were introduced within the intake to assess the performance of the technique under non-ideal conditions.

6.3.1 Disturbance 1 (D1): Horizontal 75 mm PVC and Filter Media Flow Obstructions

To create a complex velocity profile, horizontal flow obstructions were installed within the intake just upstream of the metering area. Although the dimensions of the obstructions were not scaled from a typical obstruction that would exist at a hydro plant (*e.g.*, trash rack beam), the complex velocity profile that resulted was used to address the integration accuracy of the various sampling strategies. Figure 6.10 is a photograph of D1. Expanded metal (25 mm) was attached to the walls of the intake, 320 mm upstream of the first set of transducers. A 180 mm high by 60 mm deep bat of pig hair filter media was fixed to the upper piece of expanded metal centered a distance of 160 mm from the ceiling of the intake. A second bat of pig hair, 135 mm x 100 mm, was attached 290 mm on center from the intake floor. D1 also included a 75 mm PVC tube 340 mm from the ceiling of the intake.

Figure 6.11 illustrates the velocity profile measured using an 20 minute continuous traverse for a 345.1 l/s flowrate. The added disturbances had a dramatic effect on the velocity profile; this can be seen by comparison with undisturbed profiles (*e.g.*, Figure 6.4). It is quite clear that the position of the flow obstructions corresponded directly with the velocity deficits observed in the traverse. Figure 6.11 also illustrates that the profile approached reverse flow behind the upper flow obstruction.

A range of sampling strategies were tested for the D1 flow condition at three discharge levels (approximately 250, 350 and 460 l/s). Table 6.4 includes summary data for this sequence of testing and Appendix E contains a more detailed table of the D1 test results. For the disturbed flow conditions, the highest level of GL sampling was 10. The GL12 traverse resulted in a disproportionately high number of 'laned' data at the first sampling level (upper boundary). This was likely due to a high concentration of entrained air that collected behind the upper obstructions and then floated to the upper boundary of the intake.

Table 6.4 Summary of testing and results for D1 flow condition.

Sampling Strategy	*Total Sampling Time [min]**	*No. of Flowrates Tested*	*Number of Tests*	*Average Absolute Value of Discharge Error [%]*
CTR20	20	3	8	0.70
CTR12	12	3	7	0.74
CTR8	8	3	7	0.80
CTR6	6	3	7	1.50
CTR4	4	3	7	0.70
GL10	20	3	7	1.03
GL8	16	3	7	1.84
GL6	12	3	7	4.26
GL4	8	3	5	8.03
GL2	4	1	3	38.29
* does not include positioning time required for GL tests (2-3 min)				

Figure 6.12 illustrates the discharge measurement errors calculated for the D1 test condition; to maintain a reasonable scale, 4 of 5 GL4 tests were not included in the figure (approximate errors of -10 %) and all of the GL2 results were not plotted. For this testing

series, the range in errors was exceptionally larger than for uniform flow conditions; the minimum error was 0.01 % for a CTR8 test at 460.3 l/s and the maximum error was -39.69 % for a GL2 test at 461.8 l/s. In general, the CTR sampling strategies produced superior results. The average absolute value of discharge error was around 1 % for the continuous runs. Again, no appreciable improvement in accuracy was observed by performing slower traverses.

For GL tests, the accuracy decreased as the number of sampling levels, N, was reduced. This is best explained using Figures 6.13 and 6.14. Both figures include a the same continuous profile, generated by averaging the normal velocities for 100, 1 cm windows. Figure 6.13 includes the 4 measured normal velocities for a subsequent GL4 test; these samples lie close to the continuous traverse data, indicating that the velocity profile was stable over long durations. Also included in the figure is a 7^{th} order polynomial fit to the 100 data points of the continuous traverse. By inspection, the polynomial fit does not trace the actual profile very well. However, the discharge calculated using this polynomial, by simply averaging 1000 equally spaced points on the polynomial, agrees with the integral of the continuous data to within less than 1.0×10^{-14} l/s. Tests results revealed that the GL4 integration was in error by almost -10%. This result appears to be contradictory since a four level Gauss-Legendre integration exactly evaluates the integral of a 7^{th} order polynomial. The reason for the discrepancy is that the best fit polynomial does not necessarily pass through the true profile at the GL ordinates, x_i. The GLN traversing strategy evaluates the integral of the $(2N\text{-}1)^{th}$ order polynomials *that pass through the sampled points*; polynomials passing through these points are not necessarily the best fit to the entire profile. Figure 6.14 further illustrates this point. In this case, a 19^{th} order polynomial was fit to the 100 point profile. Again, the agreement between the integral of the polynomial and the profile was excellent. In this case, the higher order polynomial closely traced the actual profile, even the smaller features. The GL10 samples lie both on the true profile and in close proximity to the best fit polynomial. Consequently, accurate discharge measurements (*i.e.*, AAE of 1.03 %) were obtained using the GL10 traverses.

Discharge measurement errors were quite repeatable at each flow rate tested, but errors ranged considerably from one flow rate to the next. Similar to results from prior tests, this suggested that a systematic offset error occurred but changed as each new testing sequence was commenced. Referring to Figure 6.12 the considerable difference between two separate test sequences at 462 l/s (greater than 2 %, on average) confirms that the bias was not flow dependent, rather changed from test sequence to test sequence.

Figure 6.15 is a plot of the measurement errors with respect to flowrate. To maintain a reasonable scale, the errors for GL2 runs were not plotted. Looking at the continuous traverse data, a subtle bias to positive errors can be detected. The average error for all the continuous traverses was calculated as 0.51 %; two possible explanations for this positive bias are: 1) the actual calibration of the ADM electronics is biased high (+0.39 % for the calibration and +0.41 % for the verification); and/or 2) a slight offset error exists. The former explanation is more likely since the high bias is consistent with discharge. If the zero offset was in error consistently, by say 0.1 cm/s, this effect would be less significant at higher discharges.

It is important to highlight the difference in total sampling time between CTR and GL strategies. Keeping in mind that the specific results are directly applicable only to the laboratory conditions tested, the CTR strategies were considerably more efficient. For example, the CTR4 tests, which required 4 minutes of sampling time yielded an average absolute value of error equal to 0.70 %. The 8 level GL tests required 16 minutes of sampling time (not including the time to position the transducers) and the average absolute value of the error was 1.84 %.

Testing the various sampling strategies in D1 conditions yielded interesting results and revealed some very significant points regarding the accuracy of Gauss sampling strategies applied to unfavorable flow conditions:

1) A $(2N\text{-}1)^{th}$ order polynomial may be fit to a complex velocity profile, and yield an integral very close to the true discharge. However, if the Gauss positioned velocity

samples are not coincident with that best fit polynomial, there is potential for significant systematic error. For complex velocity profiles with numerous inflections, only high order Gauss sampling strategies should be employed.

2) All of the continuous sampling strategies produced repeatable discharge measurements for each testing sequence, however considerable variability in error occurred over the range of flowrates. Similar to the undisturbed test sequence, these results suggested that an offset error had occurred.

3) Considering the time required to carry out the sampling strategies versus the accuracy obtained, the CTR method was considerably more efficient.

4) Comparing the results obtained for undisturbed flow, for both CTR and GL sampling strategies, the repeatability of discharge measurement was similar. The discharge measurement accuracy of the CTR traverses was not compromised in the disturbed flow, however low order GL strategies produced considerable systematic error. For the disturbed flow condition, the merit of sampling the entire velocity profile through continuous traversing outweighed the error resulting from the assumption that the profile is stable.

6.3.2 Disturbance 2 (D2): 4 Horizontal 75 mm PVC Obstructions

To gain understanding of how the ADM technique would perform under complex flow conditions with small scale turbulence (relative to the pathlengths), four 75 mm PVC tubes were installed across the intake 320 mm upstream of the leading transducer faces. D2 is illustrated in Figure 6.16. The upper tube was located 170 mm from the intake ceiling and the second tube was installed a further 170 mm below. The lower tubes were installed at the same distances from the intake floor.

Figure 6.17 illustrates the velocity profile obtained from a CTR20 traverse at 453.1 l/s. Normal velocity profiles from both the X and Y transducer pairs are shown. The

increased level of turbulence, or vortex shedding, behind the cylindrical obstructions was evident in the individual pair profiles. The figure also illustrates that the lower velocity regions directly corresponded with the position of the flow disturbances.

A smaller range of sampling strategies was tested for the D2 flow condition than for the D1 condition. Table 6.5 and Figure 6.18 summarize the results obtained from this sequence of testing. Appendix E contains a more detailed table of the D2 test results.

Table 6.5 Summary of testing and results for D2 flow condition.

Sampling Strategy	*No. of Flowrates Tested*	*Number of Tests*	*Average Absolute Value of Discharge Error [%]*
CTR20	3	3	0.23
CTR4	3	7	0.60
GL10	3	7	0.64
GL4	3	6	1.01

On average, all of the sampling strategies tested for the D2 flow condition produced quite accurate discharge measurements. The CTR20 traverse yielded the lowest average absolute value of discharge error, 0.23%. The GL4 sampling strategy performed much better under D2 conditions than for the previous disturbance; Figure 6.19 illustrates why this is the case. Included in the plot is a 100 window average normal velocity profile derived from a continuos profile, a 7^{th} order polynomial fit to the profile, and the GL4 normal velocity samples. On average, the best fit polynomial is in close proximity to the actual GL sampled velocities, particularly for the intermediate ordinates that are heavily weighted in the summation. Thus, the GL traverse evaluated the integral of a 7^{th} order polynomial that would have properly represented the true velocity profile and an accurate discharge measurement was obtained.

The repeatability of error was similar to the results outlined for previous flow conditions, indicating that the 2 minute duration was sufficient for discrete sampling in the GL tests and that the 4 minute traverse was not too short for sampling the profile and the reference discharge. Figure 6.10 does indicate, however, that the error bias of the GL4 increased as

the flow rate was increased. This suggests that the GL4 was an inadequate sampling strategy for integrating this velocity profile.

Figure 6.20 illustrates the error distribution of the CTR and GL with respect to the three discharges measured. Again, the apparent slight positive bias (average value of 0.39 %) was likely a result of the original calibration. A second contribution to this positive average was the systematic error of the GL4 tests at that increased with flowrate.

6.3.3 Disturbance 3 (D3): 1 Horizontal 150 mm PVC Obstruction

To further evaluate the performance of the ADM technique in unfavorable flow conditions, a 150 mm PVC pipe was installed upstream of the metering section. For disturbance D3, illustrated in Figure 6.21, the pipe was fixed horizontally at the midpoint of the intake. Although the dimensions of the obstruction were not directly scaled to a typical obstruction in the field (*e.g.*, trash-rack beam), the test provided valuable information on the performance of ADM in flows with larger scale turbulence.

Figure 6.22 illustrates the component X and Y profiles for a flowrate of 257.7 l/s. The velocity profile was quite uniform in the undisturbed region with a deficit behind the obstruction. Clearly, the variability of the sampled velocities was higher behind the obstruction.

For the three discharge levels, CTR20, 8 and 4 and GL10, 8 and 4 sampling strategies were evaluated under D3 conditions. The results are summarized in Table 6.6 and Figure 6.23. A detailed table of the D3 test results is contained in Appendix E.

Table 6.6 Summary of testing and results for D3 flow condition.

Sampling Strategy	*No. of Flowrates Tested*	*Number of Tests*	*Average Absolute Value of Discharge Error [%]*
CTR20	2	2	0.34
CTR8	3	6	0.61
CTR4	3	6	0.52
GL10	3	6	0.69
GL8	3	6	0.49
GL4	3	6	4.60

Excluding the 4 level GL tests, the overall accuracy of the ADM technique was quite good. Again the CTR20 resulted in the least average absolute value of discharge error, calculated to be 0.34 %. It was clear that the GL4 strategy was inadequate for this flow condition. The explanation for the poor performance of lower level GL strategies presented for D1 condition is equally applicable to the GL4 strategy in this case.

Figure 6.24 provides similar information as the previous distribution of errors plot for D2. Excluding the GL4 tests, which clearly had a positive systematic error, a slight positive bias was evident (0.51%); this systematic error can primarily be attributed to the slight bias of the original calibration.

The repeatability of the discharge error was good. For all the sampling strategies tested, at each discharge level the range of discharge measurement error was calculated. The average value of this range was calculated to be 0.43 %. The repeatability of error from one test to the next indicated that, although there was significant variability in the velocity profile, particularly at the mid levels, the traverses were sufficiently long to capture this variability. No appreciable improvement in repeatability resulted by increasing the traverse time from a CTR4 to a CTR20. Again, the systematic error of the GL4 changed with flowrate. Opposite to the results of observed for flow disturbance D2, the systematic error was lower for larger discharges. This dependency indicated that the GL4 strategy was inadequate.

Testing of the D3 flow condition strengthened previous observations, for example, the continuous traverses were found to be more efficient than the discrete level GL sampling strategies. This testing sequence also revealed that larger scale vortices perpendicular to the plane of the acoustic paths did not adversely effect the velocity measurements.

6.3.4 Disturbance 4 (D4): 1 Vertical 150 mm PVC Obstruction

A 150 mm PVC pipe was installed vertically upstream of the metering section, as shown in Figure 6.25. The pipe was located in the center of the intake, 320 mm upstream of the metering section. This configuration was tested to address the impact of large scale vortices, rotating in the same plane of the acoustic paths, on the performance of ADM.

Figure 6.26 includes the X and Y velocity measurements at a flow rate of 453.0 l/s. This particular profile was sampled using a CTR4 traverse. As expected, the variability of the normal velocity measurements was extremely high, relative to D3, due to the vortex shedding off the cylinder in the plane of the acoustic paths.

For the three discharge levels, CTR20, 8 and 4 and GL10, 8 and 4 sampling strategies were tested. The results are summarized in Table 6.7 and Figure 6.27. A detailed table of the D4 test results is contained in Appendix E.

Table 6.7 Summary of testing and results for D4 flow condition.

Sampling Strategy	*No. of Flowrates Tested*	*Number of Tests*	*Average Absolute Value of Discharge Error [%]*
CTR20	3	3	2.03
CTR8	3	6	2.22
CTR4	3	6	1.92
GL10	3	6	1.93
GL8	3	6	1.65
GL4	3	6	2.76

The addition of flow disturbance D4 significantly reduced the accuracy of the ADM technique. For the 6 sampling strategies tested, the average error ranged from 1.65 %

(GL8) to 2.75 % (GL4). Figure 6.28 illustrates the distribution of errors with discharge. Two important characteristics of the errors were identified from this plot. First, all of the discharge measurements were biased high, and secondly, the magnitude of error increased with discharge.

Figure 6.29 supports the explanation of the observed errors. The low velocity zone, located downstream of the pipe, likely extended into the velocity metering area, but tapered off further downstream of the obstruction. There are two defensible reasons for the high discharge measurements: 1) the angle of the resultant velocity vector that each transducer pair samples is less than the assumed value for both of the transducer pairs; and 2) the normal velocity profile across the intake (i.e., from wall to wall) changes as the water passes through the metering section. The resultant of the flow on either side of the obstruction is more aligned with the respective acoustic paths in the upstream half of the metering section, serving to increase the travel time differences of the acoustic paths. These 'half flow' resultants straighten as the distance from the obstruction increases; this would reduce the influence on the second acoustic path downstream of the pathline intersection. As a result, averaging the two pathline measured velocities does not reduce the cross flow error. Secondly, if the zone of separation extends into the metering section but tapers before crossing the acoustic pathlines, higher velocities in the sampled portion of the flow net will bias the discharge measurement. These explanations highlight the inherent assumption being employed in ADM: In the horizontal plane, the normal velocity profile is consistent along the depth of the metering section.

Considering the previous explanation for the positive bias in the discharge measurement, it is quite clear why the errors increase with flow rate. As the flow rate increases, the separation zone extends further into the metering section (dimension 'd' in Figure 6.29 increases). Thus, the high velocity zones at either side of the disturbance extend further into the upstream segments of the acoustic pathlines, resulting in higher velocity samples.

Although the accuracy under D4 conditions was relatively low, the repeatability of the discharge measurements was good. For all the sampling strategies tested, at each

discharge level the range of discharge measurement error was calculated. The average value of this range was calculated to be 0.37 %. The repeatability of error from one test to the next indicated that, although there was significant variability in the velocity profile, the traverses were sufficiently long to capture this variability and produce repeatable discharge measurements.

The high variability of the velocity data warranted further analysis and discussion. The variability is best explained using Figure 6.30. As a vortex advects across the acoustic path, the acoustic pulses traveling tangent to the vortex are accelerated in the same direction that the leading edge of the vortex rotates and decelerated if the pulse travels in the opposite direction. For the geometry shown in Figure 6.30 and at stage 1, the average velocity measurement along the chordal path is greater than the time averaged pathline velocity. When the vortex center is coincident with the pathline, the net influence on the pathline velocity is zero (stage 2 in the figure). After the center of the vortex passes the acoustic path, the influence of the vortex on the travel time reverses. The same vortex would have the inverse effect on a the velocity measurement from a crossed acoustic pathline.

The oscillatory effect on the pathline velocities is easily identified by inspecting a short time series of X and Y pathline measurements, as shown in Figure 6.31. This figure contains approximately 30 seconds of data logged while the transducers were stationary, 200 mm above the intake floor at a discharge of approximately 190 l/s. The inverse effect between the two pathline measurements is obvious; the Y time series is virtually a mirror image of the X pathline velocities.

The ability of the acoustic cell to 'see' the vortices prompted a frequency analysis of the data logged for the D4 flow condition. Fifteen minutes of velocity measurements were logged with the transducers held stationary in a flow of approximately 190 l/s. A spectral analysis was performed on velocity data from a single acoustic path (X) to identify the dominant oscillation frequency. Figure 6.32 illustrates the results. The peak of the variance density plot corresponds to a frequency of 0.24 Hz. From Tritton (1977), the

Strouhal number for a cylindrical obstruction at a Reynolds number of 3.2×10^4 is approximately 0.20 (based on experimental results). Equation (6.3) for the Strouhal number, was used to calculate the shedding frequency.

$$St = \frac{n'D}{V}, \tag{6.3}$$

where St = Strouhal number ($\cong 0.20$),

n' = vortex shedding frequency,

D = diameter of the obstruction (0.168 m), and

V = average free stream velocity (0.19 m/s).

The shedding frequency, based on previous experimental data, was calculated to be 0.23 Hz; this is in excellent agreement with the observed value of 0.24 Hz. The spectral analysis confirms that the ADM is quite responsive to large scale vortices that rotate in the same plane as the acoustic paths.

Although the discharge measurement accuracy of the ADM technique was relatively poor for the D4 testing series, these results are likely the most valuable. A number of significant points have been brought to light:

1) ADM, regardless of the sampling strategy used, is susceptible to systematic error when large scale obstructions that are aligned perpendicular to the plane of the acoustic paths are located shortly upstream of the metering section. This is relevant to field situations where the metering plane (*i.e.*, stop-log guides) is only a few meters downstream of the trash-racks. However, if the separation zone of the disturbance is consistent over the *depth* of the metering section, the influence will not be as pronounced. Thus, if the depth of the metering plane is minimized by increasing the pathline angles and/or reducing the path lengths, the profile will be more consistent over the metering section and the error will be reduced.

2) The ADM technique clearly tracked large scale vortices in the test flume. However, the frequency of shedding under laboratory conditions was low (below 0.75 Hz). In field conditions where velocities may approach 10 m/s the shedding frequency may reach or exceed the nyquist frequency; aliasing error may result under these conditions.

3) Under low frequency, large scale vortex shedding conditions, the repeatability of the CTR and GL test results was quite good within each flowrate test sequence.

6.3.5 Disturbance 5 (D5): Downstream Vertical Convergence

A downstream vertical convergence was added to the exit structure of the intake, as shown in Figure 6.33. 105 mm downstream of the trailing transducers, the ceiling of the intake was sloped at 45° down to height of 0.500 m. This modification forced the flow to rapidly converge from the 1 m^2 metering area to a 0.25 m^2 exit over a distance of only 0.50 m. This testing series was undertaken to indirectly evaluate the cosine response of the acoustic cell. As typical low-head intakes converge rapidly in the vertical direction at the stop-log guides, the system would be required to resolve the normal velocity profile under non-parallel flow conditions.

Figure 6.34 is a 100 window average normal velocity profile sampled at a flow rate of 460.7 l/s using a CTR20 traverse. As expected, the normal velocity measurement at the lower stations were greater than those measured towards the top of the intake.

The results of the D5 tests are summarized in Table 6.8 and Figure 6.35. A detailed table of the D5 test results is contained in Appendix E.

Table 6.8 Summary of testing and results for D5 flow condition.

Sampling Strategy	*No. of Flowrates Tested*	*Number of Tests*	*Average Absolute Value of Discharge Error [%]*
CTR20	3	3	2.21
CTR8	3	6	2.03
CTR4	3	6	2.32
GL10	3	6	1.90
GL8	3	6	1.58
GL4	3	6	2.17

The average absolute value of discharge error was quite high relative to the other disturbance scenarios. The results were quite repeatable from one measurement to the next, but the errors varied significantly across flowrates.

The distribution of errors, plotted in Figure 6.36, illustrates two significant results of this testing series: 1) virtually all of the errors are positive; and 2) the positive error increases with discharge. To a degree, this result was expected while observing the individual tests. As previously described, the vertical convergence forced the flow through an area of 0.25 m^2 over a short transition distance. Understandably, this results in a considerable head difference between the forebay and the tailrace relative to earlier tests. At peak discharge, this distance was approximately 180 mm under D5 conditions compared to less than 75 mm for the same flow without the convergence. In addition, the water surface of the flooded volume surrounding the metering section was not completely calm. At higher discharges, water was swelling from the downstream transducer ports. At the time of testing, it was suspected that some of the water re-circulated upwards and out of the downstream ports and returned into the metering area via the upstream transducer access ports. Figure 6.37 illustrates this explanation. Dye was injected in the flooded area near the upstream ports. The colored water was drawn into the metering area and then exited at the downstream ports. In addition to the actual flow, the ADM system was likely measuring a secondary re-circulation at the top of the intake resulting in positive errors that increased with flow rate.

Unfortunately, little was concluded from the D5 series of testing due to the re-circulation problem. For the low discharge (173 l/s), where the re-circulation effect was minimal, the average discharge error over all the sampling strategies was 0.23 %. This suggests that the acoustic cell resolved the normal velocity component under vertically converging flow conditions, however, it would be prudent to quantitatively address the cosine response using a more direct testing approach.

6.4 DISCUSSION OF ERRORS

As for any measurement comparison study, it is important to identify and attempt to quantify the sources of error in both the reference discharge and ADM systems. The majority of the errors discussed herein are applicable to field conditions, however the change of scale significantly influences their values. The approximations were based on an average flow rate of 300 l/s and the physical conditions of the experimental set-up. Assuming the errors identified are independent, the total error was computed by taking the square root of the sum of the squared errors; this approach has been used for similar error budgets (*e.g.*, Lowell and Hirschfeld, 1979).

6.4.1 Reference Discharge

Systematic error of the MAG in-line flowmeter calibration consisted of the volume calculation of the storage tanks and the calibration error of the water level gauge; the total of these components was estimated to be ±0.14 %. Some leakage around the switch plate that directs overflow into the volumetric tanks resulted in a missed volume of water. For 300 l/s, this was estimated to be 0.66 %.

The filling time of the volumetric tank was measured using a stopwatch with 0.1 s scale that translated to a ±0.07 % error in discharge measurement; this coupled with the reaction time error resulted in an estimated random timing error of ±0.4 %. The timing error was combined with the float gauge reading error (±0.09 %) and the water level error

(±0.53 %) to yield a random error of ±0.66 % for each MAG meter calibration trial. This measurement was repeated for 5 trials, resulting in a random error of ±0.29 %.

The instrument error of the MAG flowmeter is composed of the manufacturers calibration error (systematic) and the random instrumentation error. Developers of the instrument estimated the accuracy of the meter to be ±1.0 %, however, the literature does not include a breakdown of this value. For estimation purposes, this error was subdivided into ±0.5 % systematic and ±0.5 % random error. Since the systematic error of the manufacturer's calibration was absorbed in the lab calibration, this value was not included in the total of the reference discharge measurement error of ±0.67 %. The total random error for the MAG meter readings was estimated to be ±0.58 %. Table 6.9 lists the estimated errors for the reference discharge measurement.

Table 6.9 Reference discharge measurement errors.

Error Source	*Systematic Error [% of discharge]*	*Random Error [% of discharge]*
Reference Discharge		
calibration	±0.14	±0.29
leakage	±0.66	-
instrument	±0.5 *	±0.5**
Total	±0.67	±0.58
* not included in the total ** reduced with longer sampling durations		

6.4.2 ADM

Sources of uncertainty of the ADM system were classified in two general categories: 1) velocity measurement uncertainty which encompass errors associated with the cell geometry, VDV instrumentation errors and flow related uncertainties; and 2) discharge calculation uncertainty which includes geometric and integration errors.

6.4.2.1 Velocity Measurement

Geometric

From equations (5.2) and (5.3) it is clear that the path length measurement error directly translates to path velocity measurement error. Five measurements, accurate to 1 mm, were taken for each path which translates to ±0.08 % systematic error. The path angles in the horizontal plane were measured to within 0.25 degrees which translated to a possible systematic error in discharge measurement of ±0.7 %. The systematic misalignment of the cell to the vertical was estimated to be approximately 0.3 degrees, which translates to an uncertainty in discharge measurement of only ±0.002 %. The tolerances of the carriage guide system allowed for a ±0.2 degree movement in the vertical/flow direction plane; this was classified as random error and estimated to be ±0.0006 % of the flowrate.

Non-water path time error addresses the fact that the acoustic pulse must travel through the potting material of the transducer before entering the water and prior to reaching the ceramic surface of the receive transducer. This error is canceled in the transit-time difference of the pathline velocity calculation, but the speed of sound measurement is affected. A conservative estimate of this effect translates to a systematic error of -0.17 % in discharge.

Some velocity measurements close to the upper and lower boundaries of the metering section were corrupted due to echoing or air pockets trapped against the intake ceiling. This effect precluded testing of higher order GL strategies (*e.g.*, N=14, 16) because the extreme measurement levels were so close to the boundaries relative to the beam pattern diameter. Random and systematic error estimates of ±0.6 % were approximated for the continuous traverses. No value was assessed for the GL traverses since tests of GL strategies (N of 12 or greater) that resulted in poor boundary measurement were not considered. It is noteworthy to state that this error source would be significantly less in field applications where the intake height is much greater relative to the acoustic beam diameter.

Instrumentation

The zero offset uncertainty of the instrument is discussed in Appendix D. Calibration testing revealed that the pathline transit-time differences varied over a range of 4 digital counts in still water conditions. This corresponds to a range of nearly 5 % in normal velocity measurements. The re-calibration of the zero offset corrected the pathline biases, but the possibility of some drift remained. The change in zero offset was, on average, ±0.37 counts between bucket tests (Appendix D). This translated to a ±0.43 % error in discharge. It is important to note that this estimate would be reduced by more than an order of magnitude for a field application where the velocities are significantly greater and the relative resolution of the instrumentation would be much better.

Transit-time measurement is limited by the clock speed and the digital resolution of the instrument. Authors documenting past error studies of ADM systems (*e.g.*, Lowell and Hirschfeld, 1979) indicated that this error is truly random and varies by ±1 digital count of the instrument. For the relatively low velocities tested in the laboratory, this translates to a ±1.16 % random error. This does not directly translate to a ±1.16 % error in discharge measurement because the discharge was calculated from many velocity samples (*e.g.*, 8 Hz for 4 minutes or n=1935). Dividing 1.16 % by $(n)^{1/2}$, for a minimum n of 1935 results in a random instrument timing error of ±0.026 % with respect to discharge.

Flow Related

Voser *et al.* (1996) explain that positioning transducers such that the transducer face protrudes into the main flow results in two systematic errors of opposite sign. Figure 6.38 is used to explain this effect. First, because the transducers are not flush with the conduit wall, the smaller velocities in the boundary layer are not sampled. If corrections are not made, this primary effect results in a positive systematic error in the chordal average velocity measurement. The second systematic protrusion error is due to the

reduced and redirected water velocity close to the transducer face; this results in a negative bias in the velocity measurement. Voser (1996) estimated that, when considering both conflicting effects, the protrusion error was likely within ±0.5 %. Recognizing that this value was calculated for a specific geometry (*i.e.*, 2 m conduit, 45 degree path angles, similar size transducers), it was considered appropriate for approximation purposes.

Leakage behind the transducer faces within the slots of the intake walls was also a potential source of systematic error in the laboratory experiment. This effect is also illustrated in Figure 6.38. The possible leakage area was approximately 7.5 mm wide; given that leakage could occur at either side of the metering section, the potential leakage area was nearly 1.5 % of the total area. However, leakage flow had to redirect perpendicular to the normal flow direction. A systematic error of -0.4 % was estimated for this effect.

6.4.2.2 Discharge Measurement

Geometric

Geometric errors that directly translated to discharge measurement error were also estimated. Clearly, any error in measurement of the metering section area translates directly to discharge measurement error. To determine the flow metering area, 4 height and width measurements were taken at 3 equally spaced locations over the length of the discharge metering section. The area was calculated to be 0.9998 ±0.00047 m^2; this translates directly to a discharge calculation error of ±0.05 %.

Random transducer positioning error resulted from error within the position control system and incorrectly defining the beginning level of the traverse. The former effect was considered to be negligible for the GL traverses because the positioning system precisely located and maintained stationary positions. However the instantaneous error of position during a continuous traverse could reach 2000 encoder counts, or 1.41 mm. A

discrepancy in normal velocity of 0.9 % was estimated for a position error of 1.41 mm. Recognizing that this effect would be minimized over the duration of the traverse, a random error of ±0.2 % was arbitrarily applied to the complete discharge measurement.

Since the true center point of the beam pattern created by the transducers was not accurately known, defining the zero position of the carriage was estimated be only accurate to 2 mm, resulting in a potential systematic position error of ±0.20 %. However, for the CTR traverse, the majority of this error would cancel out of the measurement. Measurements obtained too close to the upper boundary would be low, but this deficit would be compensated since lower boundary samples would be obtained further from the intake floor than intended. A systematic error of ±0.10 % was assigned to the CTR sampling strategy for this effect.

Voser *et al.* (1996) indicated that relative errors due to incorrect positioning of acoustic transducers when using Gauss integration techniques can lead to an error of "several thousandths." Given that typical positioning errors associated with this estimate were only ±0.05 % of the intake diameter, the position error effect was scaled to ±0.4 %.

Integration Error

Clearly, the integration method used is a potential source of discharge measurement uncertainty. A single value was not estimated since it is largely dependent on the characteristics of the profile being measured. It can be stated, however, that the uncertainty resulting from a continuous traverse is predominantly random. If an intake is traversed excessively fast, the random fluctuation of the velocity profile would not be adequately sampled. The repeatability of the CTR tests from one measurement to the next, at the same flow rate, suggested that the overall random uncertainty was quite small (roughly ±0.20 % to ±0.50 %). The traverses performed in the laboratory were not excessively fast to the point that the profile was under sampled and large random errors dominated.

In the case of a discrete profiling technique, such as the GL traverse, systematic integration errors would be dominant. As explained in Section 6.3.1, if an insufficient number of sampling levels are used, the GL techniques will not evaluate the integral of the true best fit polynomial, rather of an $(2N\text{-}1)^{th}$ order polynomial that passes through the sampled velocity points. If the profile geometry was consistent, a systematic error would be the result. This effect is more pronounced when the flow conditions are complex and the profile contains numerous inflections. The various GL tests performed under disturbed flow conditions resulted in systematic errors roughly between 9.0 % and 0.1 % for N values ranging from 4 to 10. Certainly for lower order GL strategies, a significant portion of these systematic errors was attributed to integration uncertainty.

Table 6.10 summarizes the estimated errors of the ADM system in the context of the laboratory experiment. Not including the unknown integration errors, the total systematic error was ±1.00 % and ±0.89 % for the CTR and GL sampling strategies, respectively. The total random error was estimated to be ±0.63 % for the CTR traverses and ±0.026 % for the GL results. A number of the systematic uncertainties were likely absorbed by the laboratory calibration of the ADM system. Not including such uncertainties resulted in an estimate of ±0.44 % and ±0.59 % values of systematic uncertainty for the CTR and GL methods, respectively. It can not be overemphasized, however, that accurate calibration of field discharge systems is very difficult and the accuracy of the calibration is only as good as the reference discharge measurement method used. Thus, systematic errors due to field conditions, such as the path angle measurement error, will not be identifiable.

Table 6.10 ADM errors.

Error Source	*Systematic Error [% of discharge] (CTR/GL)*	*Random Error [% of discharge] (CTR/GL)*
Velocity Measurement		
geometric		
path length	±0.08 *	-
path angle	±0.70 *	-
vertical alignment	-0.002 *	±0.0006
non-water path time	-0.17 *	-
boundary effects	±0.6/ - *	±0.6/ -
instrumentation		
zero offset	±0.43	-
transit-time measurement	-	±0.026
flow		
protrusion error	±0.5 *	-
leakage	-0.4 *	-
Discharge Calculation		
geometric		
area	±0.05	-
transducer position	±0.1/±0.4	±0.2/ -
integration **	-	-
Total	±1.00/±0.89	±0.63/±0.026
Total (excluding systematic errors absorbed in calibration (*))	± 0.44/±0.59	±0.63/±0.026
** integration errors not included in total		

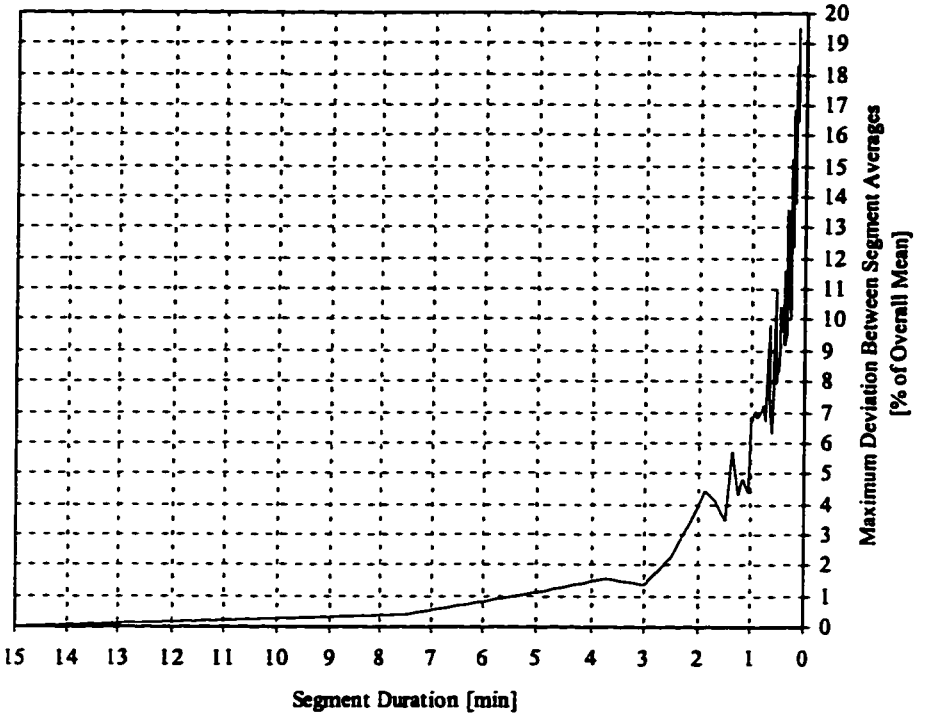

Figure 6.1 Variability of segment average velocity (Q=185.8 l/s, no filter media).

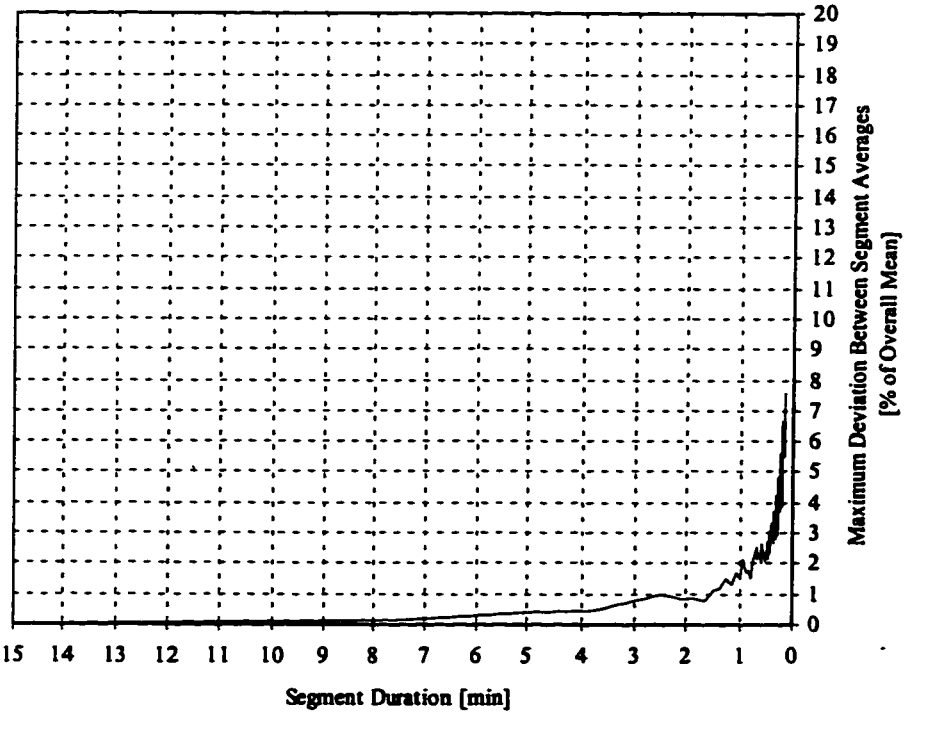

Figure 6.2 Variability of segment average velocity (Q=286.0 l/s, filter media).

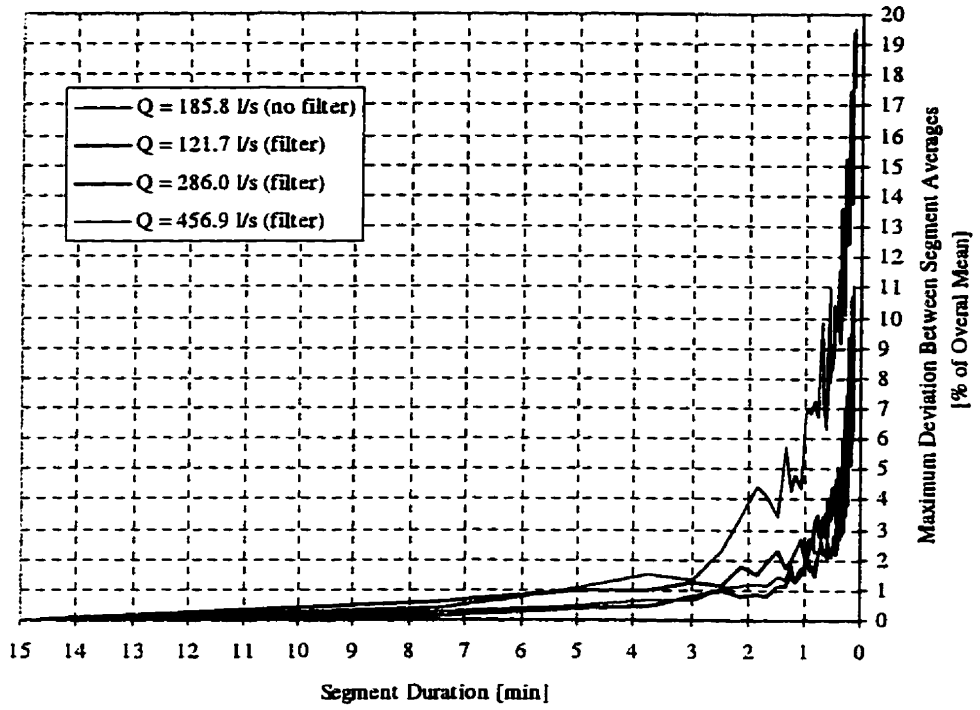

Figure 6.3 Variability of segment average velocity (all flowrates tested).

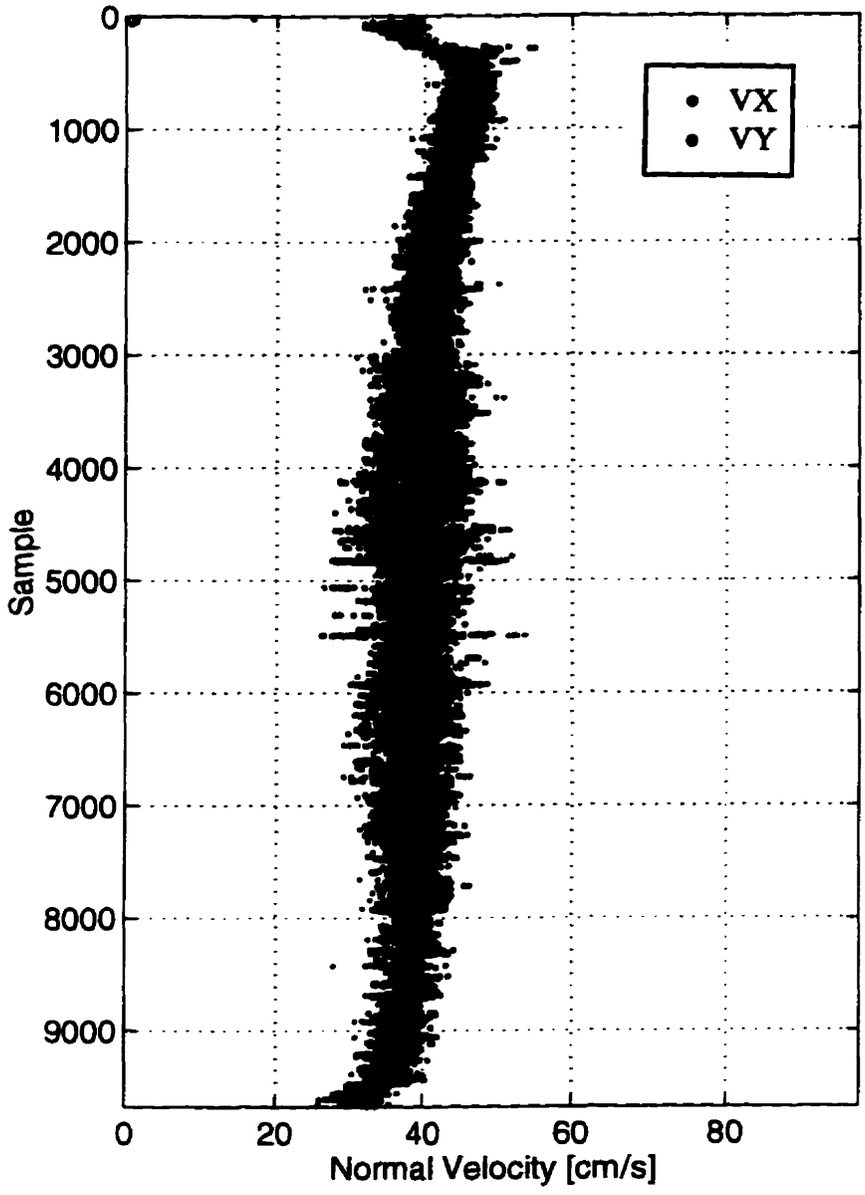

Figure 6.4 Undisturbed velocity profile (CTR20, Q=388.1 l/s)

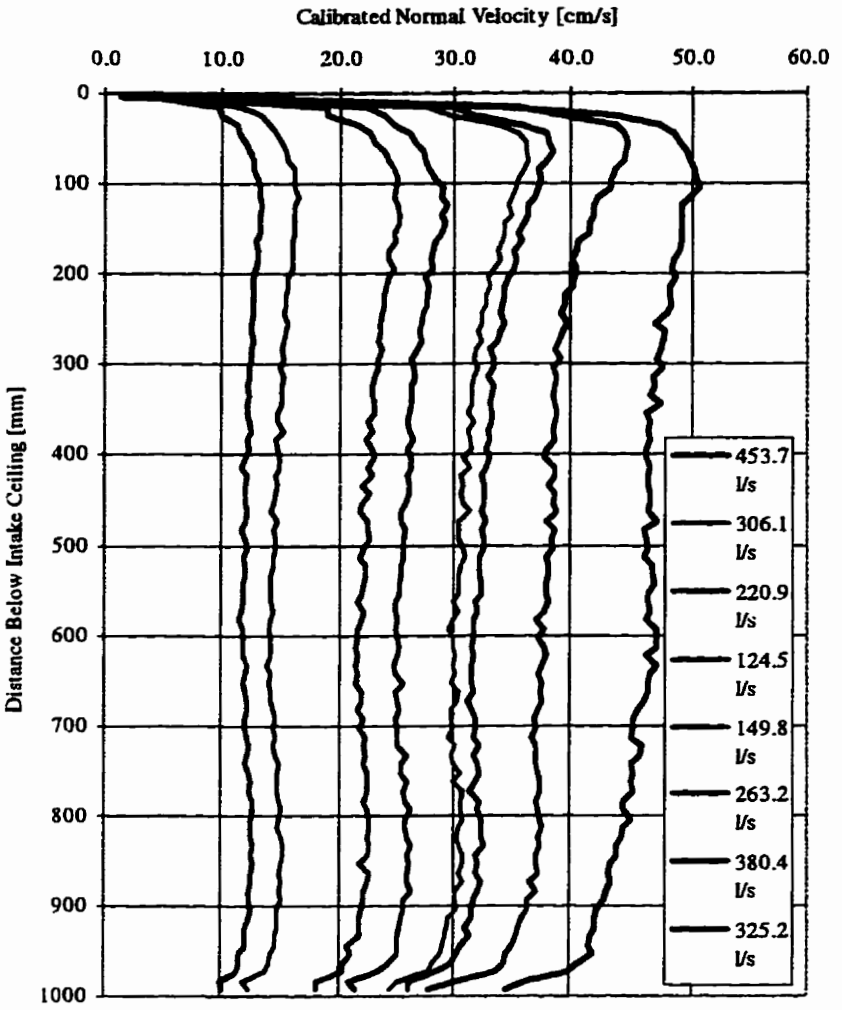

Figure 6.5 Velocity profile for 8 flowrates (undisturbed).

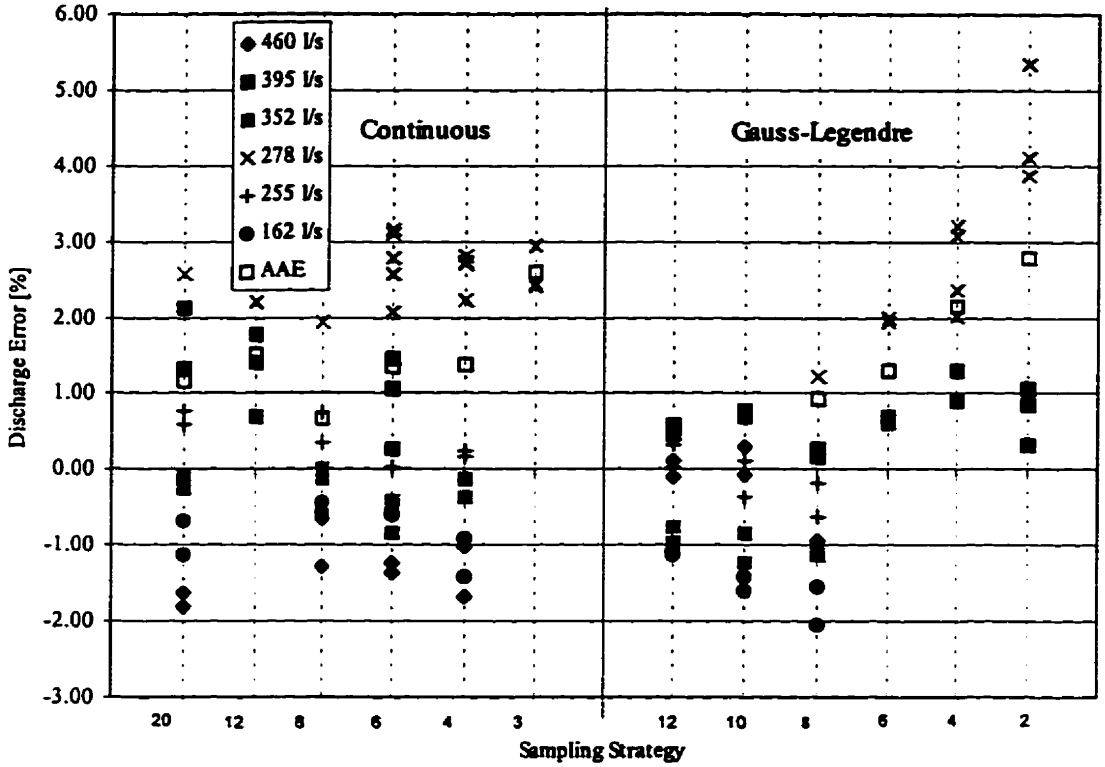

Figure 6.6 Sampling strategy comparison results.

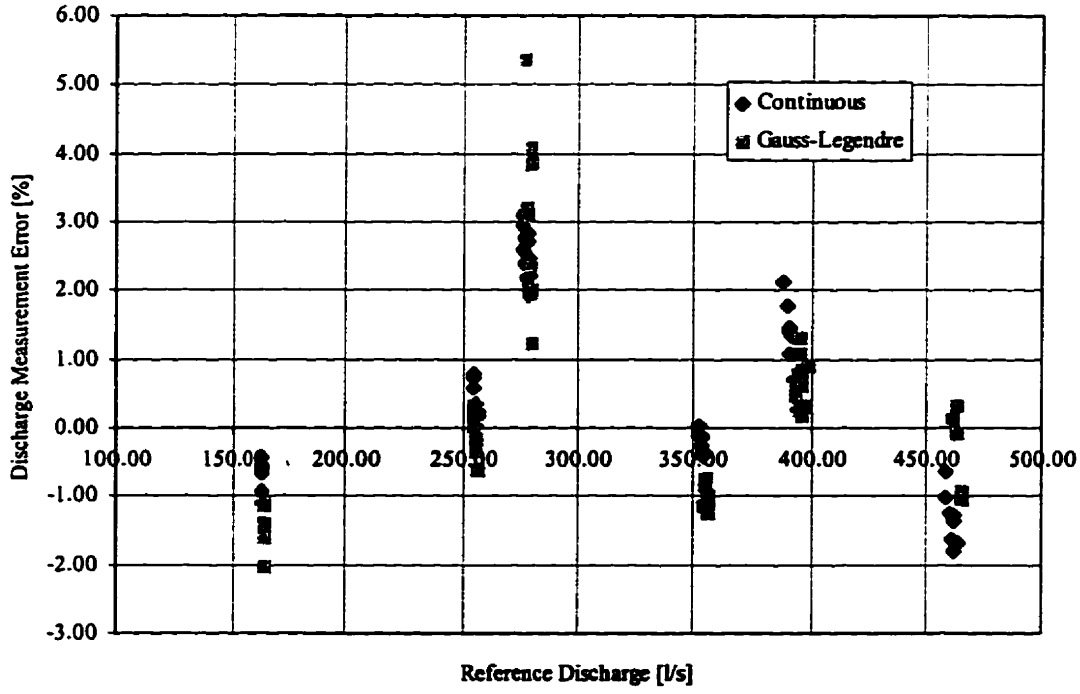

Figure 6.7 Distribution of discharge measurement error with flowrate (undisturbed).

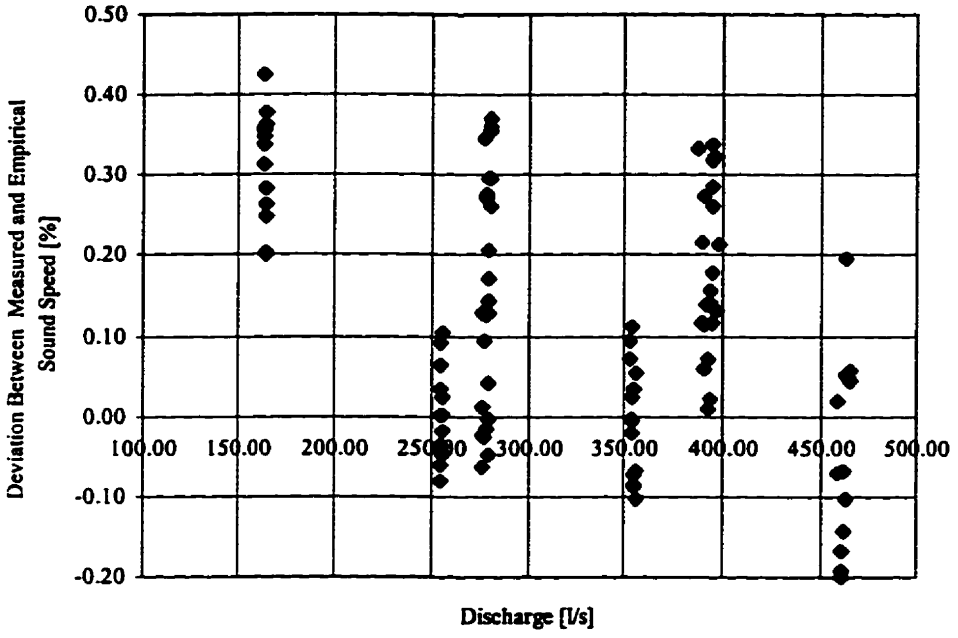

Figure 6.8 Distribution of speed of sound discrepancy with flowrate.

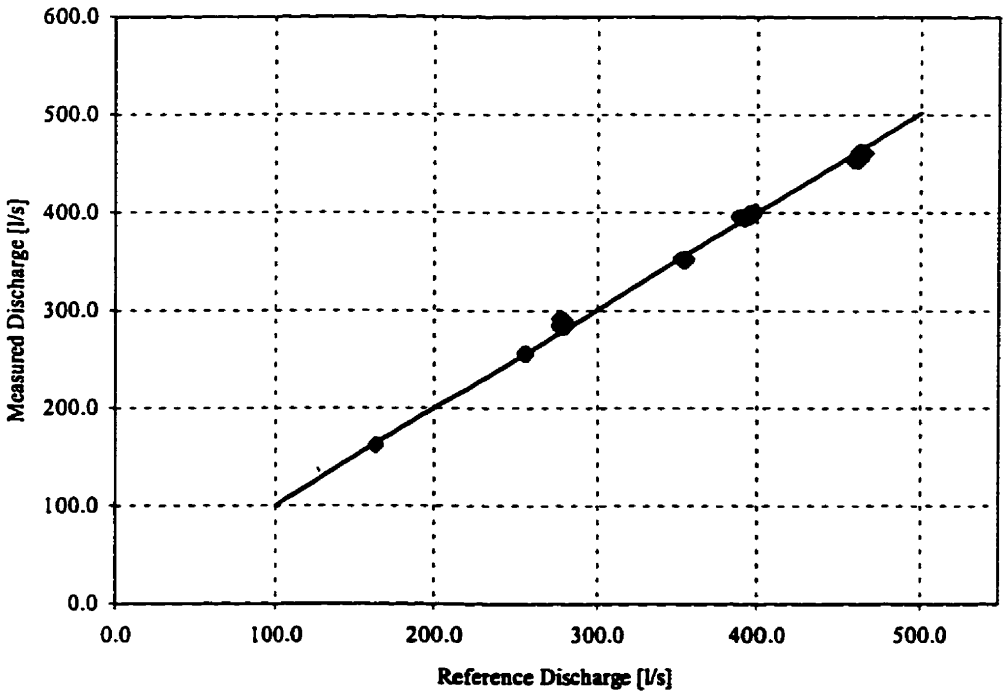

Figure 6.9 Verification of calibration.

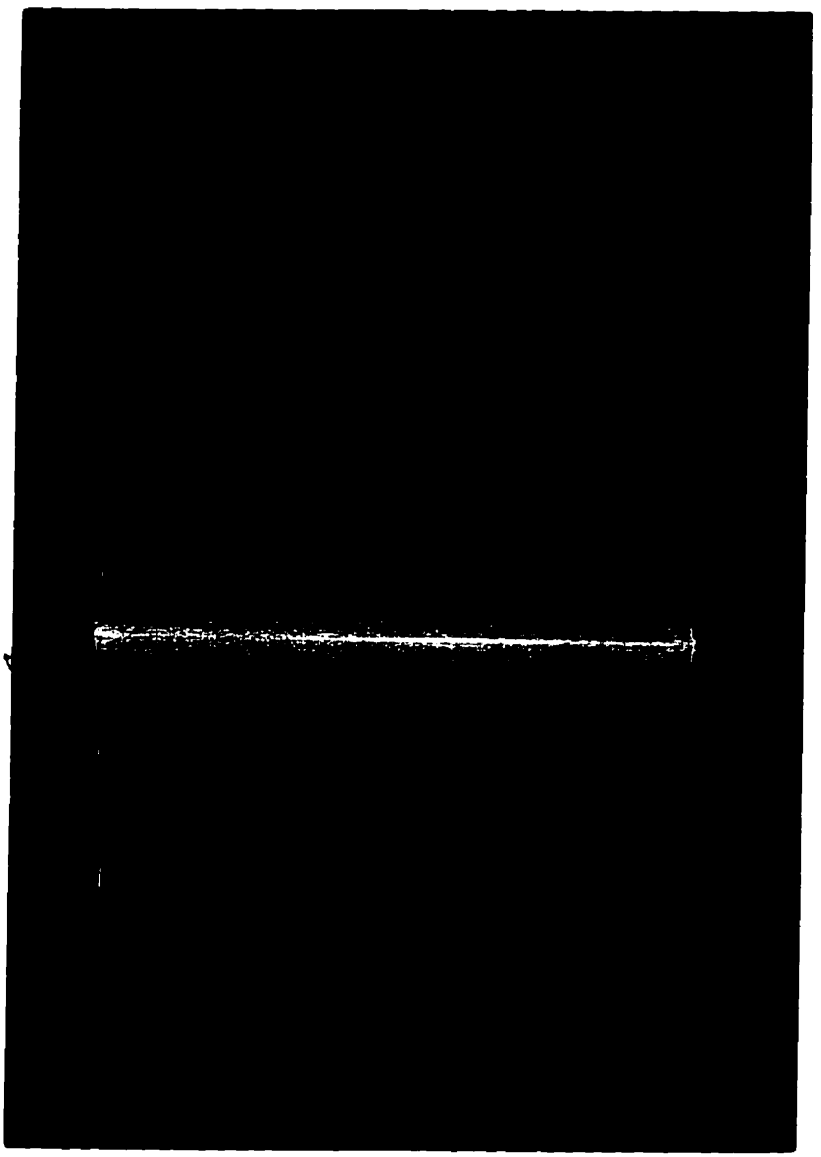

Figure 6.10 Disturbance 1.

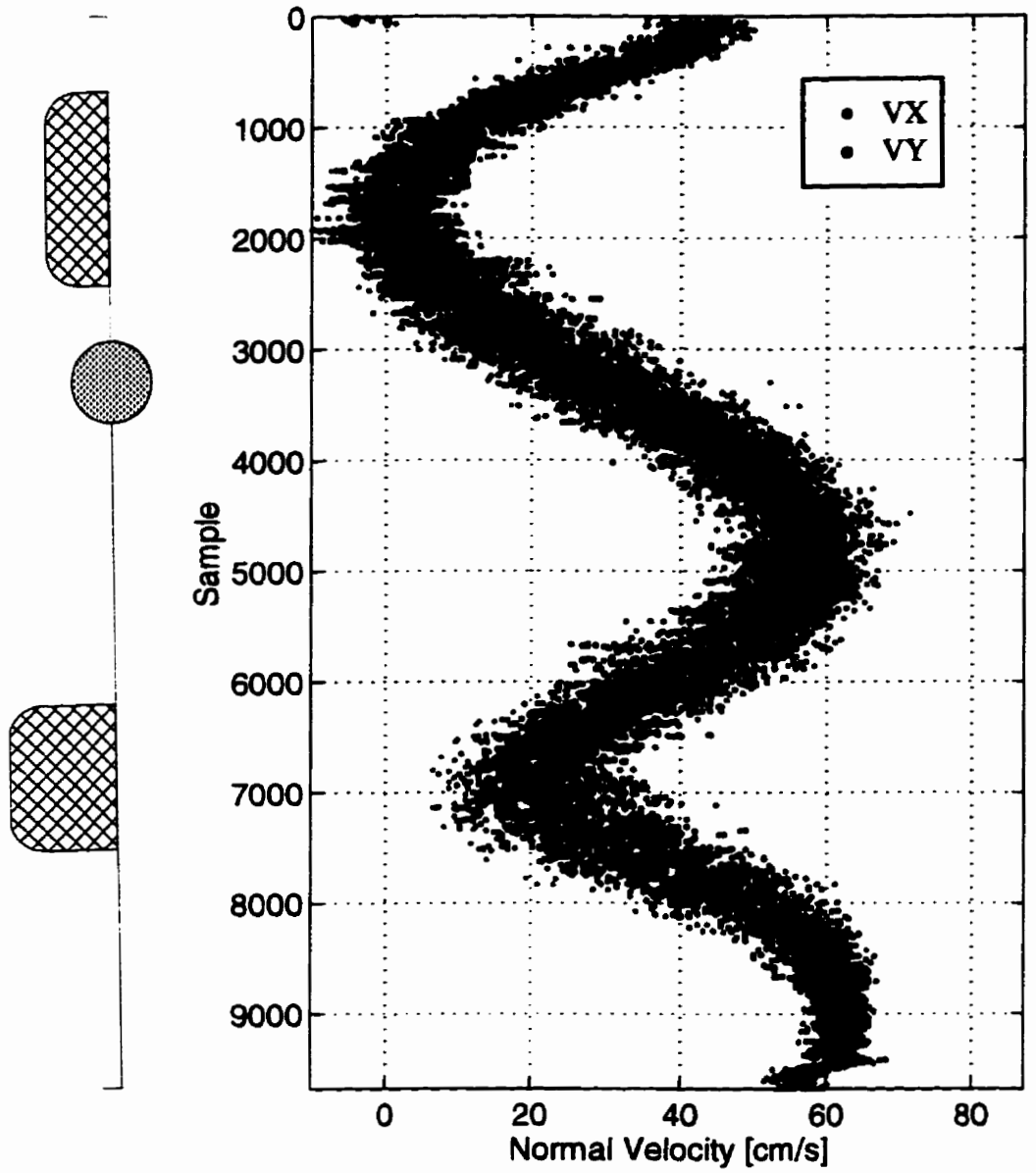

Figure 6.11 Velocity profile for D1 flow condition (CTR20, Q=345.1 l/s)

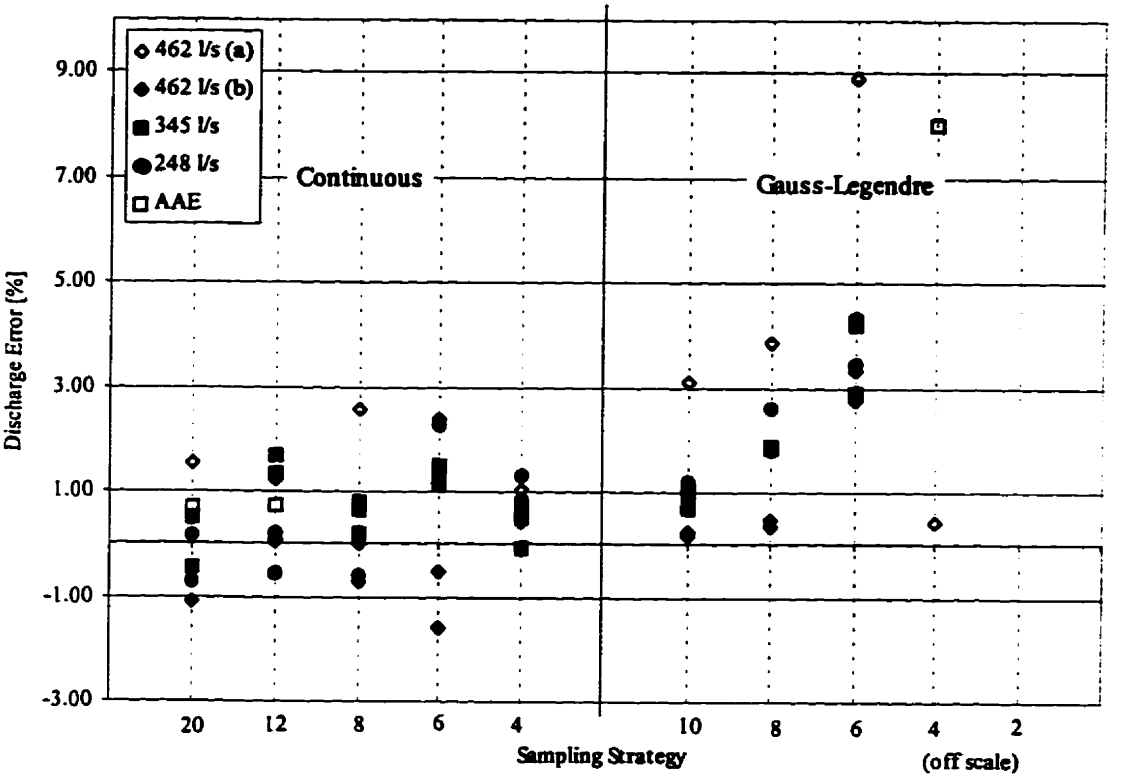

Figure 6.12 Comparison of sampling strategies for D1 flow condition.

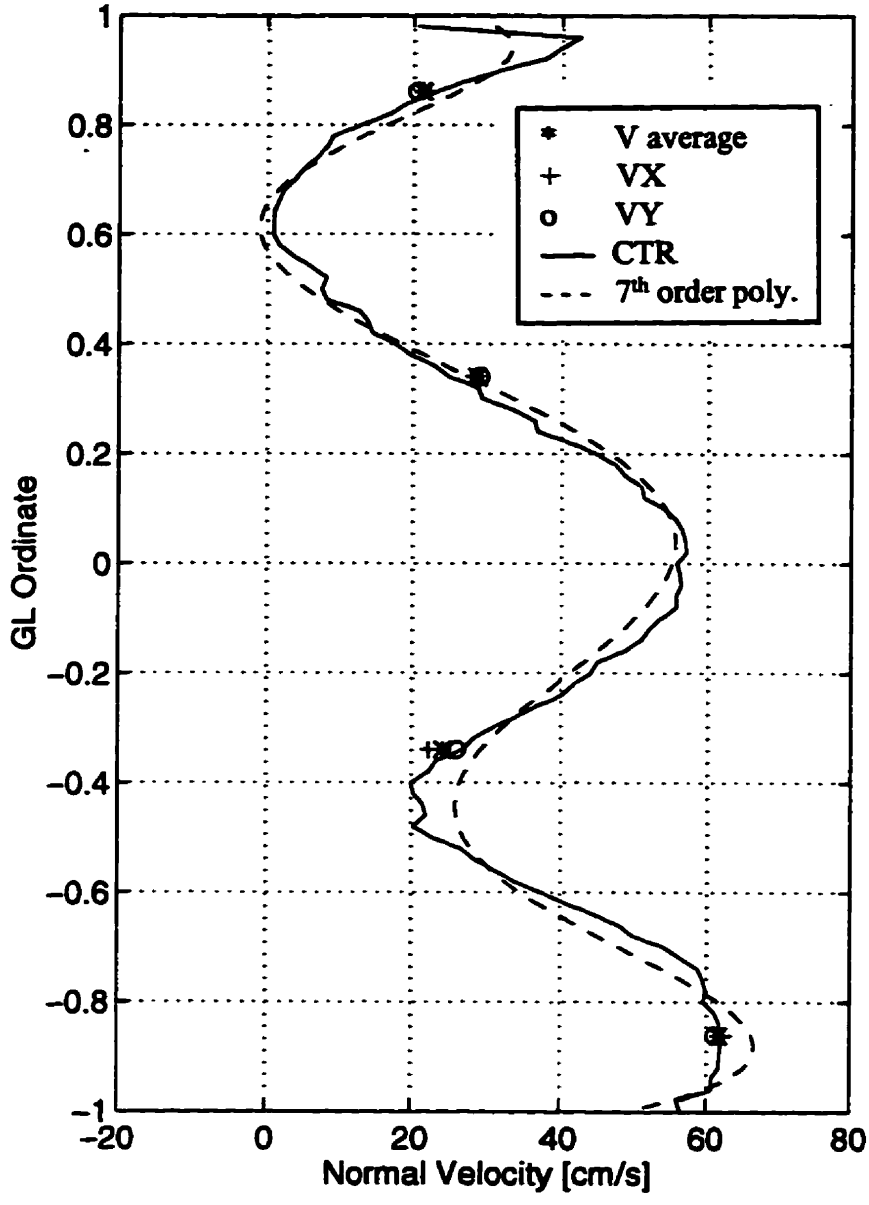

Figure 6.13 Smoothed velocity profile, GL4 measurements and 7th order polynomial fit (D1 flow condition).

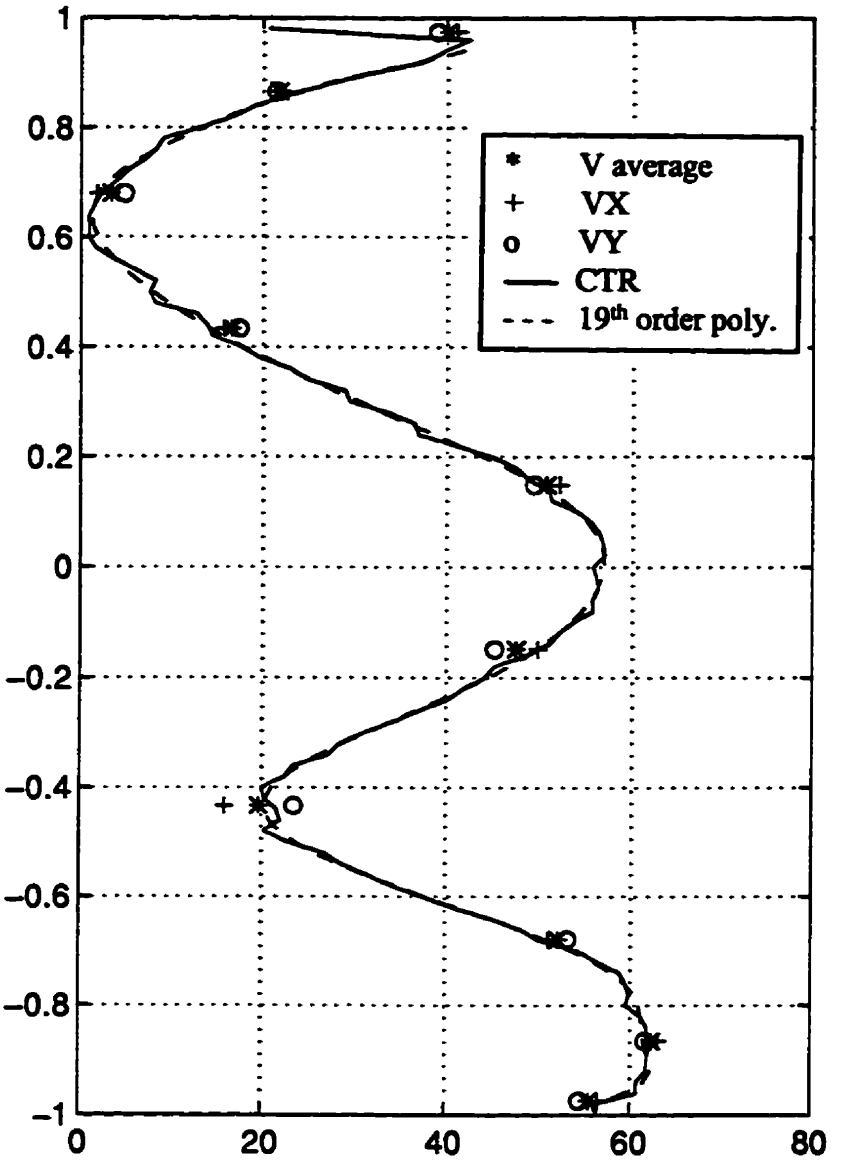

Figure 6.14 Smoothed velocity profile, GL10 measurements and 19th order polynomial fit (D1 flow condition).

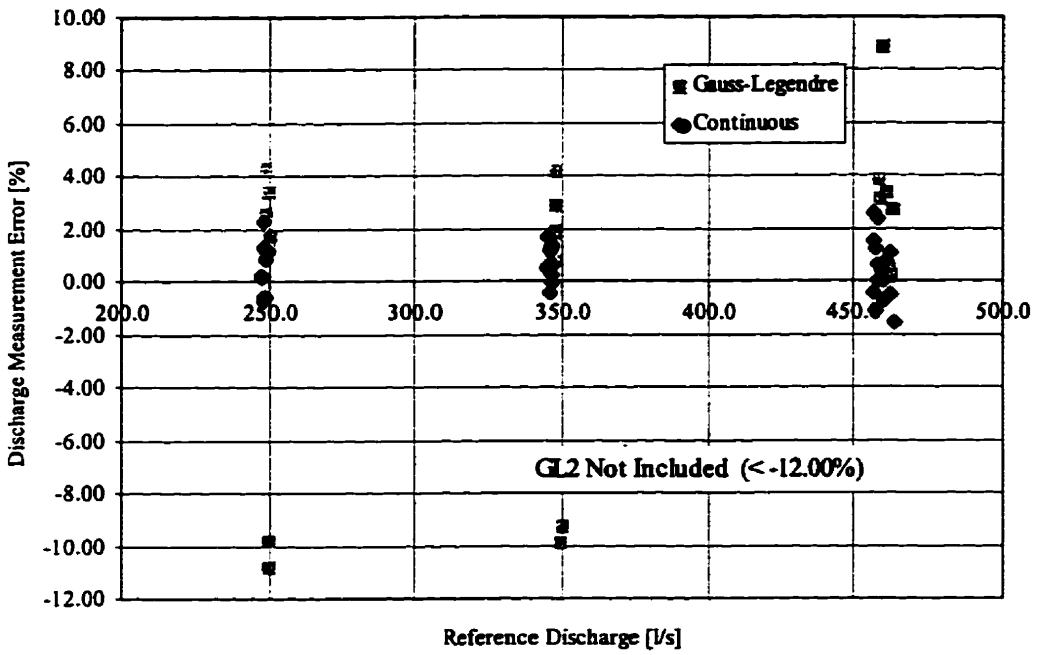

Figure 6.15 Distribution of error with flowrate (D1 flow condition)

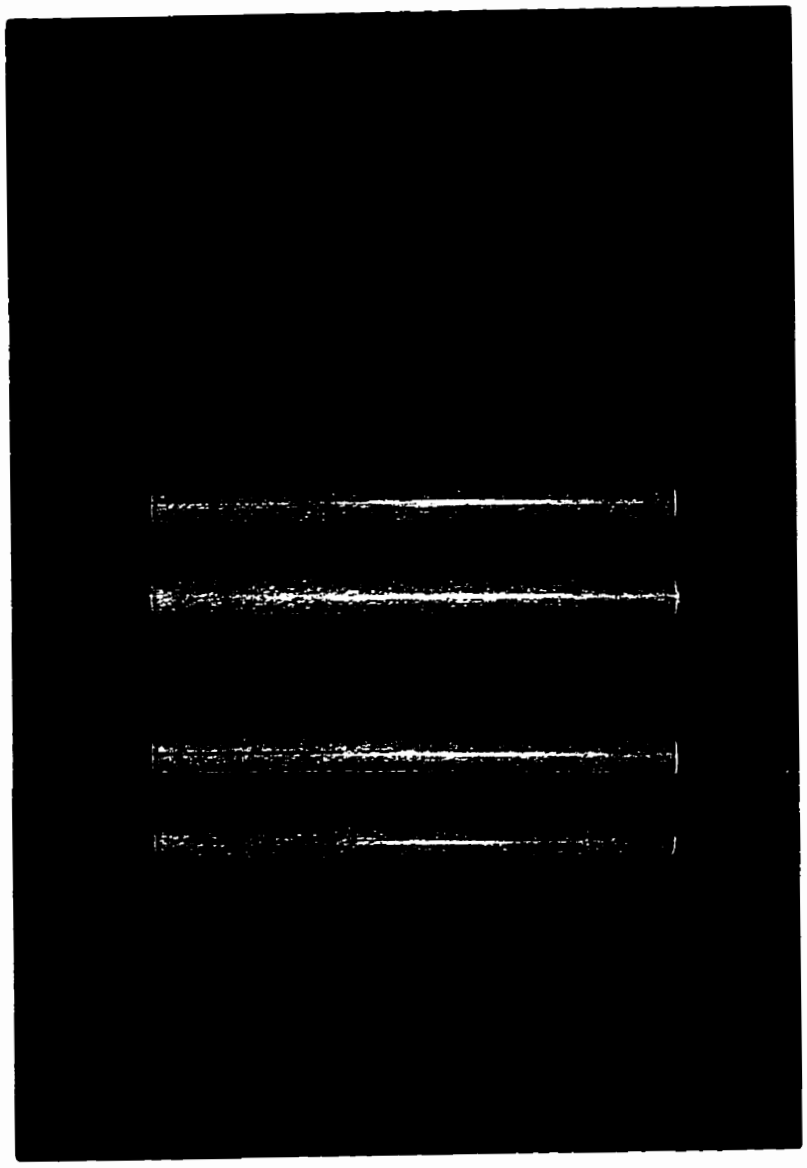

Figure 6.16 Disturbance 2.

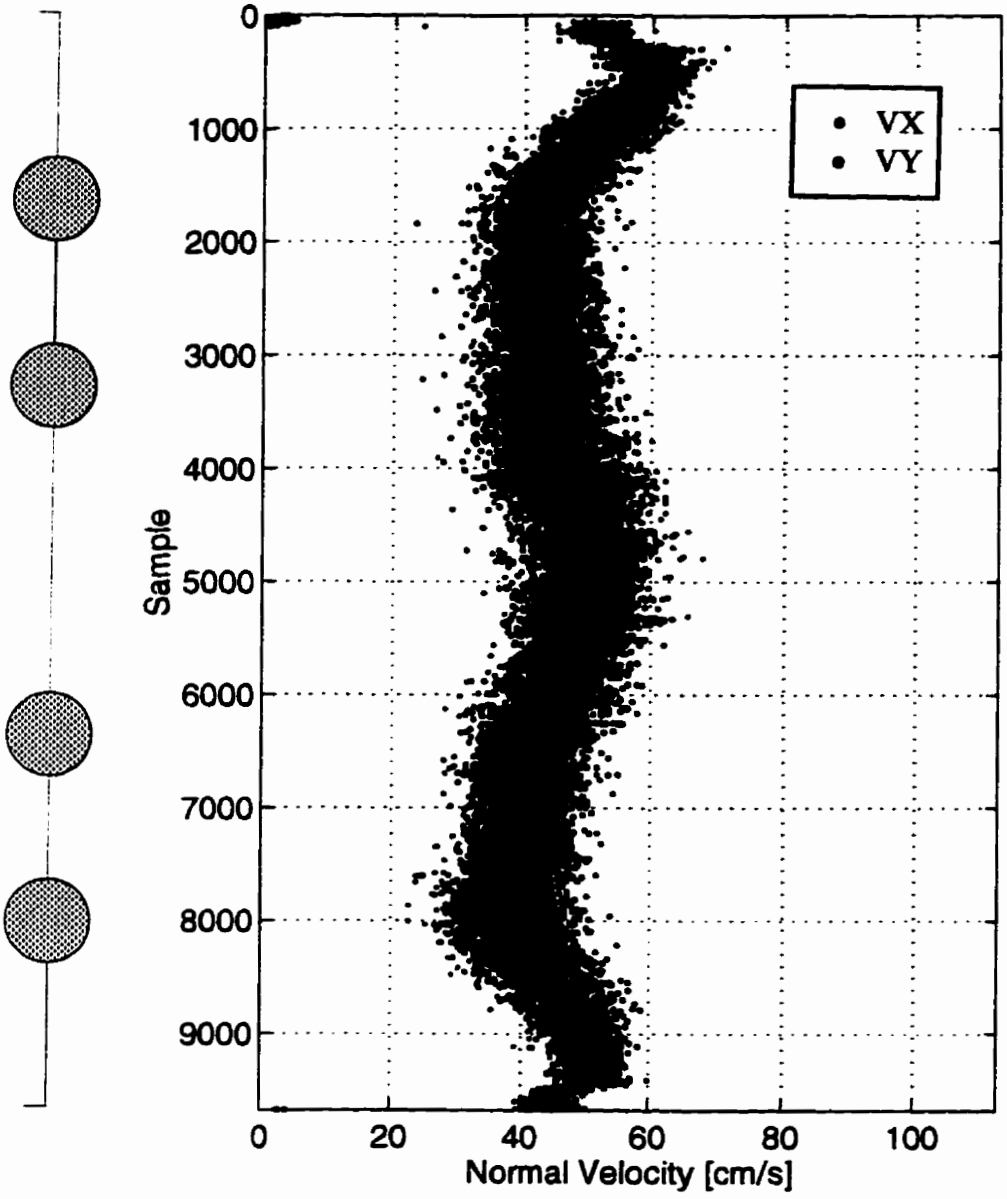

Figure 6.17 Velocity profile for D2 flow condition (CTR20, Q=453.1 l/s)

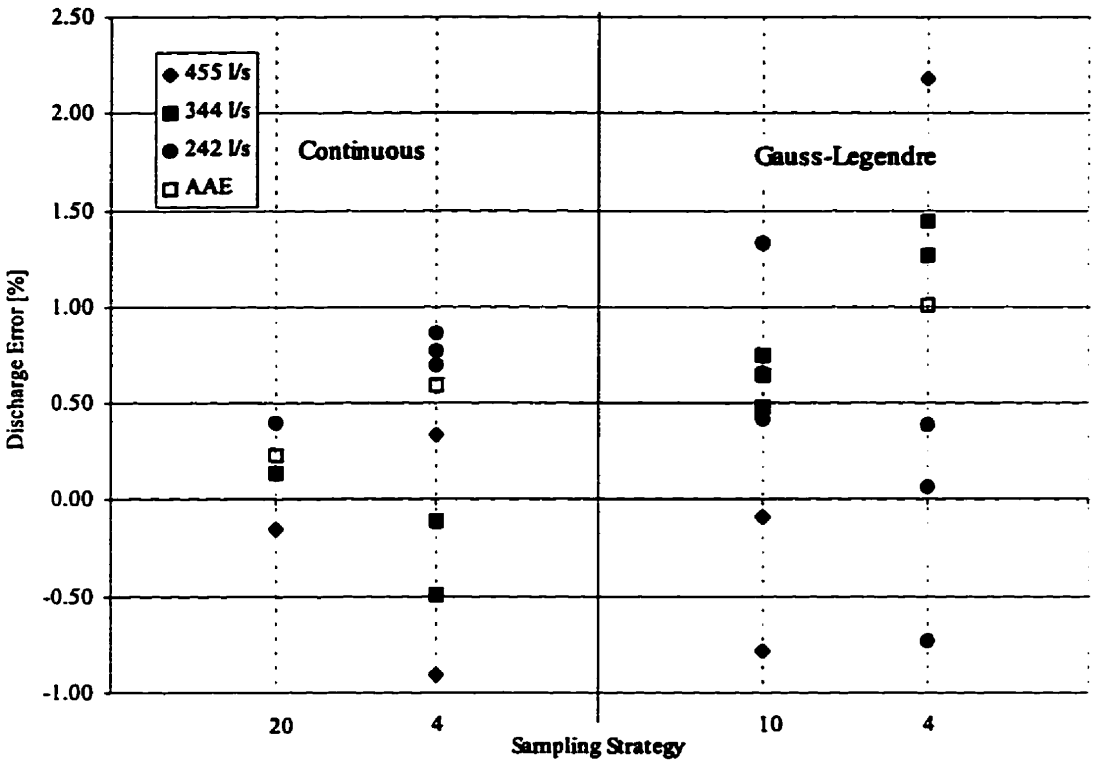

Figure 6.18 Comparison of sampling strategies for D2 flow condition.

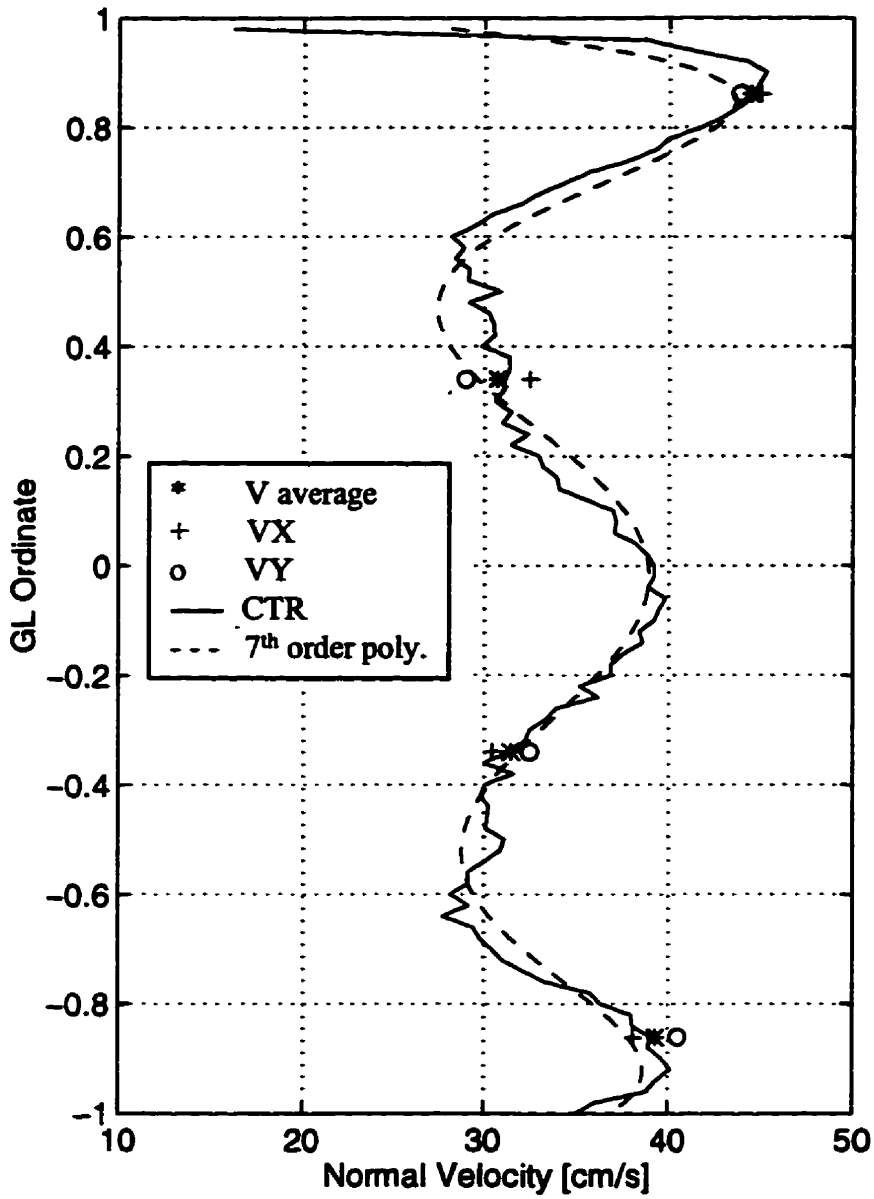

Figure 6.19 Smoothed velocity profile, GL4 measurements and 7th order polynomial fit (D2 flow condition).

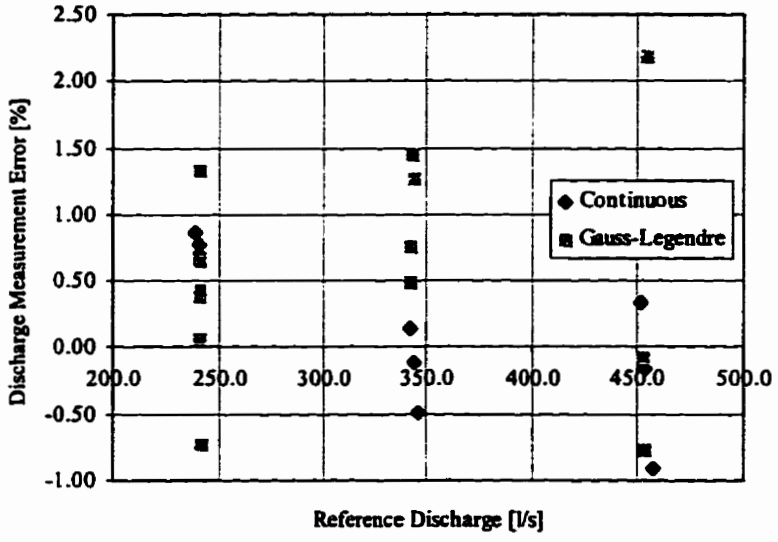

Figure 6.20 Distribution of error with flowrate (D2 flow condition).

Figure 6.21 Disturbance 3.

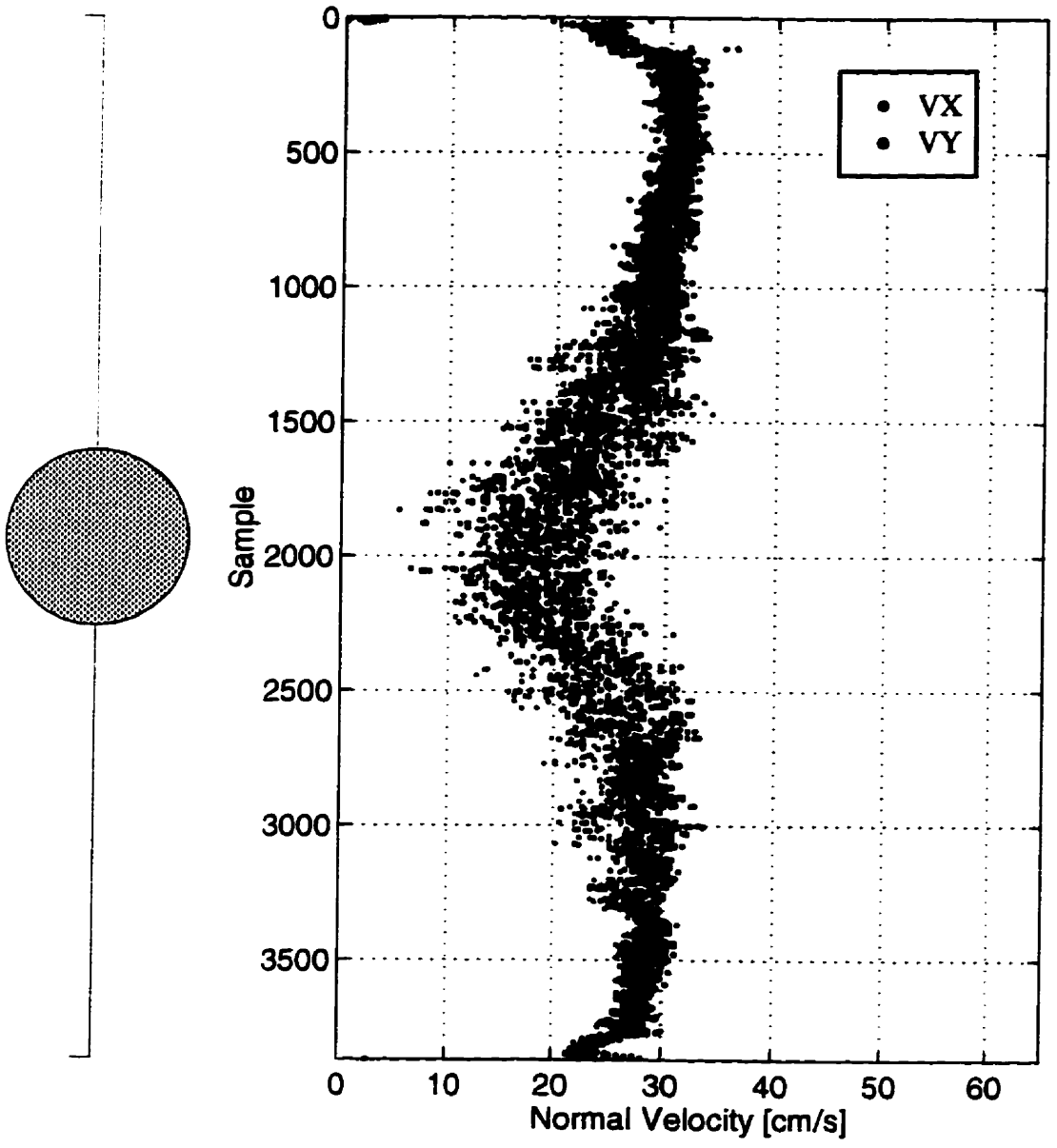

Figure 6.22 Velocity profile for D3 flow condition (CTR8, Q=257.7 l/s).

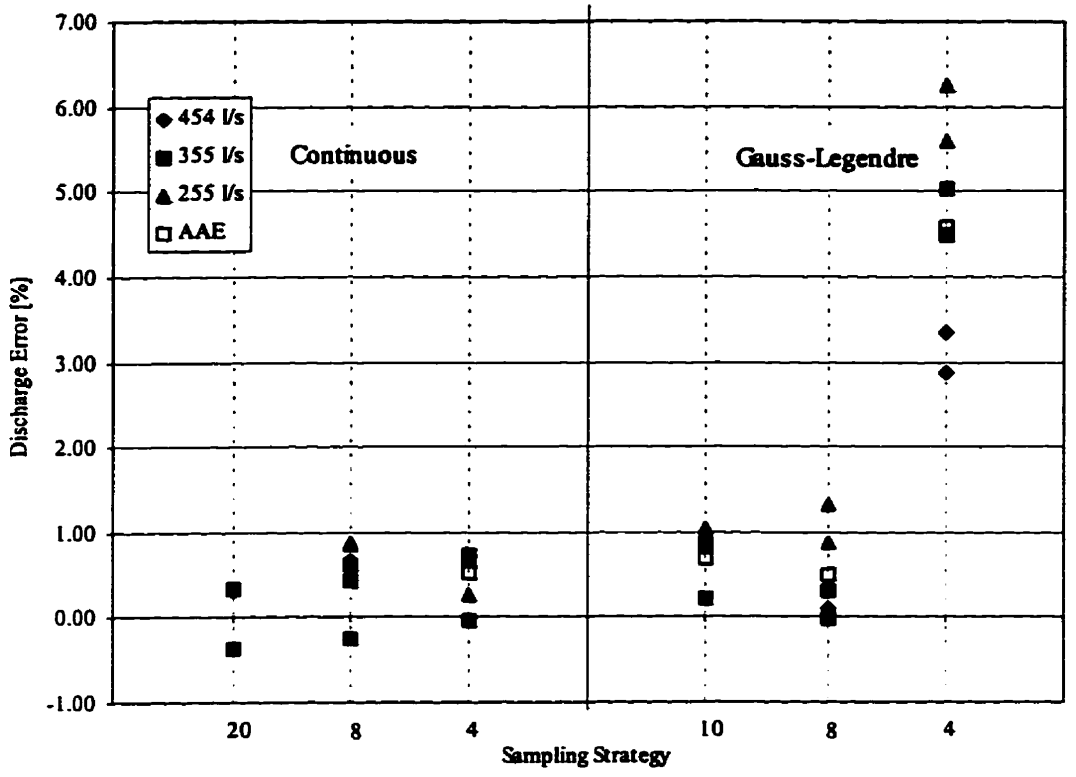

Figure 6.23 Comparison of sampling strategies for D3 flow condition.

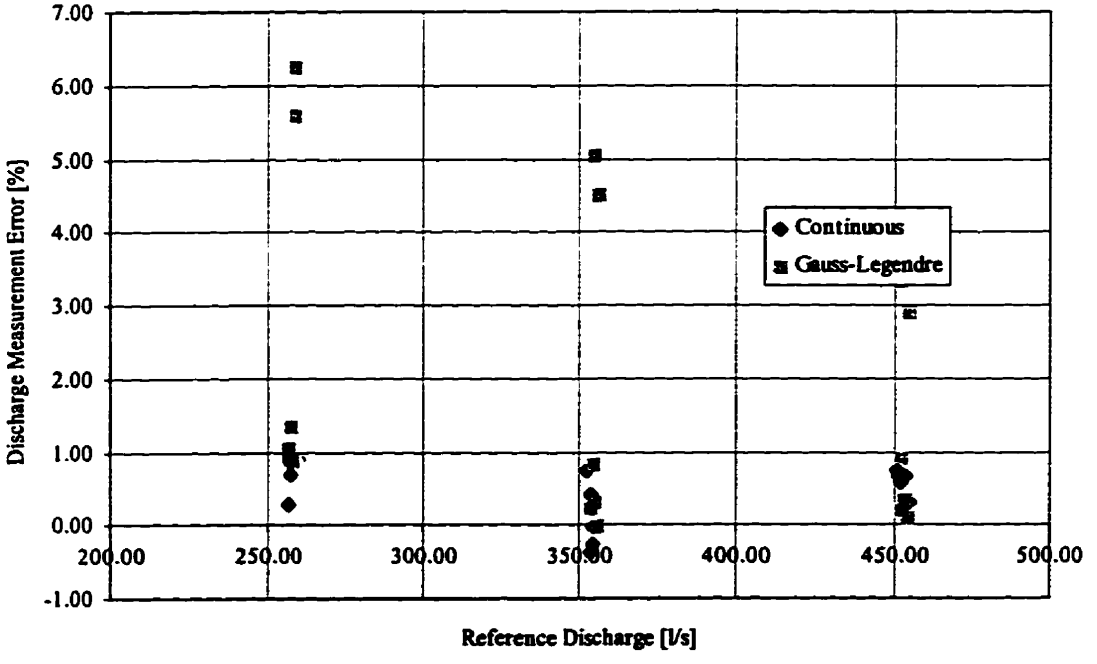

Figure 6.24 Distribution of error with flowrate (D3 flow condition).

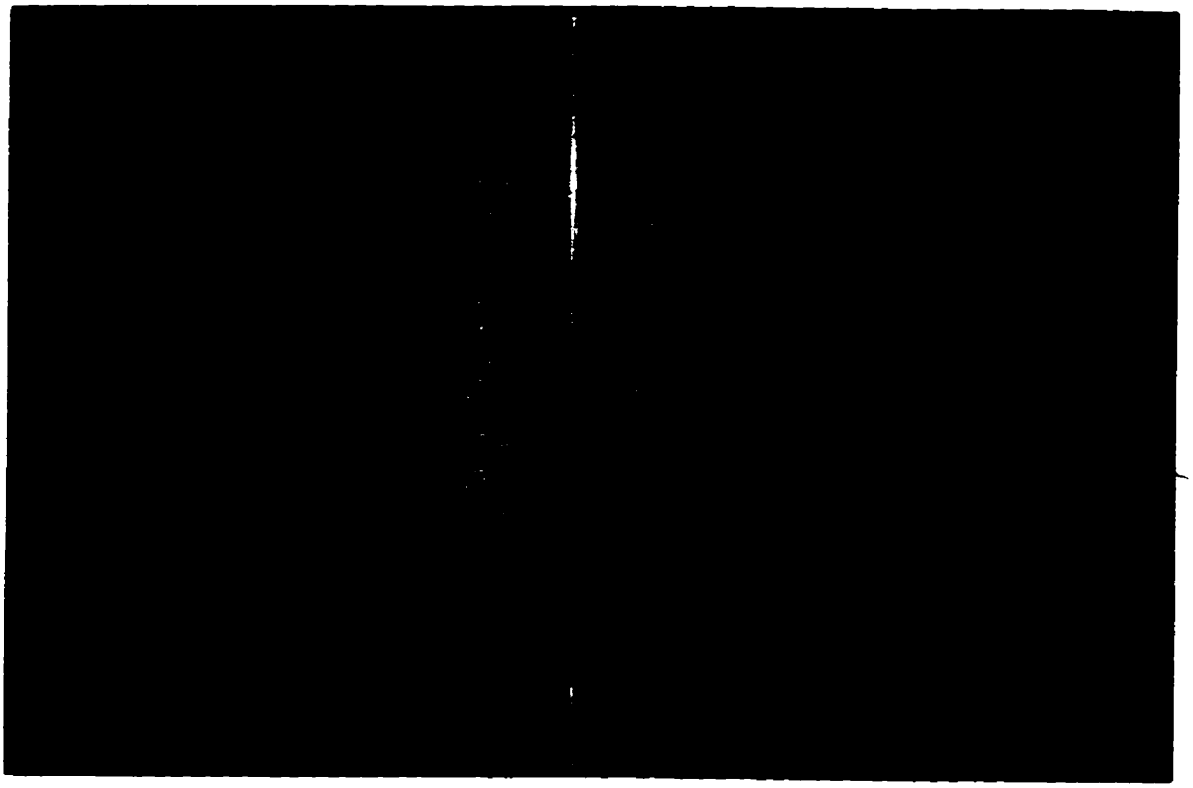

Figure 6.25 Disturbance 4.

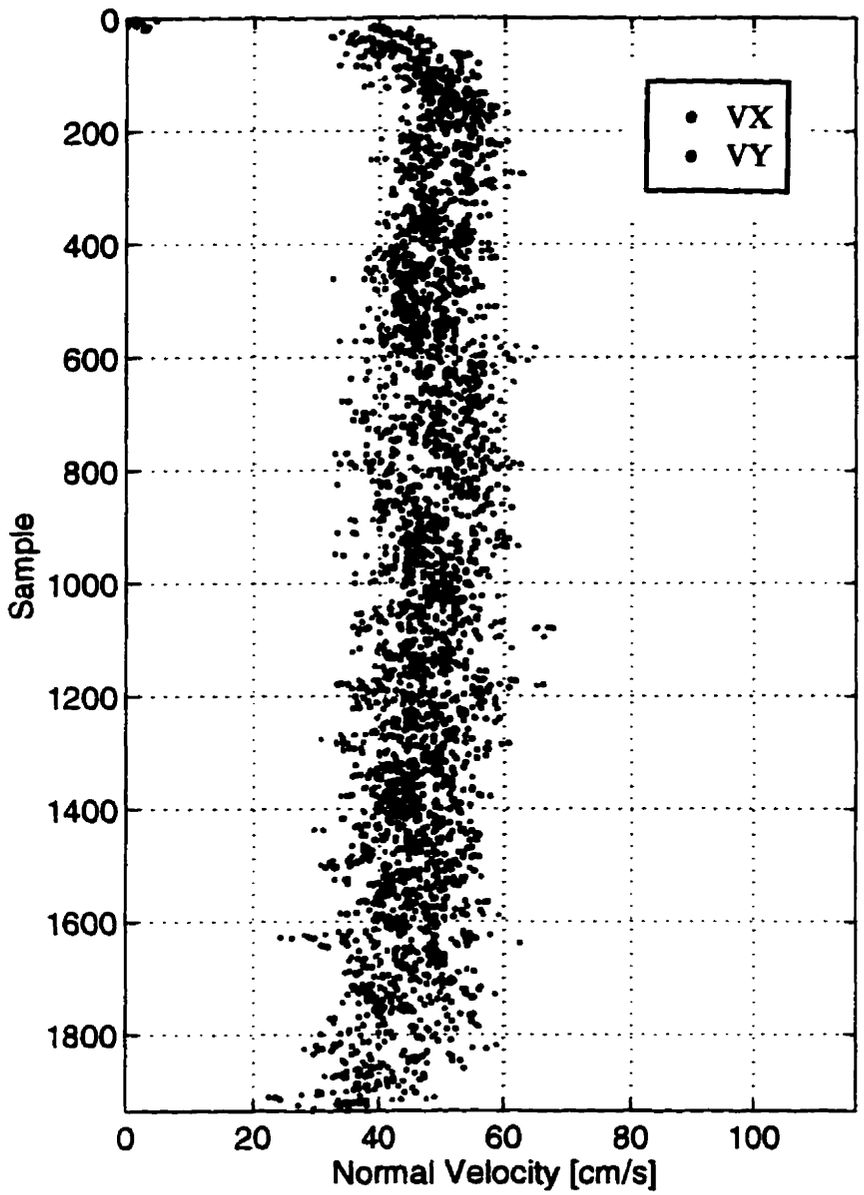

Figure 6.26 Velocity profile for D4 flow condition (CTR4, Q=453.0 l/s)

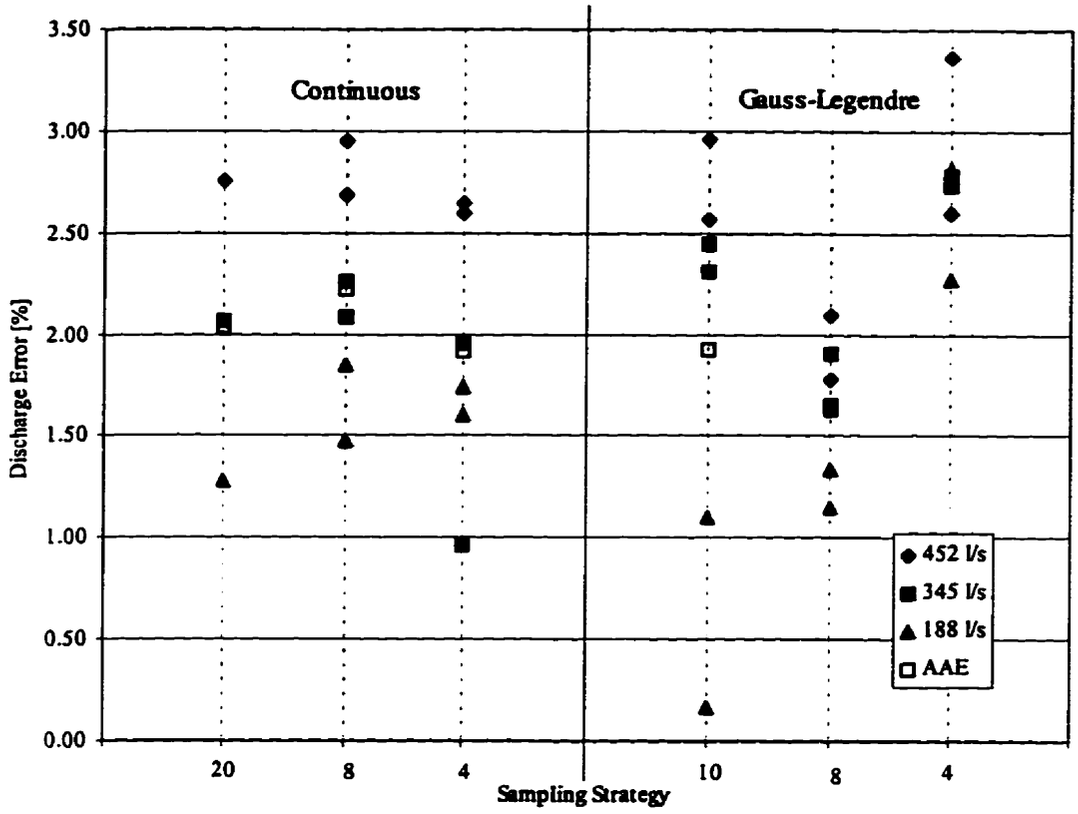

Figure 6.27 Comparison of sampling strategies for D4 flow condition.

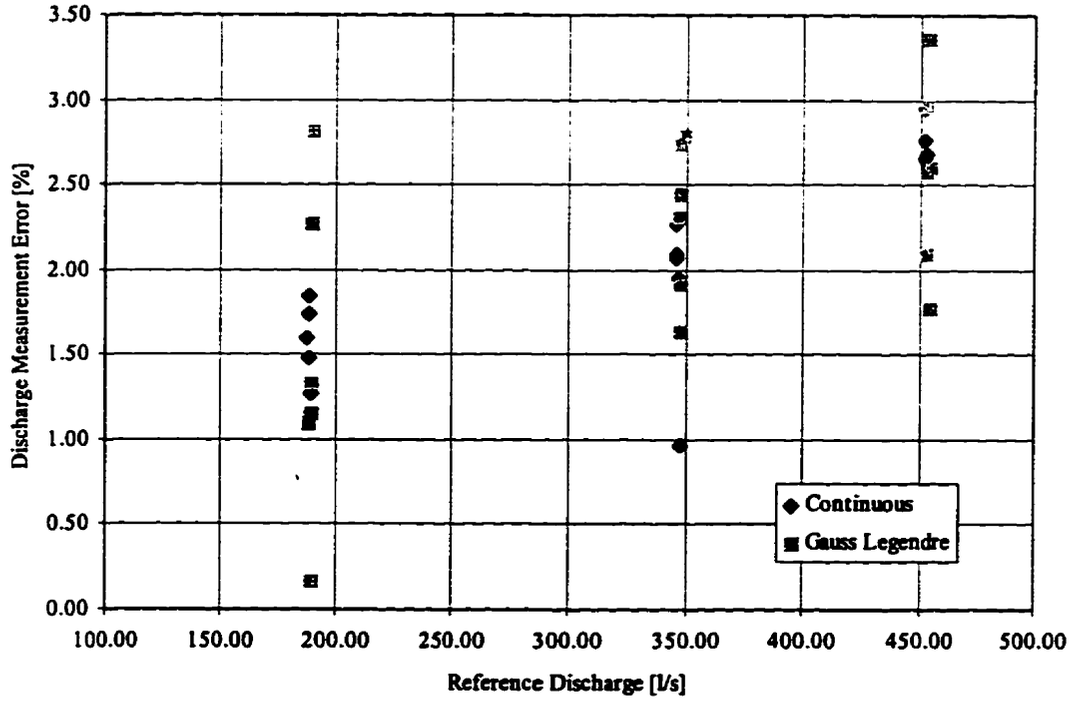

Figure 6.28 Distribution of error with flowrate (D4 flow condition).

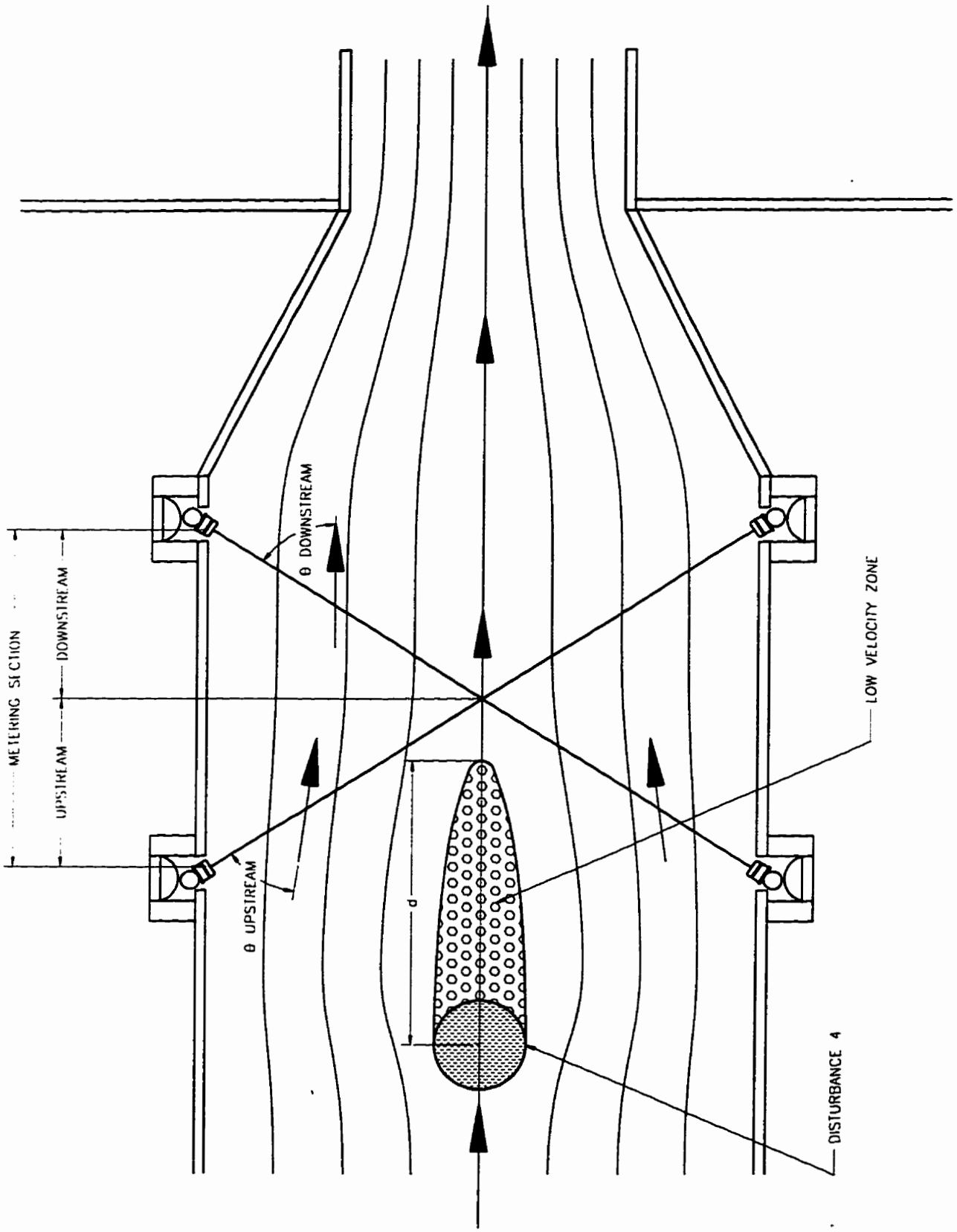

Figure 6.29 Plan drawing of D4 and metering section.

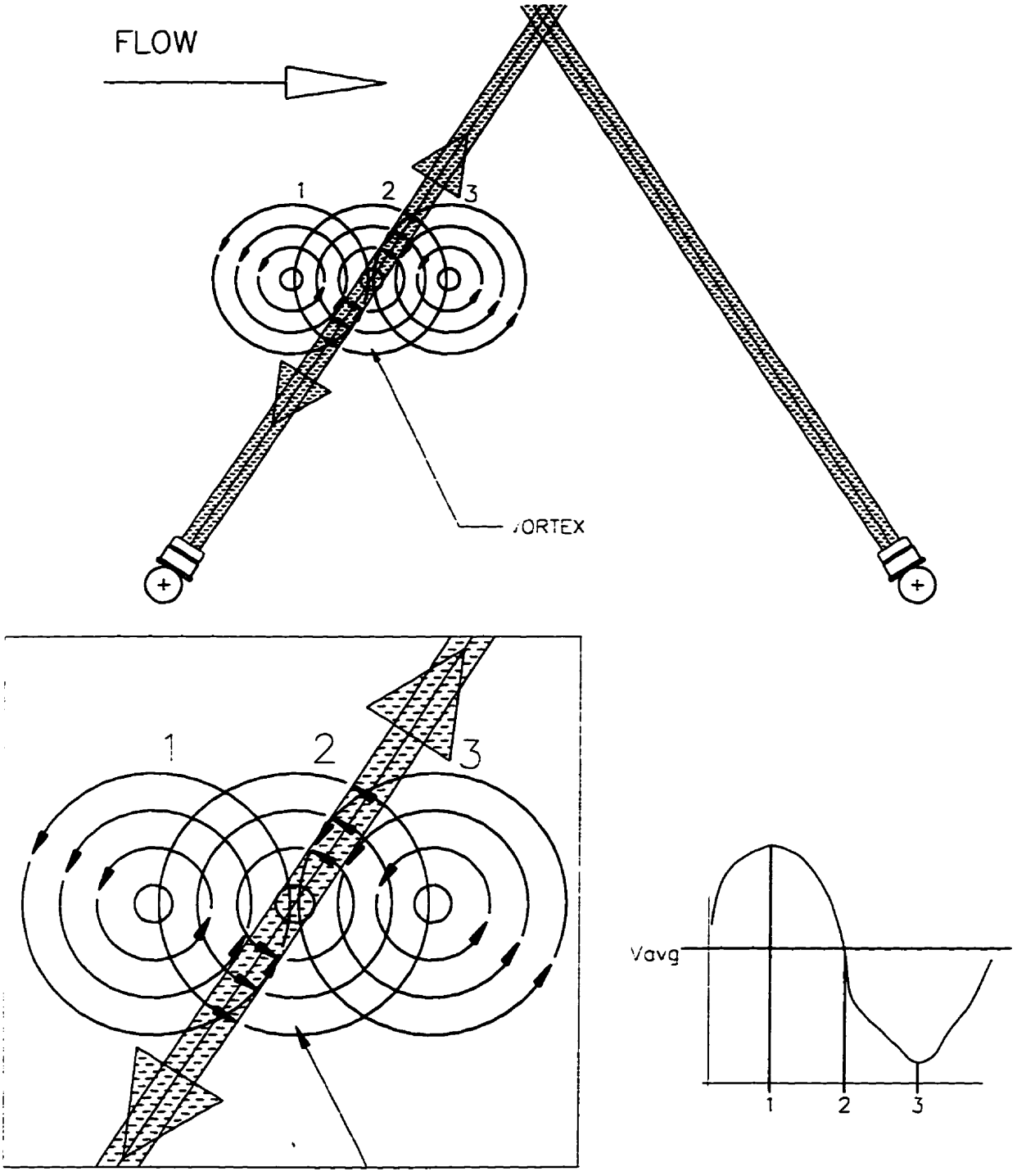

Figure 6.30 Advection of vortex across acoustic path.

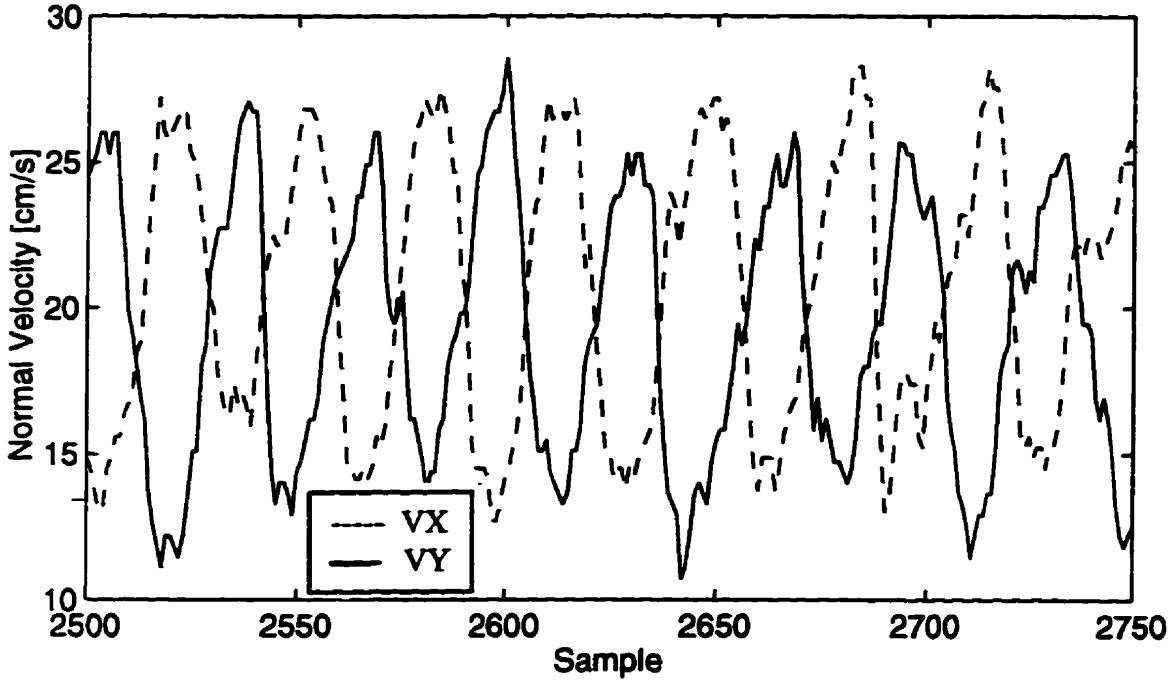

Figure 6.31 Braiding of X and Y velocity measurements due to vortex shedding (D4 flow condition).

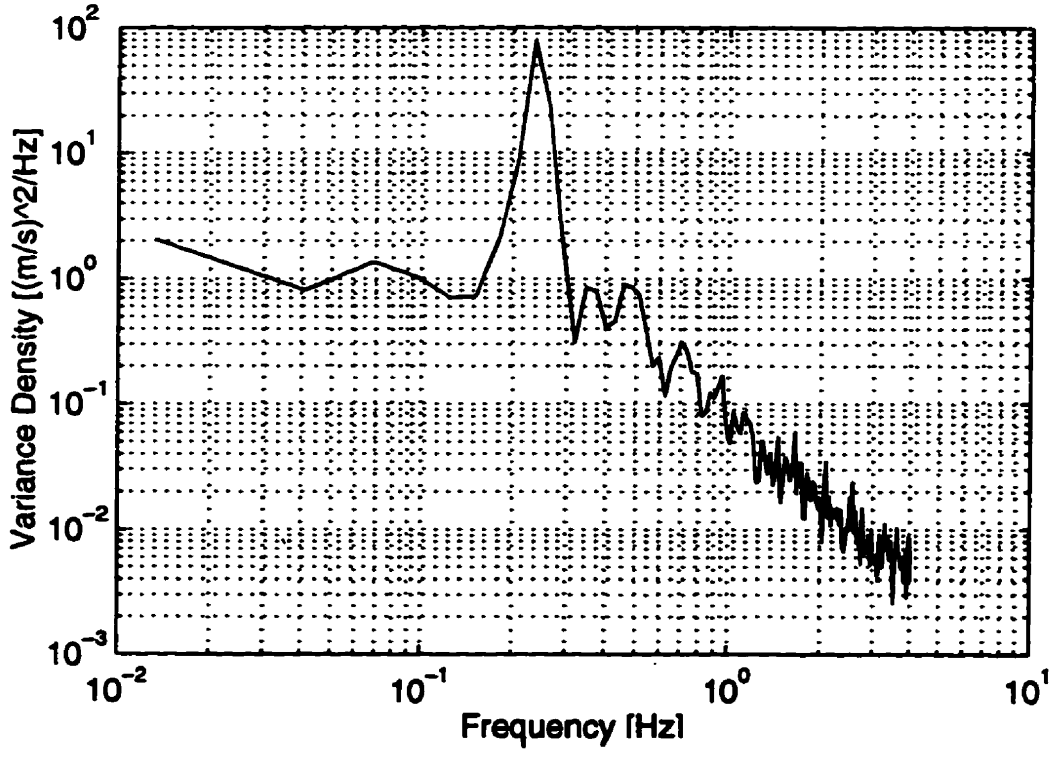

Figure 6.32 Variance density of 15 minute stationary record (D4 flow condition). (50 degrees of freedom, Δf=0.028 Hz).

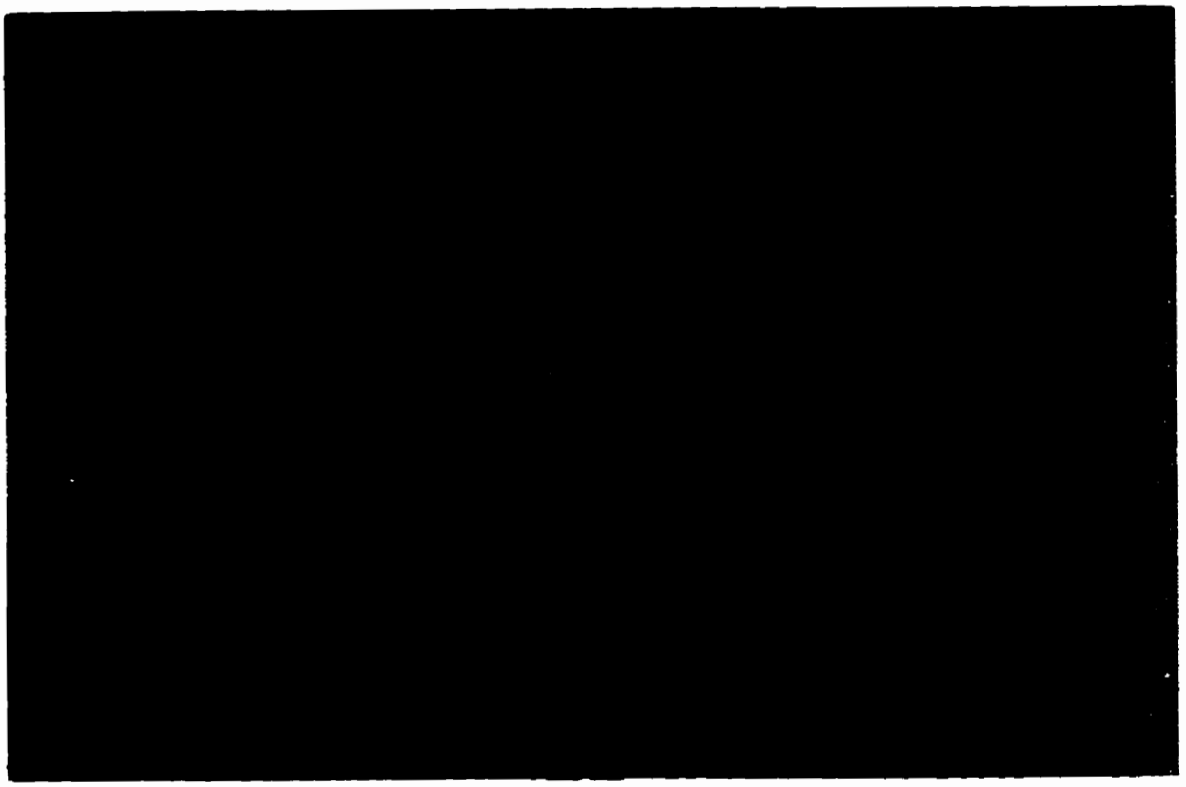

Figure 6.33 Disturbance 5.

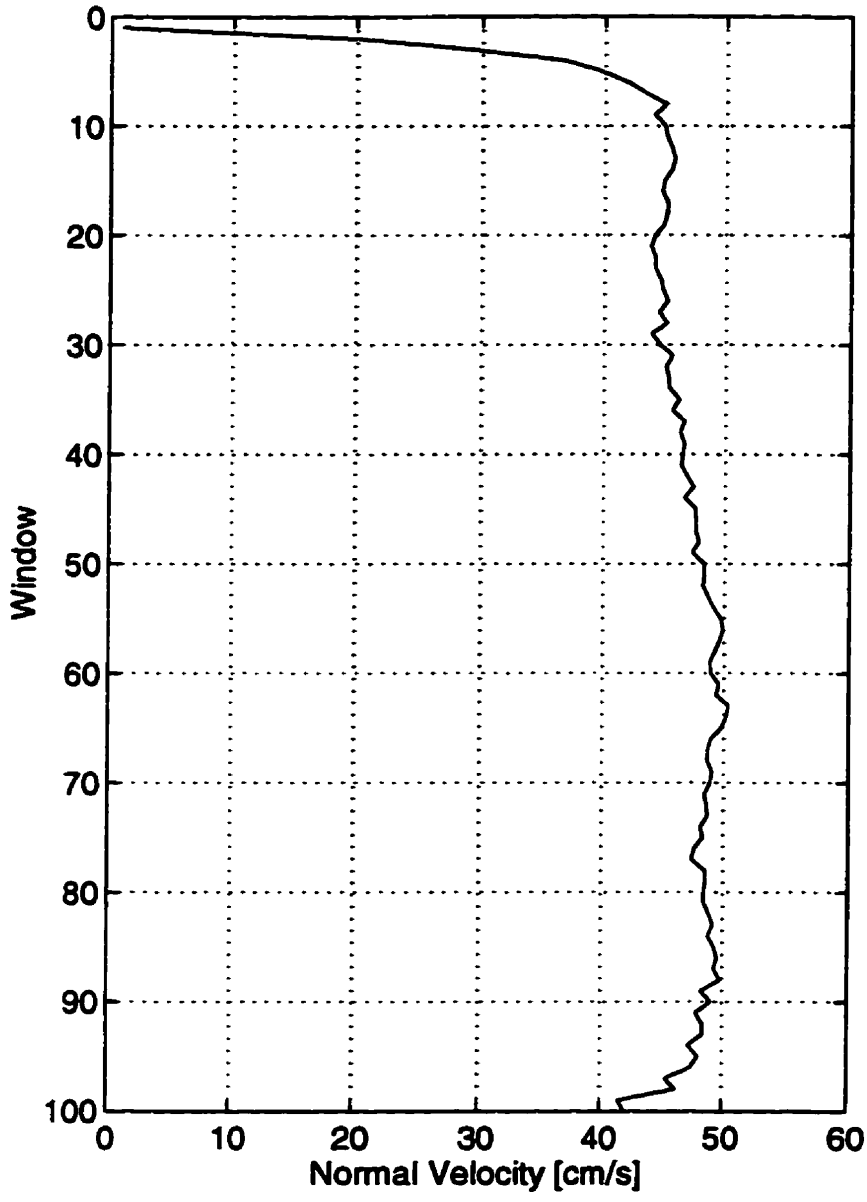

Figure 6.34 Smoothed velocity profile for D5 flow condition (Q=460.7 l/s).

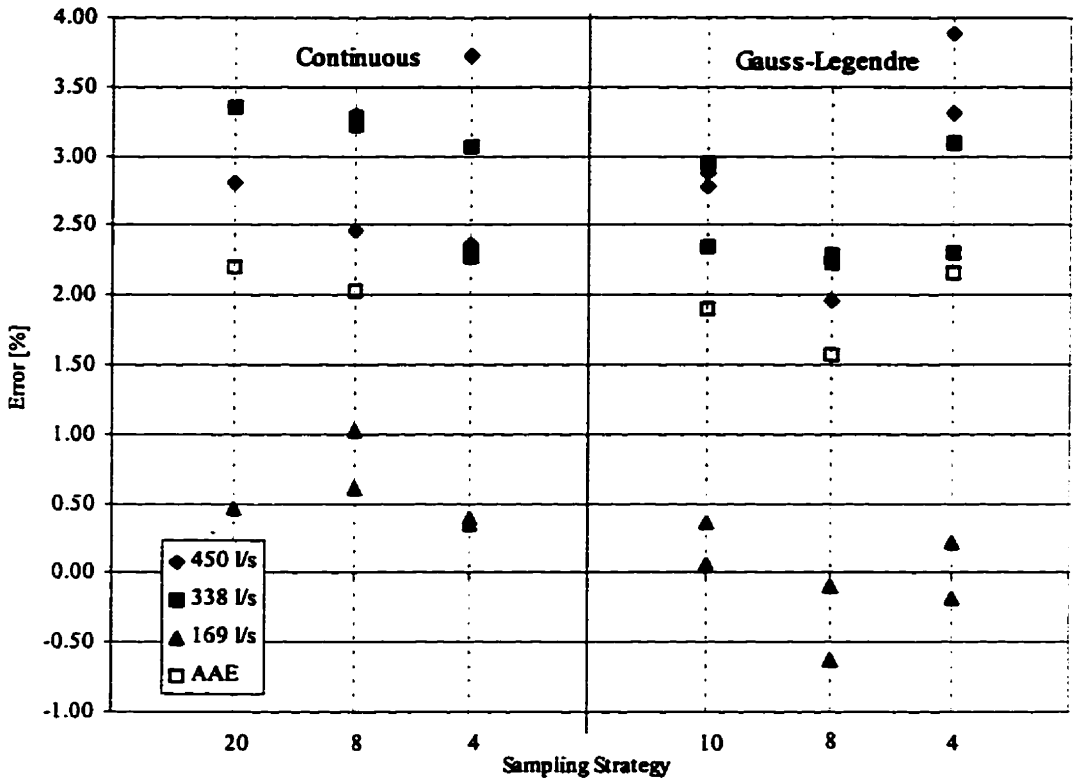

Figure 6.35 Comparison of sampling strategies for D5 flow condition.

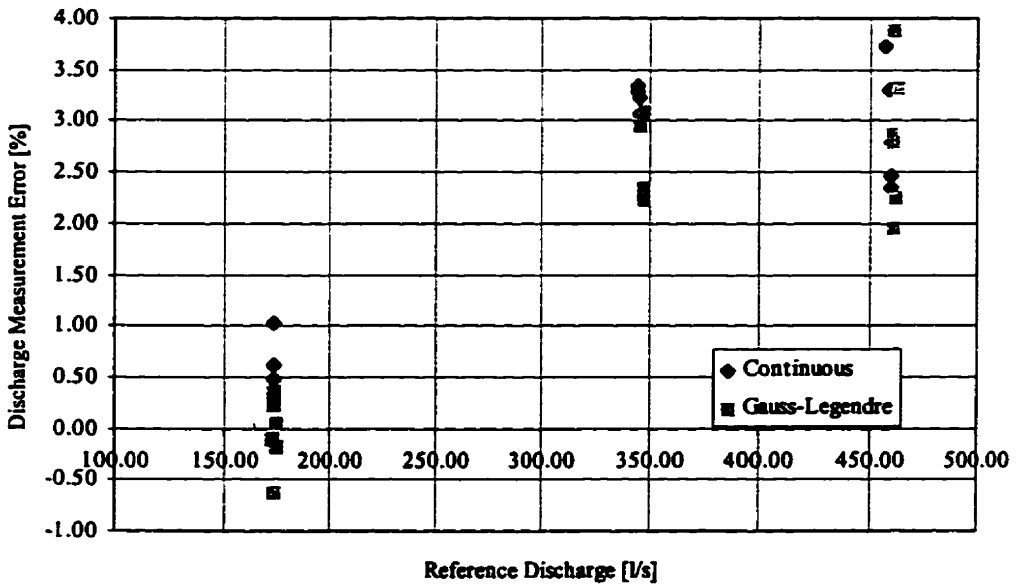

Figure 6.36 Distribution of error with flowrate (D5 flow condition).

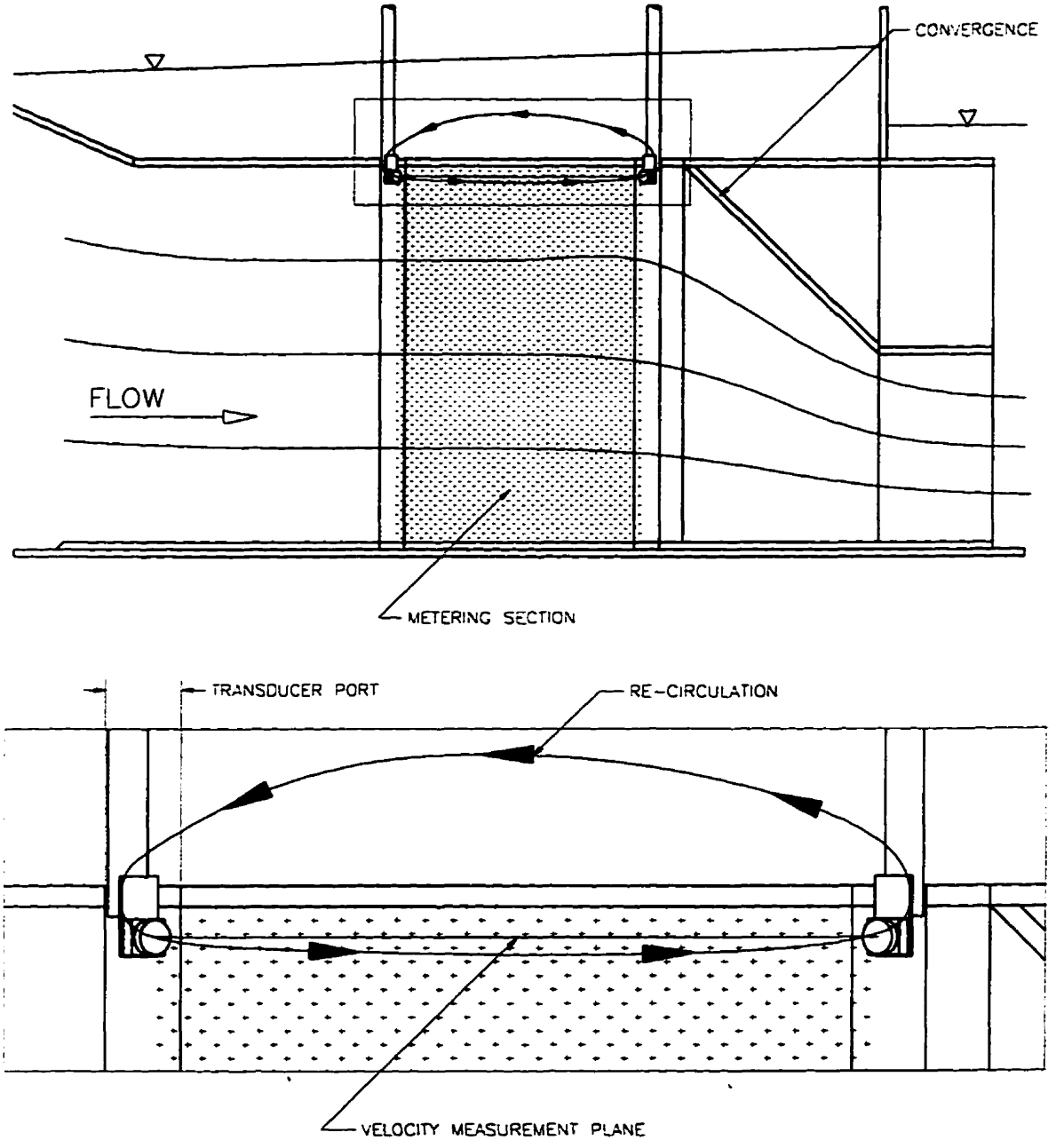

Figure 6.37 Circulation in D5 flow condition.

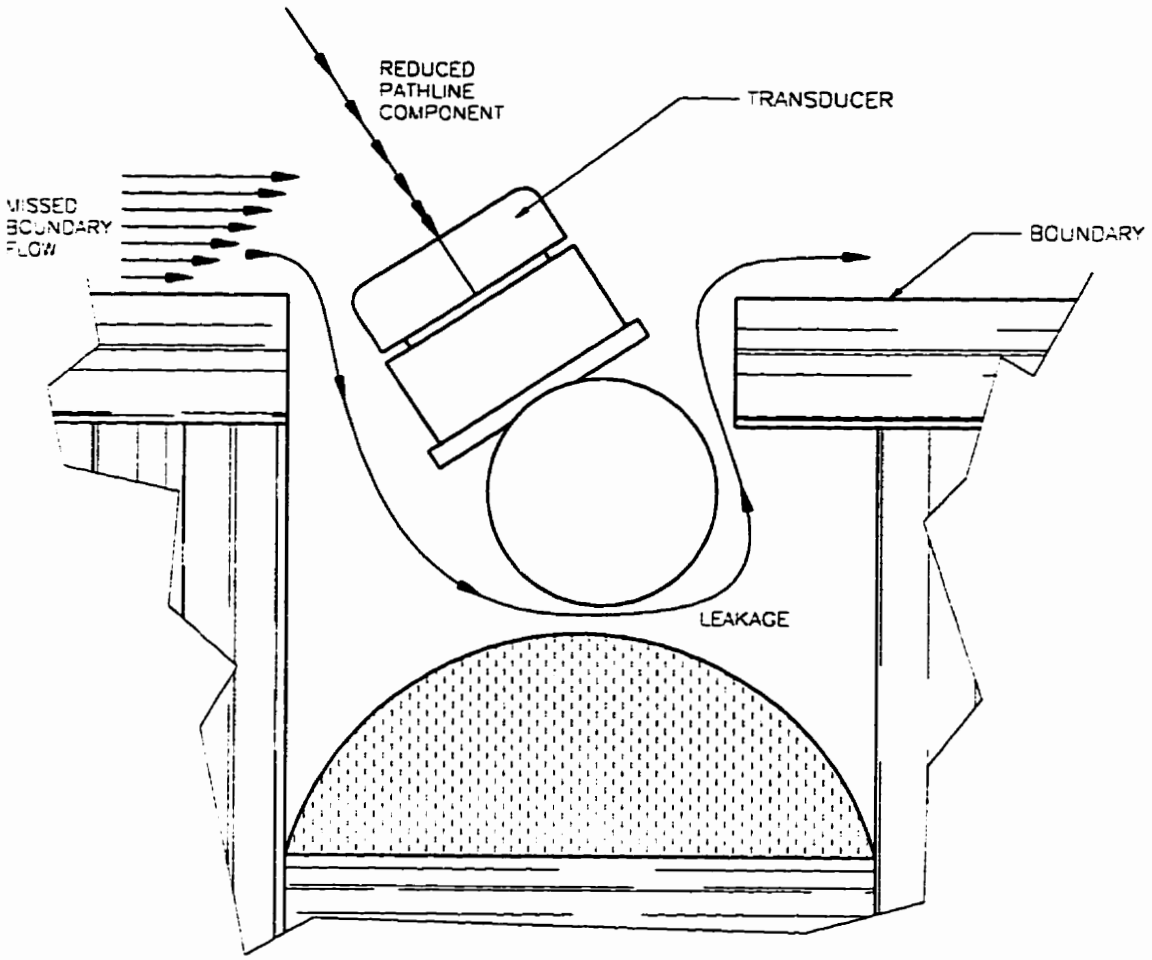

Figure 6.38 Protrusion effect and leakage.

CHAPTER 7
SUMMARY AND RECOMMENDATIONS

7.1 SUMMARY OF RESULTS

It is imperative that generator/turbine unit performance relationships be accurately known to efficiently produce hydroelectricity. Of the information required to develop these relationships, discharge is the most difficult to obtain. The current-meter technique is the traditional approach employed at low-head plants. One shortcoming of this technique is the inability to accurately integrate the complex velocity profiles observed at low-head plants with a limited number of point velocity measurements.

It has been proposed that transit-time acoustic velocimetry be applied to performance testing at low-head hydroelectric plants. The proposed technique involves continuously traversing an array of acoustic cells down the stop-log guides while measuring the chordal average normal water velocity. The primary function of this technique is to provide a complete integration of the complex velocity profile typical to low-head plants, which will lead to more accurate discharge measurement and, in turn, improved accuracy of performance testing. The initial development of this technique consisted of laboratory testing of a single acoustic cell at the Hydraulics Research and Testing Facility, University of Manitoba.

A model intake structure was constructed to evaluate the performance of the acoustic cell, consisting of two crossed acoustic paths, under varying flow conditions. The ADM system was successfully calibrated and verified to the reference discharge measurement resulting in a systematic difference of less than 0.5 %.

Various continuous and discrete Gauss-Legendre sampling strategies were evaluated under favorable (*i.e.*, relatively uniform) flow conditions and complex velocity profiles. In agreement with the literature, higher order discrete sampling techniques performed as

well or better than the continuous sampling strategy in favorable flow conditions. However, under these conditions, the susceptibly of lower order GL traverses to systematic integration error was well-defined. The repeatability of the continuous traverses, suggested that the variability of the velocity profile was adequately sampled to reduce the random error of the integration.

Introducing a number of complexities to the flow profile provided valuable insight to the performance of the ADM technique and various sampling strategies under non-favorable flow conditions. Simple continuous traversing, in general, resulted in more accurate discharge measurement than GL sampling. The systematic error of lower order GL integration dramatically increased from the results obtained in favorable flow conditions whereas continuous traversing produced relatively accurate discharge measurements. Furthermore, when considering the time requirements of the two sampling methods, the continuous method was certainly more efficient.

Introducing a large scale vertical disturbance shortly upstream of the metering section resulted in relatively poor discharge accuracy using ADM. The explanation for this error was two-fold, first the resultant velocity direction of the portion of flow sampled by each individual acoustic path was different; this translated to a positive bias in the calculated average normal velocity. Secondly, the separation zone behind the disturbance was not consistent over the length of the discharge measurement section. This testing series illustrated that, to determine accurate line averages of velocity, the velocity distribution and direction in the plane of the acoustic paths must be consistent over the length of the measurement section. The direct implication of this statement is that short metering sections should be used.

A downstream convergence was added to the intake ceiling in an attempt to address the effects of non parallel flowlines in the vertical plane. However, a circulation problem precluded any definitive statements on the performance of ADM under these conditions.

An optimal continuous traverse rate was not identified from the test results. A limited number of tests for each flow disturbance, traverse rate and discharge level were performed. This, in combination with the variability in measurement error across flowrates, precluded a statistically grounded comparison between every sampling strategy. However, in light of the testing results, it can be concluded that the upper limit of the traverse rate was not reached. At this point, assumption of velocity profile stability would be violated and the random error of the CTR integration would dominate. The repeatability of the CTR4 traverses indicated that this was not the case.

Sources of error for the ADM technique were identified and estimated in the context of the laboratory experiment. The considerable systematic uncertainty, primarily due to the zero offset of the instrumentation and path angle measurement, was absorbed in the calibration. Integration error was not directly calculated, however it can be stated that this error would primarily consist of random error for a continuous traverse and systematic error for a discrete sampling technique.

The results from this study suggested that the proposed technique will provide improved discharge measurement accuracy over the existing current-meter practice. The argument of continuous versus discrete sampling techniques is certainly applicable as the current-meter method is based on discrete velocity measurements in both dimensions of the metering plane. In addition, high frequency flow phenomena (*e.g.*, vortex shedding) and flow reversals can be accurately measured using this technique.

Based on the work documented in this thesis, a number of conclusions pertinent to the field application of traversing ADM can be made:

1) Lower order Gauss-Legendre sampling techniques (*e.g.*, $N \leq 8$) are susceptible to systematic error for complex velocity profiles. In a qualitative manner, this statement also applies to other methods where few discrete velocity samples are made.

2) Random error would be the primary component of the integration error for a continuous traverse method.

3) Relative to discrete sampling techniques, the continuous traverse method is potentially more efficient.

4) Considerable systematic error can result if the velocity profile, in the same plane as the acoustic paths, is not consistent over the length of the metering section.

7.2 RECOMMENDATIONS

After reviewing the literature on discharge measurement techniques and performing considerable laboratory testing of the proposed ADM technique, a number of recommendations for future research and practice are proposed.

Recommendations for Future Laboratory Testing

Promising results from the continuous traverse ADM tests suggested that this technique should be further pursued. Additional evaluation of the single cell configuration is necessary. First, the performance of the single cell should be studied for water speeds in the typical range of the field application. Under these conditions, vibration and aliasing effects would be addressed. Secondly, the cosine response of the acoustic paths should be directly tested since flows in low-head applications typically converge in the vertical direction. Furthermore, assessment of the ability to resolve the normal velocity component for different path angles would be valuable. These additional evaluations are best-suited to tow-tank testing, where the normal velocity component can be directly compared to a reference value (*i.e.*, cart speed); this would eliminate the discharge calculation error from the evaluation.

'Multiple cell' testing is recommended. Disturbance effects, such as the protrusion effect, certainly require attention. Also, the effect of cross-flow between cells on the accuracy of resolving the average normal velocity component should be studied. Again, testing at a tow-tank facility would support a direct evaluation of these effects.

Unlike existing stationary ADM installations, the proposed technique is intrusive because a carriage would be lowered across the turbine intake. Further study should be devoted to improving the geometry of the carriage to reduce the disturbance effects. Non-prismatic elliptical sections could be used to reduce the disturbance effect of the transducer struts; such sections have been used for mounting Ott meters to traversing carriages.

Recommendations for Field Discharge Measurement for Performance Testing

The D4 testing series revealed key limitations of ADM to resolving the true normal velocity component when the velocity profile in the plane of the acoustic paths is not of constant shape and/or direction over the length of the metering section. This is a realistic situation if the metering section is in close proximity (*e.g.*, less than 5 length scales) to upstream vertical disturbances such as large trash-rack beams. The planar velocity profile may also change if the intake rapidly converges in the horizontal direction. This effect is reduced by shortening the metering section through larger path angles and/or shorter path lengths, but these measures have their shortcomings. Larger path angles increase the potential for systematic discharge error due to path misalignment. Also, timing error becomes a concern since transit-time differences are reduced if path angles are increased or the path lengths are reduced. A definite trade-off exists, which warrants careful consideration.

Systematic errors associated with measuring the normal velocity component using ADM were identified. Since an accurate calibration cannot be performed in the field, these errors should be accurately calculated and the measurements should be adjusted accordingly.

After comparing the performance of a range of continuous and discrete (Gauss-Legendre) sampling strategies, a few recommendations can be stated regarding the sampling strategies used for performance testing of low-head hydroelectric turbines. Low order Gauss-Legendre sampling strategies can produce significant systematic errors when sampling a complex velocity profile. Moreover, limited level discrete sampling strategies may not adequately integrate a complex velocity profile and should be avoided. Continuous traversing of high-frequency velocity measurement instrumentation may better capture a complex velocity profile. The stability of the velocity profile will affect the random error of a discharge measurement from a continuous traverse method.

Instrumentation containing signal recognition circuitry that is capable of identifying missed acoustic pulses (due to attenuation) should be employed. It is quite likely that some air entrainment and suspended material would be present in the field. Lower frequency transducers should be considered for field application as: 1) the lower frequency signals are less susceptible to attenuation; and 2) missed pulses would be easier to identify.

The laboratory testing results suggest that traversing instrumentation that measures a single chord average normal velocity at a high sampling rate can be used to accurately calculate total discharge. Given this, considerable attention should be devoted to the current research and field testing of the acoustic scintillation flow measurement method by Lemon *et al.* (1996).

REFERENCES

American Society of Mechanical Engineers, 1992. Standard PTC-18, "Performance Test Code for Hydraulic Turbines."

Bell, P.W. and Lemon, D.D., 1996. Measuring Hydraulic Turbine Discharge with the Acoustic Scintillation Flowmeter, *Proceedings IGHEM Seminar - Montreal'96*, Paper n. 20.

Birch, R. and Lemon, D.D., 1995. Non-Intrusive Flow Measurement Techniques for Hydroelectric Applications, *Proceedings of the 1995 International Conference on Hydropower*, ASCE, v. 3, pp. 2049-2058.

Birch, R. and Lemon, D.D., 1993. Acoustic Flow Measurement at the Rocky Reach Dam, *Proceedings Waterpower '93*, ASCE, pp. 2187-2196.

Clay, C.S. and Medwin, H., 1977. Acoustical Oceanography, John Wiley & Sons Inc..

Clifford, S.F. and Farmer, D.M., 1983. Ocean Flow Measurements Using Acoustic Scintillation, *Acoustical Society of America*, v. 74, n. 6, pp. 1826-1832.

Dube, L., 1985. Turbine Efficiency Measurement by Ultrasonic Methods, *Water Power & Dam Construction*, May 1985, pp. 15-19.

Flint-Peterson, L. and Rajaratnam, N., 1987. A Method to Measure Discharge in Pipelines, *Journal of Pipelines*, n. 6, pp. 319-323.

Grego, G., 1996. Comparative Flowrate Measurements at the Caneva Generating Plant Unit 2, *Proceedings IGHEM Seminar - Montreal'96*, Paper n. 14.

Gulliver, J.S. and Arndt, R.E.A., 1991. Hydropower Engineering Handbook, McGraw-Hill Inc..

International Electrotechnical Commission, 1991. Standard IEC-41-1991, "Field acceptance tests to determine the hydraulic performance of hydraulic turbines, storage pumps and pump-turbines."

Lanning, C.C. and Ehrhart, R.W., 1977. Application of Acoustic Velocity Flowmeters, *Journal of American Water Works Association*, v. 69, pp. 102-105.

Lawrence, R.S., Ochs, G.R., and Clifford, S.F., 1972. Use of Scintillations to Measure Average Wind Across a Light Beam, *Applied Optics*, v. 11, n. 2, pp. 239-243.

Lemon, D.D., 1995. Measuring Intake Flows in Hydroelectric Plants With an Acoustic Scintillation Flowmeter, *Proceedings of the 1995 International Conference on Hydropower*, ASCE, v.3, pp. 2039-2048.

Levesque, J., 1994. Measuring Flow with Pressure-Time Current Meter Methods, *Hydro Review*, v. 13, n. 5, 99. 102-109.

Lowell, F.C. and Walsh, J.T., 1991. Performance Analysis of Multipath Acoustic Flowmeters Under Various Hydraulic Conditions, *Proceedings of the International Conference on Hydropower*, ASCE, v. 3, pp. 2041-2050.

Lowell, F.C. and Hirschfeld, F., 1979. Acoustic Flowmeters for Pipelines, *Mechanical Engineering*, v. 101, n. 10, pp. 23-35.

Mikhail, A., 1994. Turbine Performance Testing Using the Intake Current-Meter System (ICMS), *Proceedings Canadian Electrical Association Conference*, Engineering and Operating Division.

Missimer, J.R., March, P.A., Voss, A.W. and Sullivan, C., 1986. A Comparison of Flow Measurements Using Acoustic and Volumetric Techniques at Raccoon Mountain Dumped Storage Plant, *Proceedings 4th International Symposium on Hydro Power Fluid Machinery*, pp. 239-243.

MSR, 1992. *Product Operator Manual*, "MSR Magmeter, Magnum Version 2.00," MSR Edmonton, Canada.

Nielsen, K.L., 1964. Methods in Numerical Analysis, 2nd Ed., Macmillan.

Nystrom, J.B., 1991. Application of Personal Computers to Field Flow Measurement, *Proceedings International Conference on Hydropower*, v. 3, pp. 2254-2263.

Schuster, J.C., 1975. Measuring Water Velocity by Ultrasonic Flowmeter, *Journal of the Hydraulics Division*, ASCE, v. 101, n. 12, pp. 1503-1517.

Simpson, M. and Oltmann, R., 1993. Discharge-Measurement System Using an Acoustic Doppler Current Profiler with Applications to Large Rivers and Estuaries, U.S. Geological Survey Water Supply Paper n. 2395.

Spencer, D., 1986. R&D Status Report, Advanced Power Systems Division, *EPRI Journal*, v. 18, n. 8, pp. 41-43.

Sugishita, K., Sakurai, A., Tanaka, H. and Suzuki, T., 1996. Evaluation of Error of Acoustic Method and its Verification by Comparative Field Tests, *Proceedings IGHEM Seminar - Montreal'96*, Paper n. 31.

Tritton, D.J., 1977. Physical Fluid Dynamics, Van Nostrand Reinhold, Ltd..

Trivett, A., Bowen, A.J., and Snow, J., 1996. VDV: An Environmental Flow Sensor With Some Unique Capabilities, *Proceedings Oceanology International*.

Trivett, A., Bowen, A.J., Bowers, C., Bowers, K., McKay, R., Snow, J., and Woodside, S., 1995. VDV: A New Oceanographic Sensor, *Proceedings 1995 Canadian Coastal Conference, CCSEA*, v. 2, pp. 867-874.

Trivett, A., Terray, E.A. and Williams III, A.J., 1991. Error Analysis of an Acoustic Current Meter, *IEEE Journal of Oceanic Engineering*, v. 16, n. 4, pp. 329-337.

Voser, A., 1996. CFD-Calculations of the Protrusion Effect and Impact on the Acoustic Discharge Measurement Accuracy, *Proceedings IGHEM Seminar - Montreal '96*, Paper n. 35.

Voser, A., Bruttin, C., Prenat, J., and Staubli, S., 1996. Improving Acoustic Flow Measurement, *International Water Power & Dam Construction*, v. 48, n. 4, pp. 30-34.

Walsh, J.T., Ludewig, P., Knowlton, R., Hermo, M., and Halas, R., 1996. Performance of an 18 path Acoustic Flowmeter at Robert Moses Niagara Power Plant Unit 13, *Proceedings IGHEM Seminar - Montreal '96*, Paper n. 22.

Winstone, C.R., 1989. Manitoba Hydro Technical Report, " Ott meter program: Long Spruce Generating Station."

APPENDIX A

GAUSS-LEGENDRE INTEGRATION

A. GAUSS-LEGENDRE INTEGRATION

Consider the following integral

$$I = \int_{a'}^{b'} v(h)dh \,. \tag{A.1}$$

The principle of Gaussian integration is to find the best subdivision of the interval [h_0, h_1], the value of the function at these points and the coefficients to multiply the functional values to yield the value of the definite integral. To keep the algebra simple and to maintain generality, the integral is transformed to [-1,1] using

$$h = \frac{(h_1 + h_0)}{2} + \frac{(h_1 - h_0)}{2} x \,. \tag{A.2}$$

With this transformation, the integral is given by

$$I = \int_{h_0}^{h_1} v(h)dh = \frac{(h_1 - h_0)}{2} \int_{-1}^{1} v\left(\frac{(h_1 - h_0)x + (h_1 + h_0)}{2}\right)dh = \int_{-1}^{1} f(x)dx \,. \tag{A.3}$$

The Gauss-Quadrature integration rule can be written as

$$I \cong \sum_{i=1}^{N} w_i f(x_i) = w_1 f(x_1) + w_2 f(x_2) + w_3 f(x_3) + \cdots + w_N f(x_N) \,. \tag{A.4}$$

This integration rule has $2N$ unknown constants consisting of the weights w_i and the ordinates x_i. It can be shown (*e.g.*, Nielsen, 1965) that these constants can be determined so that the integration rule is exact for all polynomials of order less than or equal to $2N$-1.

If the highest order of the polynomial $f(x)$ is $2N$-1, then $f(x)$ may be written as

$$f(x) = a_0 + a_1 x + a_2 x^2 + a_3 x^3 + \cdots + a_{2N-1} x^{2N-1}. \tag{A.5}$$

From this,

$$\begin{aligned} \int_{-1}^{1} f(x)dx &= \left(a_0 x + \tfrac{1}{2} a_1 x^2 + \tfrac{1}{3} a_2 x^3 + \tfrac{1}{4} a_3 x^4 + \cdots + \frac{1}{2N} a_{2N-1} x^{2N} \right) \Bigg|_{-1}^{1} \\ &= 2a_0 + \tfrac{2}{3} a_2 + \tfrac{2}{5} a_4 + \cdots. \end{aligned} \tag{A.6}$$

Substituting x_i (i = 1 to N) into the polynomial of equation (A.5) yields the N values of equation A.5

$$f(x_i) = a_0 + a_1 x_i + a_2 x_i^2 + a_3 x_i^3 + \cdots + a_{2N-1} x_i^{2N-1}. \tag{A.7}$$

Equation (A.4) can then be written as

$$\begin{aligned} \int_{-1}^{1} f(x)dx = {} & w_1 \left(a_0 + a_1 x_1 + a_2 x_1^2 + a_3 x_1^3 + \cdots + a_{2N-1} x_1^{2N-1} \right) \\ & + w_2 \left(a_0 + a_1 x_2 + a_2 x_2^2 + a_3 x_2^3 + \cdots + a_{2N-1} x_2^{2N-1} \right) \\ & + w_1 \left(a_0 + a_1 x_3 + a_2 x_3^2 + a_3 x_3^3 + \cdots + a_{2N-1} x_3^{2N-1} \right) \\ & \vdots \\ & + w_N \left(a_0 + a_1 x_N + a_2 x_N^2 + a_3 x_N^3 + \cdots + a_{2N-1} x_N^{2N-1} \right) \\ = {} & a_0 (w_1 + w_2 + w_3 + \cdots + w_N) \\ & + a_1 (w_1 x_1 + w_2 x_2 + w_3 x_3 + \cdots + w_N x_N) \\ & + a_2 (w_1 x_1^2 + w_2 x_2^2 + w_3 x_3^2 + \cdots + w_N x_N{}^2) \\ & \vdots \\ & + a_{2N-1} (w_1 x_1^{2N-1} + w_2 x_2^{2N-1} + w_3 x_3^{2N-1} + \cdots + w_N x_N^{2N-1}) \end{aligned} \tag{A.8}$$

Since equations (A.6) and (A.8) must be identical for all values of a_i, the coefficients of a_i must be equal. This results in the following system of $2N$ equations.

$$\begin{aligned} w_1 + w_2 + w_3 + \cdots + w_N &= 2 \\ w_1 x_1 + w_2 x_2 + w_3 x_3 + \cdots + w_N x_N &= 0 \\ w_1 x_1^2 + w_2 x_2^2 + w_3 x_3^2 + \cdots + w_N x_N^2 &= \tfrac{2}{3} \\ w_1 x_1^3 + w_2 x_2^3 + w_3 x_3^3 + \cdots + w_N x_N^3 &= 0 \\ &\vdots \\ w_1 x_1^{2N-1} + w_2 x_2^{2N-1} + w_3 x_3^{2N-1} + \cdots + w_N x_N^{2N-1} &= 0 \end{aligned} \tag{A.9}$$

This system of equations is reduced to a set of linear equations if the x_i are assigned to be the zeros of the orthogonal Legendre polynomials (hence the name, Gauss-Legendre). The Legendre zeros and the resulting weights w_i are listed in Table A.1.

The truncation error of a N^{th} order GL integration is proportional to the $2N^{th}$ derivative of the function being integrated, evaluated at a point c' between a' and b'. Table A.1 includes the truncation error for N from 2 to 12.

Table A.1 Gauss-Legendre ordinates, weights and truncation error.

N	*Ordinates,* x_i	*Weights,* w_i	*Truncation Error* $(a' < c' < b')$
2	±0.577 350 269	1.000 000 000	$\frac{f^{(4)}(c')}{135}$
4	±0.339 981 044 ±0.861 136 312	0.652 145 155 0.347 854 845	$\frac{f^{(8)}(c')}{3{,}472{,}875}$
6	±0.238 619 186 ±0.661 209 387 ±0.932 469 514	0.467 913 935 0.360 761 573 0.171 324 492	$\frac{f^{(12)}(c')2^{13}[6!]^4}{[12!]^3 13!}$
8	±0.183 434 643 ±0.525 532 410 ±0.796 666 477 ±0.960 289 857	0.362 683 783 0.313 706 646 0.222 381 035 0.101 228 536	$\frac{f^{(16)}(c')2^{17}[8!]^4}{[16!]^3 17!}$
10	±0.148 874 339 ±0.433 395 394 ±0.679 409 568 ±0.865 063 367 ±0.973 906 529	0.295 524 225 0.269 266 719 0.219 086 363 0.149 451 349 0.066 671 344	$\frac{f^{(20)}(c')2^{21}[10!]^4}{[20!]^3 21!}$
12	±0.125 233 409 ±0.367 831 499 ±0.587 317 954 ±0.769 902 674 ±0.904 117 256 ±0.981 560 634	0.249 147 046 0.233 492 537 0.203 167 427 0.160 078 329 0.106 939 326 0.047 175 336	$\frac{f^{(24)}(c')2^{25}[12!]^4}{[24!]^3 25!}$

APPENDIX B

POSITION CONTROLLER PROGRAMS

DMC PROGRAM: CTR20
POSITION CONTROLLER PROGRAM

```
#CTR20
KI 1
TL 9.5
ER 2000
OE 1
C=1
SP 1179
AC 10000
DC 10000
DP 0
MG " "
MG "CTR20 - CONTINUOUS TRAV"
MG "20 MIN, 9676 REC"
MG " "
MG "VERIFY AT STATION 00000"
MG " "
MG "IF NOT, RESET DMC NOW!"
WT 5000
MG " "
MG "BEGIN TIMING"
MG " "
WT 10000
MG "TRAVERSING"
PA -1415197
BG
AM
MG " "
MG "TRAVERSE COMPLETE"
MG " "
MG "TL SET TO 9.5, SP 6000"
MG "TO POSITION 0: PR 1,415,197"
MG " "
EN
```

DMC PROGRAM: GL8
POSITION CONTROLLER PROGRAM

```
#GL8
KI 1
TL 9.5
ER 2000
OE 1
SP 8000
AC 20000
DC 20000
DP 0
MG " "
MG "GL8 - 8PT GAUSS-L"
MG "2 MIN/STA, 968 POINTS/LEVEL"
MG " "
MG "VERIFY AT STATION 00000"
MG " "
MG "IF NOT, RESET DMC NOW!"
WT 5000
MG " "
MG "BEGIN TIMING"
MG " "
WT 10000
MG "TRAVERSING"
PA -28099
BG
AM
MG " "
MG "AT STATION 1"
WT 120000
MG "TRAVERSING"
PA -143879
BG
AM
MG " "
MG "AT STATION 2"
WT 120000
MG "TRAVERSING"
PA -335733
BG
AM
MG " "
MG "AT STATION 3"
WT 120000
MG "TRAVERSING"
PA -577800
BG
AM
MG " "
MG "AT STATION 4"
WT 120000
MG "TRAVERSING"
PA -837397
BG
AM
```

```
MG " "
MG "AT STATION 5"
WT 120000
MG "TRAVERSING"
PA -1079464
BG
AM
MG " "
MG "AT STATION 6"
WT 120000
MG "TRAVERSING"
PA -1271319
BG
AM
MG " "
MG "AT STATION 7"
WT 120000
MG "TRAVERSING"
PA -1387098
BG
AM
MG " "
MG "AT STATION 8"
WT 120000
MG " "
MG "STOP LOGGING DATA"
MG "RETURNING TO STATION 0000"
PA 0
BG
AM
MG " "
MG "AT STATION 0, PROGRAM COMPLETE"
MG " "
EN
```

APPENDIX C

MATLAB SCRIPTS FOR POST-PROCESSING

MATLAB SCRIPT: CTR 1.2
POST-PROCESSING OF CONTINUOUS TRAVERSE DATA

```
% ************************************************************
% CTR_12
% ************************************************************

% Version: 1.2 (12/05/96)

% Script file to clean Magmeter and VDV data and to calculate measured
% discharge from VDV velocity measurements.
% The calibrated slew rate of the DTV circuits and zero offset adjustments are
% applied.

% Input files:
%     _ v*.log   logged vdv data
%       m*.log   raw magmeter data (reference discharge)
%
% Output files:
%       <datafile>.res     % discharge measurement results and error
%       <datafile>.w       % used by GL Mfiles to extract expected average velocity

disp(' ')
disp('**********************')
disp('CTR_1.2')
disp('**********************')
disp(' ')
clear

% filename specification and data loading
   load c:\users\kevin\logfiles\dist4\v?????.log
   load c:\users\kevin\magfiles\dist4\m?????.txt
   f=v?????;
   m=m?????;
   testname='Test ?????';
   datafile='d?????';

% ************************************************************
% User defined trial specific parameters.
   dstart=??;                    % number of records prior to record 0
   temp=??.??;                   % temperature of water [deg C]
   depth=1.???;                  % depth of water [m]
   duration=??;                  % number of minutes of traverse [min]
% ************************************************************

% ************************************************************
% Define other parameters.
   lowdev=40;                    % acceptable deviation from expected average [cm/s]
   highdev=40;                   % acceptable deviation from expected average [cm/s]
   numwindow=200;                % number of windows to break logfile into for Q calculation
   threshold=20;                 % maximum standard deviation acceptable of Mag data [l/s]
   height=0.9985;                % height of intake [m]
   width=1.0013;                 % width of intake [m]
   thetaX=57.14;                 % angle between X pathline and net flow [deg]
   thetaY=57.06;                 % angle between Y pathline and net flow [deg]
```

```
   lX=117.0;                    % X pathlength [cm]
   lY=117.1;                    % Y pathlenght [cm]
   salinity=0;                  % salinity of water
% ********************************************************

% calculate total number of records logged during traverse
   nrec=duration*60*8.063;

% assign vectors for v and c counts
   vX=f(:,1);
   vY=f(:,2);
   cX=f(:,3);
   cY=f(:,4);

% assign vector names to V and C original VDV calibrated values
   VXv=f(:,5);
   VYv=f(:,6);
   CXv=f(:,7);
   CYv=f(:,8);

% determine the reference discharge from raw Magmeter output
   o_mag=m;
   o_magm=mean(m);
   c_mag=(8.69369+1.1062*m);  %(calibration performed on 96/10/20)

% clean Magmeter data
   c_magmeantemp=mean(c_mag);
   tmean=mean(c_mag);
   tc_mag=c_mag;
   c_maglen=length(c_mag);
   xm=(1:c_maglen);
   gc_mag=c_mag;
   not9999=(1:c_maglen);
   while std(tc_mag(not9999))>threshold;  % eliminate data until below specified std
      diff=max(abs(tc_mag(not9999)-mean(tc_mag(not9999))));
      worst=find(abs(tc_mag-mean(tc_mag(not9999)))==diff);
      firstworst=worst(1);
      tc_mag(firstworst)=9999;
      not9999=find(tc_mag~=9999);
   end
   g_cmagindex=not9999;                  % indeces of retained Mag data
   b_cmagindex=find(tc_mag==9999);       % indeces of discarded Mag data

% calculate mean and stdev of Mag data
   c_magmean=mean(c_mag(g_cmagindex));
   c_magstd=std(c_mag(g_cmagindex));
   ref_Q=c_magmean;

% plot Magmeter data
   figure(1)
   plot(g_cmagindex,c_mag(g_cmagindex),'g+',b_cmagindex,c_mag(b_cmagindex),'r+');
   xlabel('Sample')
   ylabel('Calibrated Discharge [l/s]')
   axis([0 c_maglen 0 1.4*c_magmean])
   text(.2*c_maglen,.8*c_magmean,'MAGQ_cal, std(MAGQ_cal)');
   text(.2*c_maglen,.6*c_magmean,num2str(c_magmean));
```

```
   text(.4*c_maglen,.6*c_magmean,num2str(c_magstd));
   grid
   title(testname)

% output reference Q data to display
   disp('o_magm   ref_Q    c_magstd')
   [o_magm ref_Q c_magstd]

% calculate expected average pathline velocity
   thetaavg=(thetaX+thetaY)/2;
   expavg=ref_Q/1000/(height*width)*100*cos(thetaavg*pi/180);

% discard initial data not taken during traverse
   vX=vX(dstart+1:dstart+nrec);
   vY=vY(dstart+1:dstart+nrec);
   cX=cX(dstart+1:dstart+nrec);
   cY=cY(dstart+1:dstart+nrec);
   VXv=VXv(dstart+1:dstart+nrec);
   VYv=VYv(dstart+1:dstart+nrec);
   CXv=CXv(dstart+1:dstart+nrec);
   CYv=CYv(dstart+1:dstart+nrec);

% eliminate laned data based on expected range of normal velocities
   sp=1;
   ep=nrec;
   denX=cos(thetaX*pi/180);
   denY=cos(thetaY*pi/180);
   datX=find(VXv(sp:ep)./denX < expavg+highdev & VXv(sp:ep)./denX > expavg-lowdev);
   datY=find(VYv(sp:ep)./denY < expavg+highdev & VYv(sp:ep)./denY > expavg-lowdev);
   ldatX=length(datX);
   ldatY=length(datY);

% calculate normal velocity components and statistics
   VXvn(datX)=VXv(datX)/denX;
   VYvn(datY)=VYv(datY)/denY;
   VXvnm=mean(VXvn(datX));
   VYvnm=mean(VYvn(datY));
   stdevVXv=std(VXvn(datX));
   stdevVYv=std(VYvn(datY));

% calculate original (non-calibrated) discharge
   avgVvn=(VXvnm+VYvnm)/2;
   o_Q=avgVvn/100*height*width;

% Determine empirical speed of sound value
   avgdepth=depth/2;       %average submergence of transducers
   Cemp=1449.2+4.6*temp-0.055*temp^2+0.00029*temp^3+(1.34-0.01*temp)*(salinity-
35)+0.016*avgdepth;

% ***********************************************************
% Apply calibration to VDV data
% ***********************************************************

% time delays
   ddelayX=(687.865E-6)+8e-6;
   ddelayY=(687.865E-6)+8e-6;
```

```
% calibrated constants
   c_calv=294465;
   c_vel_constant=1/2.0*5.0/4096/c_calv;

 % scaling of velocity constant by pathlength
   c_vsclX=c_vel_constant/lX;
   c_vsclY=c_vel_constant/lY;

% determine mean VDV results
   meanvXdat=mean(vX(datX)-2.5);
   meanvYdat=mean(vY(datY)+2);
   meanvdat=(meanvXdat+meanvYdat)/2;
   meanCdat=(mean(CXv(datX))+ mean(CYv(datY)))/2;

% calculate calibrated velocities for each station and resulting Q
% remove zero offset bias and apply calibrated velocity scale
   VXc=(vX-2.5).*100^2.*CXv.^2*c_vsclX/2;
   VYc=(vY+2).*100^2.*CYv.^2*c_vsclY/2;
   VXcn(datX)=VXc(datX)/denX;
   VYcn(datY)=VYc(datY)/denY;

% calculate window means:
   xlow=0;
   ylow=0;
   window =round(nrec/numwindow);
   for i=1:numwindow
         x=find(datX>=xlow & datX<=xlow+window);
         y=find(datY>=ylow & datY<=ylow+window);
         VXwind(i)=mean(VXcn(datX(x)));
         VYwind(i)=mean(VYcn(datY(y)));
         VRwind(i)=(VXwind(i)+VYwind(i))/2;
         xlow=xlow+window;
         ylow=ylow+window;
   end

% calculate overall means
   VXcnm=mean(VXwind(:));
   VYcnm=mean(VYwind(:));
   avgVcn=mean(VRwind(:));

% calculate measured discharge and error
   c_Q=avgVcn/100*height*width;
   Qerr=(1000*c_Q-ref_Q)/ref_Q*100;

% plot calibrated results
   figure(3);
   Xscl=round(2.5*avgVcn);
   VXcn=[VXcn]';
   VYcn=[VYcn]';
   plot(VXcn(datX),datX,'y--',VYcn(datY),datY,'b-.');
   axis('ij')
   axis([-5 Xscl 0 (nrec)]);
   xlabel('Calibrated Normal Velocity [cm/s]')
   ylabel('Sample')
   text(1,nrec-.3*nrec,'c_Q =');
```

```
   text(3,(nrec-.2*nrec),num2str(c_Q))
   legend('VXc','VYc',0);
   grid
   title(testname);

% output results to display
  disp('discharge error[%]')
  [Qerr]
  disp('lenghtX stdevX lenghtY stdevY ')
  [lenX std(VXcn(datX)) lenY std(VYcn(datY))]
  disp('Cemp meanCdat')
  [Cemp meanCdat]

% write results to file
   c=[ref_Q  1000*c_Q Qerr lenX lenY Cemp meanCdat];
   eval(['save ',datafile,'.c', ' c' ,' -ascii']);
   d=[VRwind'];
   eval(['save ',datafile,'.w', ' d' ,' -ascii']);
```

MATLAB SCRIPT: GL8 1.2
POST-PROCESSING OF 8 LEVEL GAUSS-LEGENDRE DATA

```
% ********************************************************
% GL8_12
% ********************************************************

% Version: 1.2 (11/13/96)

% Script file to clean Magmeter and VDV data, scale VDV data, segment
% GL points, and calculate discharge using 8 level Gauss-Legendre integration.

% Input files:
%       v*.log   logged vdv data
%       m*.log   raw magmeter data (reference discharge)
%
% Output files:
%       <datafile>.res     % discharge measurement results and error

disp(' ')
disp('**********************')
disp('GL8_1.2')
disp('**********************')
disp(' ')
clear

% filename specification and data loading

format long
load c:\users\kevin\logfiles\dist3\v?????.log
load c:\users\kevin\magfiles\dist3\m?????.txt
load c:\users\kevin\mfiles\d?????.w
w=d?????;
f=v?????;
m=m?????;
testname='Test ?????';
datafile='d?????';
file_length=length(f);


% ********************************************************
% User defined trial specific parameters.
   dstart=??;       % number of records prior to record 0
   temp=??.??;      % temperature of water [deg C]
   depth=1.???;     % depth of water [m]
% ********************************************************

% ********************************************************
% Define other parameters.
   lowdev=40;                   % acceptable deviation from expected average [cm/s]
   highdev=40;                  % acceptable deviation from expected average [cm/s]
   nrec=968;                    % number of records/station (2 minute sampling duration)
   threshold=20;                % maximum standard deviation acceptable of Mag data [l/s]
   height=0.9985;               % height of intake [m]
   width=1.0013;                % width of intake [m]
```

```
  thetaX=57.14;                % angle between X pathline and net flow [deg]
  thetaY=57.06;                % angle between Y pathline and net flow [deg]
  lX=117.0;                    % X pathlength [cm]
  lY=117.1;                    % Y pathlenght [cm]
  salinity=0;                  % salinity of water
% ************************************************************

% assign vector to window data
  window=w(:);

% assign vectors for v and c counts
  vX=f(:,1);
  vY=f(:,2);
  cX=f(:,3);
  cY=f(:,4);

% assign vector names to V and C original VDV calibrated values
  VXv=f(:,5);
  VYv=f(:,6);
  CXv=f(:,7);
  CYv=f(:,8);

% determine the reference discharge from raw Magmeter output
  o_mag=m;
  o_magm=mean(m);
  c_mag=8.69369+1.1062*m;  %(calibration performed on 96/10/20)

% clean Magmeter data
  c_magmeantemp=mean(c_mag);
  tmean=mean(c_mag);
  tc_mag=c_mag;
  c_maglen=length(c_mag);
  xm=(1:c_maglen);
  gc_mag=c_mag;
  not9999=(1:c_maglen);
  while std(tc_mag(not9999))>threshold;  % eliminate data untill below specified std
    diff=max(abs(tc_mag(not9999)-mean(tc_mag(not9999))));
    worst=find(abs(tc_mag-mean(tc_mag(not9999)))==diff);
    firstworst=worst(1);
    tc_mag(firstworst)=9999;
    not9999=find(tc_mag~=9999);
  end
  g_cmagindex=not9999;                  % indeces of retained Mag data
  b_cmagindex=find(tc_mag==9999);       % indeces of discarded Mag data

% calculate mean and stdev of Mag data and reference Q
  c_magmean=mean(c_mag(g_cmagindex));
  c_magstd=std(c_mag(g_cmagindex));
  ref_Q=c_magmean;

% plot Magmeter data
  figure(1)
  plot(g_cmagindex,c_mag(g_cmagindex),'g+',b_cmagindex,c_mag(b_cmagindex),'r+');
  xlabel('Sample')
  ylabel('Calibrated Discharge [l/s]')
  axis([0 c_maglen 0 1.4*c_magmean])
```

```
   text(.2*c_maglen,.8*c_magmean,'MAGQ_cal, std(MAGQ_cal)');
   text(.2*c_maglen,.6*c_magmean,num2str(c_magmean));
   text(.4*c_maglen,.6*c_magmean,num2str(c_magstd));
   grid
   title(testname)

% output reference Q data to display
   disp('o_magm   ref_Q    c_magstd')
   [o_magm ref_Q c_magstd]

% discard initial data not taken during traverse
   vX=vX(dstart+1:file_length);
   vY=vY(dstart+1:file_length);
   cX=cX(dstart+1:file_length);
   cY=cY(dstart+1:file_length);
   VXv=VXv(dstart+1:file_length);
   VYv=VYv(dstart+1:file_length);
   CXv=CXv(dstart+1:file_length);
   CYv=CYv(dstart+1:file_length);

% Determine empirical speed of sound value
   avgdepth=depth/2;       %average submergence of transducers
   Cemp=1449.2+4.6*temp-0.055*temp^2+0.00029*temp^3+(1.34-0.01*temp)*(salinity-
35)+0.016*avgdepth;

% ********************************************************
% Apply calibration to VDV data set
% ********************************************************

% time delays
   ddelayX=(687.865E-6)+8e-6;
   ddelayY=(687.865E-6)+8e-6;

% calibrated constants
   c_calv=294465;
   c_vel_constant=1/2.0*5.0/4096/c_calv;

 % scaling of velocity constant by pathlength
   c_vsclX=c_vel_constant/lX;
   c_vsclY=c_vel_constant/lY;

% calculate calibrated velocities for each station and resulting Q
   denX=cos(thetaX*pi/180);
   denY=cos(thetaY*pi/180);
   VXc=(vX-2.5).*100^2.*CXv.^2*c_vsclX/2;
   VYc=(vY+2).*100^2.*CYv.^2*c_vsclY/2;
   VXcn=VXc/denX;
   VYcn=VYc/denY;


% Gauss-Legendre stations and weights.  Segmentation of VDV logfile.

num_sta=8;
gauss_xi=[0.96029; 0.796666; 0.525532; 0.183435; -0.18343; -0.52553; -0.79667; -0.96029];
gauss_wi=[0.1012285362;0.2223810344;0.3137066458;0.3626837833;0.3626837833;0.3137066458;0.22
23810344;0.1012285362];
```

```
start_pts=[28;1113;2273;3485;4714;5926;7087;8171];
end_pts=[996;2080;3241;4453;5682;6893;8054;9139];

% eliminate laned data based on expected range of normal velocities

% extract expected average from continuous profile
    index=round(gauss_xi*(-100)/2+50);

    for i=1:num_sta,
     sp=start_pts(i);
     ep=end_pts(i);
     meansta=window(index(i));
     datXtemp=find(VXcn(sp:ep) < meansta+highdev & VXcn(sp:ep) > meansta-lowdev);
     datYtemp=find(VYcn(sp:ep) < meansta+highdev & VYcn(sp:ep) > meansta-lowdev);
     datX=datXtemp+sp-1;
     datY=datYtemp+sp-1;
     ldat(i,1)=length(datX);
     ldat(i,2)=length(datY);
     Vcnm(i,1)=mean(VXcn(datX));
     Vcnm(i,2)=mean(VYcn(datY));
     stdevVn(i,1)=std(VXcn(datX));
     stdevVn(i,2)=std(VYcn(datY));
     Sta_Cdat(i,1)=mean(CXv(datX));
     Sta_Cdat(i,2)=mean(CYv(datY));

%   plot station data to check lane removal
     figure(i+3)
     tempx=[sp ep];
     expected=[meansta meansta];
     plot(datX,VXcn(datX),'y-',datY,VYcn(datY),'b-',tempx,expected,'r-')
     text(sp,meansta+highdev,num2str(i))
     axis([(sp-100) (ep+100) (meansta-1.5*lowdev) (meansta+1.5*highdev)])
end

% calculate total dicharge
   integral=0;
   totalX=0;
   totalY=0;
   for i=1:num_sta,
         Sta_avg_Vn(i)=(Vcnm(i,1)+Vcnm(i,2))/2;
         integral=integral+0.49925*gauss_wi(i)*Sta_avg_Vn(i)/100;
         Sta_avg_C(i)=(Sta_Cdat(i,1)+Sta_Cdat(i,2))/2;
         totalX=totalX+ldat(i,1);
         totalY=totalY+ldat(i,2);
   end

% calculate GL discharge measurement and error
   c_Q=integral*width
   avgVcn=mean(Sta_avg_Vn(:));
   meanCdat=mean(Sta_avg_C(:));
   Qerr=(1000*c_Q-ref_Q)/ref_Q*100;

i=[1:num_sta]';
% plot calibrated results
   figure(2);
   Xscl=round(2.5*avgVcn);
```

```
   plot(Sta_avg_Vn(i),gauss_xi(i),'r*',Vcnm(i,1),gauss_xi(i),'y*',Vcnm(i,2),gauss_xi(i),'b*');
   axis([0 Xscl -1 1]);
   xlabel('Calibrated Normal Velocity [cm/s]')
   ylabel('Station')
   text(1,.4,'c_Q =');
   text(3,.2,num2str(c_Q))
   legend('Avg','VXc','VYc',0);
   grid
   title(testname);

% output results to display
   disp('discharge error[%]')
   [Qerr]
   disp('Cemp meanCdat')
   [Cemp meanCdat]

% write calibration data to file
   c=[ref_Q  1000*c_Q Qerr avgVcn totalX totalY Cemp meanCdat];
   eval(['save ',datafile,'.res', ' c' ,' -ascii']);
```

APPENDIX D

CALIBRATION OF INSTRUMENTATION

D. CALIBRATION OF INSTRUMENTATION

D.1 MAG FLOWMETER CALIBRATION

To ensure that the reference discharge measurement was accurate, volumetric differencing was used to calibrate the MAG flowmeter. The technique simply involved subtracting the overflow from the head tank weirs from the total system capacity. The remaining flow was routed to the testing flume, and could be compared to the MAG meter readings for calibration. First, the total capacity of the pumping system was determined by measuring the filling time of two 7.35 m^3 volumetric tanks with no water flowing to the test flume; the tanks were surveyed to accurately determine their volume and to calibrate the south tank float gauge. The system capacity is summarized in Table D.1.

Table D.1 System capacity.

Pump	*Pumping Capacity [l/s]**
60 hp	221.0
75 hp	285.3
Total System Capacity	506.3
* corresponds to approximately 7.5 m lift head	

Using the total system capacity as a reference point for the differencing technique required that a constant lift head between the sump and head tank weirs be maintained. Water was added to the system and the gate on the test flume was adjusted to maintain the sump level at the same value (to within ±10 cm) as when the pump capacity was tested. The pumps are high discharge, low-head, thus there performance curves were relatively flat with head; this was confirmed beforehand by increasing the lift head by more than 1.5 m (20 %), resulting in only 2.5 % reduction in pumping capacity. Thus, small changes in the lifting head do not significantly influence the discharge measurement.

A range of flows from 100 l/s to 480 l/s were routed through the test flume. For each discharge the system was allowed to stabilize and then multiple trials were carried out to measure the overflow into the volumetric tanks. The differencing technique proved to be very repeatable with flow measurements varying by no more than 1 l/s between trials. During overflow measurement, MAG output was continuously logged to the PC. The same procedure was used to determine the MAG average flow measurement as described in Section 5.1. Figure D.1 includes the 8 calibration tests, and the resulting calibration line.

It is clear that a linear calibration is appropriate and provides a good fit, with an r^2 of 0.9999 and a standard error of 2.15 l/s. The resulting calibration relationship (D.1) was applied to raw MAG output ranging from 100 to 480 l/s to calculate the reference discharge for comparative testing with the ADM. It is worth noting that when no flow was routed to the test flume, and the system was stable there was a small negative flow offset from the MAG meter. Thus, incorporating an intercept in the calibration was appropriate, *i.e.*,

$$Q_{ref} = 8.694 + 1.106\, Q_{mraw}, \qquad \text{(D.1)}$$

where Q_{ref} = MAG reference discharge [l/s], and
Q_{mraw} = MAG raw discharge measurement [l/s].

D.2 CALIBRATION OF VDV INSTRUMENTATION

Preliminary velocity measurement comparisons were carried out in the mezzanine level variable slope test flume using Sontek acoustic Doppler velocity meters. Point velocities were sampled along the acoustic paths to determine a reference average pathline velocity. Preliminary discharge comparisons were also undertaken in the main test flume to assess the accuracy of the modified VDV package. These tests revealed that the measured water velocities were low for both the X and Y acoustic paths. A second observation was that

the X and Y velocity readings were low by different proportions. In addition, the proportional error varied with velocity. The latter two observations prompted a still water, or 'bucket test,' of the acoustics to determine if there was an electrical offset error. Following bucket testing, the pathline velocity calculation was re-calibrated by back-calculating pathline velocities from known reference discharges.

D.2.1 Still Water Testing ('Bucket Test')

Trivett *et al.* (1991), when documenting the sources of error for the BASS oceanographic current meter, a predecessor of the VDV, indicated that the zero offset of the electronics dominated the error at low flows. Since the velocities tested in the lab were in the low range of the electronics, a bucket test to assess the offset was justified.

The test flume was sealed and filled to a depth of 0.40 m. After lowering the transducers to 25 mm above the intake floor, the water was allowed to settle for over 10 hours. Following this, five tests were performed where VDV output was logged for a duration of 1.5 hours. The results are summarized in Table D.2.

Table D.2 Still water calibration results.

Trial	*Mean $V_{p,X}$ [cm/s]*	*Mean $V_{p,Y}$ [cm/s]*	*Difference [cm/s]*	*Mean $V_{p,X}$ [counts]*	*Mean $V_{p,Y}$ [counts]*	*Difference [counts]*
1	0.35	-0.39	0.73	2.00	-2.22	4.21
2	0.43	-0.45	0.88	2.47	-2.58	5.05
3	0.34	-0.44	0.78	2.01	-2.56	4.57
4	0.33	-0.41	0.74	1.94	-2.40	4.34
5	0.28	-0.43	0.71	1.65	-2.51	4.16
Average	0.4	-0.4	0.8	**2.0**	**-2.5**	4.5

From these tests, it was quite clear that an electronic offset error was present. On average, digital counts for the X pair of transducers were biased high by approximately 2.0 and the Y signal was biased low by 2.5 counts. Ideally, the mean digital counts would all have been zero indicating a transit-time difference and resulting water velocity measurement of zero. Although the zero offset errors were small relative to the range of

the electronics (±4096 counts), they were significant relative to the range of values observed in the lab; peak velocities achieved in the test flume corresponded to digital readings of approximately 250 counts. The zero offset bias explained both the disagreement between the X and Y measured velocities and the change in proportionate error as the velocity was varied. To adjust the zero offset, 2.0 counts were subtracted from the X digital data and 2.5 counts were added to the Y data.

D.2.2 Re-Calibration of the Velocity Calculation

To convert the voltage from the internal clock of the VDV package to a time measurement, the slew rate of the differential time circuit was required. Focal Technologies indicated that accurate measurement of the slew rate was difficult under bench testing conditions, even with a high frequency oscilloscope. It was recommended that a tow tank or discharge comparison calibration be undertaken to better define this value.

The re-calibration process essentially consisted of back calculating the transit-time differences in equations (5.3), (5.4), (5.6) and (5.7). For a range of discharges, 20 minute continuous traverses were used to collect non-calibrated digital records from the VDV. The average normal velocity was determined by dividing the reference discharge by the intake area; multiplying this value by the cosine of the respective path angles to evaluate the reference average pathline water velocities. The pathlengths and average sound speed measurements were then used to back calculate the average transit-time differences that would result in a velocity measurement identical to the reference value. Knowing the correct transit-time difference and the measured digital data, the average slew rate was recalculated.

Twenty calibration tests were performed for 8 different flow rates ranging from 124.5 l/s to 454.1 l/s. Table D.3 summarizes the results obtained from the calibration procedure. The calibrated slew rate was quite repeatable, with the standard deviation being less than 1.3% of the mean. Figures D.2 and D.3 illustrate the fit of the calibration; it was clear

that a linear calibration was appropriate as there was no trend in the residuals of the regression. Table D.4 summarizes the regression statistics. The 0.39 % deviation from unity may have been reduced by using a more elaborate calibration procedure (*i.e.*, not simply averaging the calculated slew rates), however this accuracy was considered acceptable relative to other uncertainties in the testing program.

Table D.3 VDV calibration results.

Trial	*Reference Discharge [l/s]*	*Calibrated Slew Rate*	*Measured c [m/s]*	*Empirical c [m/s]*	*Deviation in c [%]*	*Calibrated Discharge [l/s]*	*Error in Discharge [%]*
a	454.1	293706	1480.3	1479.0	0.09	454.0	-0.03
b	453.7	293943	1480.4	1479.9	0.03	454.0	0.07
c	454.3	293323	1479.6	1481.6	-0.13	453.7	-0.12
d	306.1	299310	1481.5	1483.3	-0.12	311.8	1.87
e	222.2	297387	1481.2	1481.6	-0.03	224.7	1.11
f	220.9	299267	1482.8	1481.6	0.08	224.8	1.76
g	221.1	299061	1483.0	1483.3	-0.02	224.8	1.66
h	124.5	288086	1488.8	1485.9	0.19	121.9	-2.06
i	149.7	291375	1481.6	1479.9	0.11	148.2	-1.00
j	149.7	290456	1481.9	1481.6	0.02	147.8	-1.26
k	149.8	290723	1481.2	1481.6	-0.03	148.0	-1.21
l	262.7	289227	1481.8	1482.4	-0.04	258.2	-1.70
m	263.2	290173	1485.9	1483.3	0.18	259.7	-1.34
n	263.2	290378	1486.3	1483.3	0.20	259.8	-1.30
o	379.7	296010	1485.7	1484.2	0.10	382.4	0.72
p	380.4	295765	1486.3	1485.0	0.09	382.7	0.61
q	379.8	297635	1490.8	1486.7	0.27	384.5	1.23
r	324.4	298607	1490.7	1486.8	0.27	329.4	1.54
s	325.7	297907	1491.5	1488.3	0.21	329.9	1.30
t	325.2	296962	1491.8	1488.3	0.23	328.5	1.00
	Mean	294465			0.09		0.14
	Standard Dev.	3774			0.12		1.31
	Standard Dev. [%]	1.28			-		-

Table D.4 VDV calibration statistics.

Statistic	*Value*
r^2	0.9991
standard error [l/s]	3.13
intercept	0
coefficient	1.0039

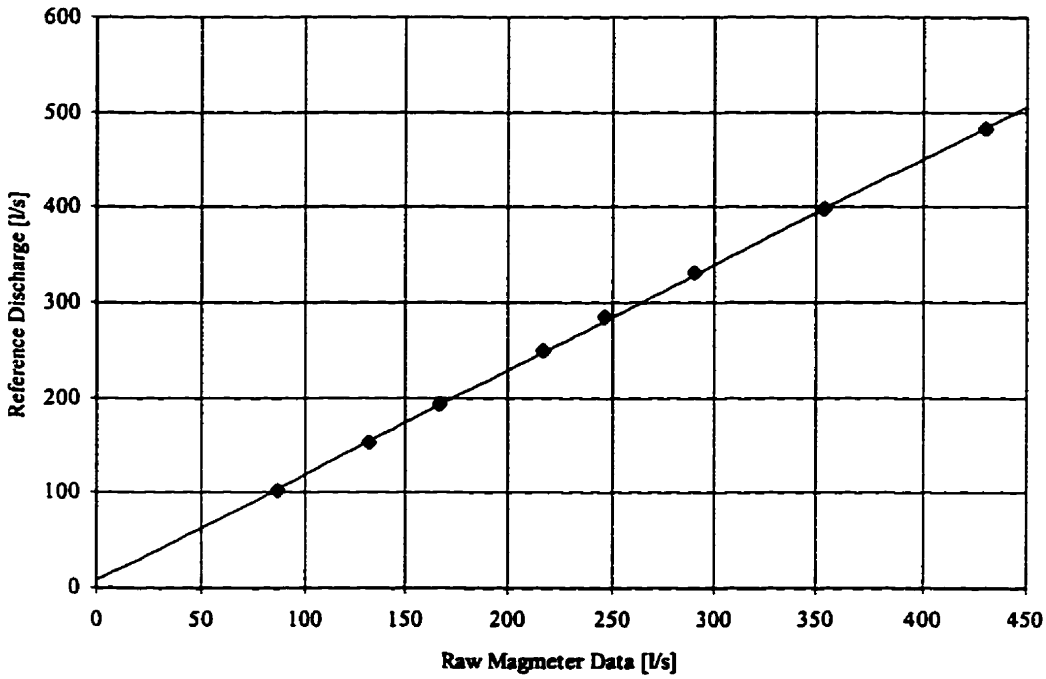

Figure D.1 MAG flowmeter calibration.

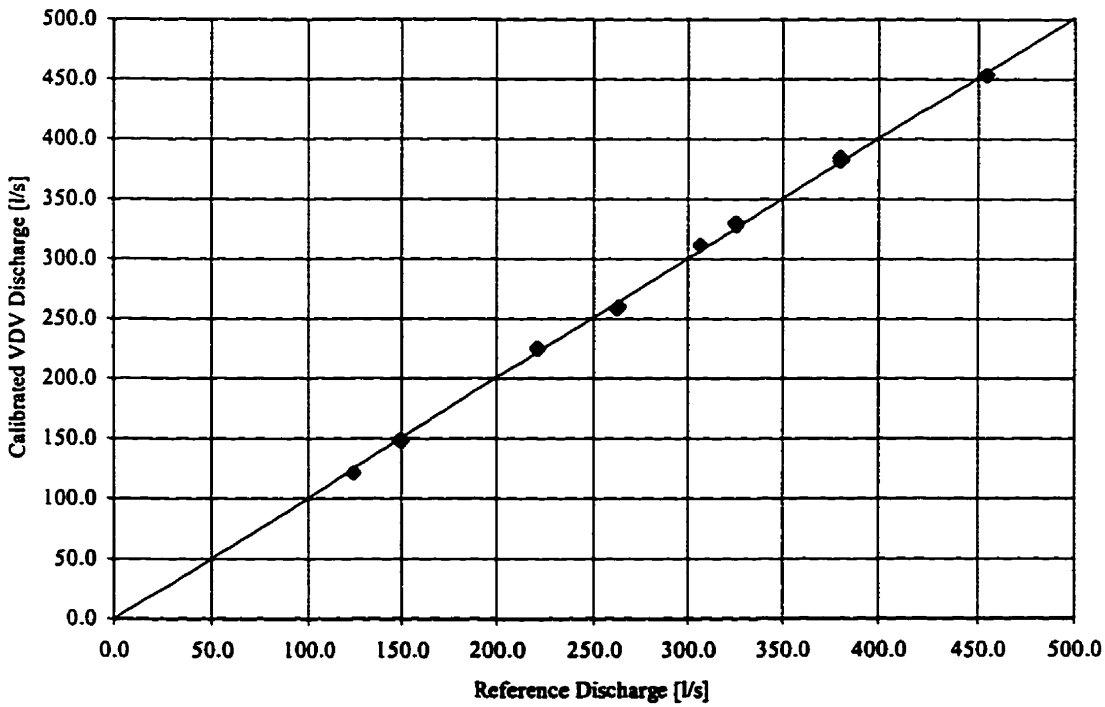

Figure D.2 VDV calibration.

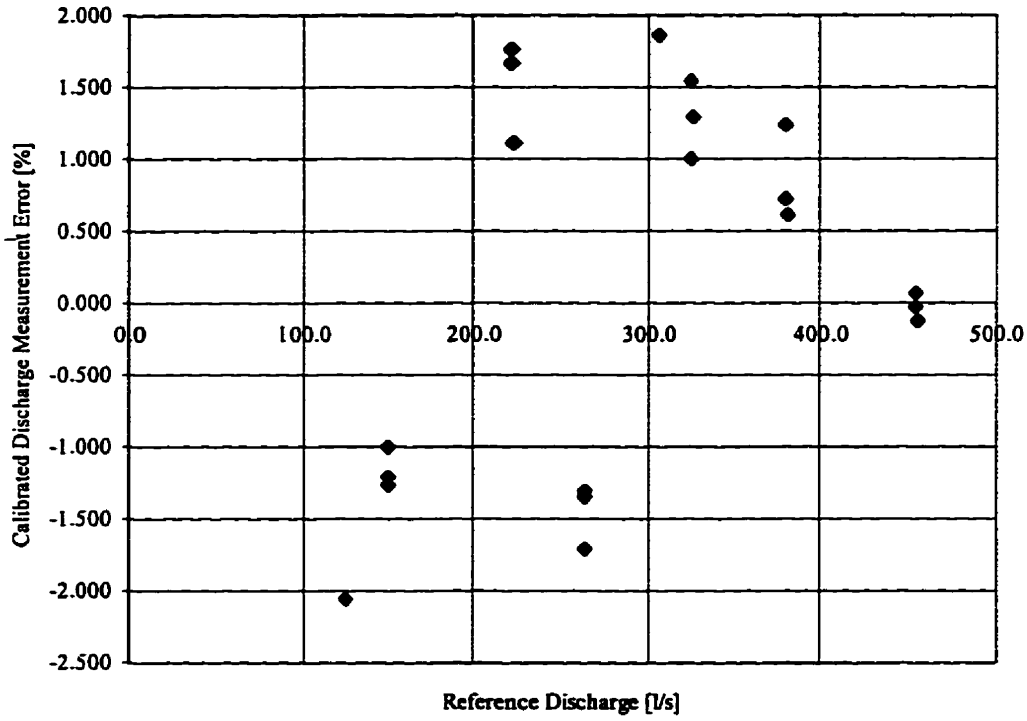

Figure D.3 Distribution of error for VDV calibration.

APPENDIX E

DETAILED TEST RESULTS

SAMPLING STRATEGY COMPARISON

Sampling Strategy Comparison: Summary of Results
* CTR - continuous, GL - Gauss-Legendre sampling strategies

Date	*Run*	*Sampling Strategy**	*Reference Discharge [l/s]*	*Measured Discharge [l/s]*	*Discharge Error [%]*	*Empirical Sound Spd. [m/s]*	*Measured Sound Spd. [m/s]*	*Sound Spd. Error [%]*
1031	a	CTR20	276.98	284.07	2.56	1479.9	1481.3	0.09
	c	CTR12	277.79	283.87	2.19	1481.6	1481.4	-0.02
	d	CTR8	278.40	283.78	1.93	1481.6	1480.9	-0.05
	e	CTR6	275.88	284.43	3.10	1481.6	1481.3	-0.02
	f	CTR6	278.62	284.39	2.07	1481.6	1481.6	0.00
	g	CTR6	276.13	283.26	2.58	1482.5	1482.6	0.01
	h	CTR6	276.30	283.97	2.78	1483.4	1483.0	-0.03
	i	CTR6	276.17	284.83	3.14	1483.4	1482.4	-0.06
	j	CTR4	278.92	285.09	2.21	1483.4	1484.0	0.04
	k	CTR4	277.56	285.06	2.70	1484.2	1486.1	0.13
	l	CTR4	278.05	285.62	2.72	1485.0	1487.0	0.13
	m	CTR4	278.63	286.47	2.81	1485.0	1486.9	0.13
	n	CTR3	276.94	283.58	2.40	1485.0	1487.0	0.13
	p	CTR3	275.85	283.95	2.94	1485.9	1487.8	0.13
	q	CTR3	279.02	285.84	2.45	1485.9	1490.3	0.30
	s	GL2	279.80	290.64	3.87	1486.8	1492.2	0.36
	t	GL2	279.41	290.83	4.09	1486.8	1492.1	0.36
	u	GL2	279.54	290.31	3.85	1486.8	1492.3	0.37
	v	GL2	276.59	291.37	5.35	1487.4	1492.5	0.35
	w	GL4	277.77	286.64	3.20	1488.3	1492.4	0.28
	x	GL4	280.28	285.93	2.01	1488.3	1492.7	0.30
	y	GL4	278.17	286.74	3.08	1488.3	1492.3	0.27
	z	GL4	279.18	285.77	2.36	1489.1	1492.2	0.21
	aa	GL6	279.05	284.49	1.95	1490.0	1492.5	0.17
	bb	GL6	278.67	284.18	1.98	1490.0	1492.1	0.14
	cc	GL8	279.86	283.32	1.24	1488.3	1492.2	0.26

Sampling Strategy Comparison: Summary of Results (continued)
* CTR - continuous, GL - Gauss-Legendre sampling strategies

Date	*Run*	*Sampling Strategy**	*Reference Discharge [l/s]*	*Measured Discharge [l/s]*	*Discharge Error [%]*	*Empirical Sound Spd. [m/s]*	*Measured Sound Spd. [m/s]*	*Sound Spd. Error [%]*
1107	a	CTR20	388.2	396.4	2.13	1476.4	1481.3	0.33
	b	CTR20	391.1	396.3	1.33	1477.3	1481.3	0.27
	c	CTR12	389.5	396.4	1.79	1478.1	1481.3	0.22
	d	CTR12	390.3	395.7	1.40	1479.0	1480.7	0.12
	e	CTR12	392.1	394.9	0.70	1479.0	1481.1	0.14
	f	CTR6	390.7	396.4	1.45	1479.9	1481.6	0.11
	g	CTR6	390.8	395.0	1.06	1479.9	1480.8	0.06
	h	CTR6	394.4	395.5	0.27	1480.8	1481.1	0.02
	i	GL12	392.8	394.6	0.45	1481.6	1481.8	0.01
	j	GL12	392.8	395.1	0.59	1482.6	1483.6	0.07
	k	GL12	393.7	396.8	0.77	1485.0	1487.1	0.14
	l	GL10	393.9	396.6	0.70	1485.9	1488.2	0.16
	m	GL8	395.5	396.2	0.18	1486.7	1491.7	0.34
	n	GL8	395.1	396.2	0.27	1486.7	1491.4	0.32
	o	GL6	396.2	398.9	0.69	1487.5	1492.3	0.33
	p	GL6	395.5	397.9	0.61	1488.3	1492.6	0.29
	q	GL4	395.3	400.4	1.30	1488.3	1492.2	0.26
	r	GL4	398.3	401.9	0.90	1489.1	1492.3	0.21
	s	GL2	395.2	399.5	1.07	1490.0	1492.6	0.18
	t	GL2	395.7	399.1	0.86	1490.0	1491.7	0.12
	u	GL2	397.6	398.8	0.32	1490.0	1491.9	0.13
1109	a	CTR20	462.1	453.7	-1.81	1481.6	1480.6	-0.07
	b	CTR20	460.9	453.4	-1.64	1483.4	1480.4	-0.20
	c	CTR8	461.7	455.8	-1.29	1483.4	1482.4	-0.07
	d	CTR8	458.4	455.5	-0.64	1484.2	1483.1	-0.07
	e	CTR6	460.3	454.6	-1.24	1485.0	1482.6	-0.17
	f	CTR6	462.0	455.7	-1.36	1485.0	1482.9	-0.14
	g	CTR4	458.5	453.9	-1.01	1485.9	1486.2	0.02
	h	CTR4	463.6	455.8	-1.68	1485.9	1486.6	0.05
	i	GL12	461.1	461.6	0.10	1485.9	1483.0	-0.19
	j	GL12	463.1	462.6	-0.10	1487.5	1486.0	-0.10
	k	GL10	462.6	464.0	0.31	1488.3	1491.2	0.20
	l	GL10	463.2	462.8	-0.08	1491.5	1492.3	0.05
	m	GL8	465.2	460.3	-1.06	1491.5	1492.4	0.06
	n	GL8	465.4	461.0	-0.94	1491.5	1492.2	0.04

Sampling Strategy Comparison: Summary of Results (continued)
* CTR - continuous, GL - Gauss-Legendre sampling strategies

Date	*Run*	*Sampling Strategy**	*Reference Discharge [l/s]*	*Measured Discharge [l/s]*	*Discharge Error [%]*	*Empirical Sound Spd. [m/s]*	*Measured Sound Spd. [m/s]*	*Sound Spd. Error [%]*
1110	a	CTR20	163.8	162.0	-1.11	1485.0	1491.4	0.43
	b	CTR20	163.8	162.7	-0.68	1485.9	1491.0	0.35
	c	CTR8	163.8	163.1	-0.43	1486.7	1491.4	0.31
	d	CTR8	163.8	162.9	-0.57	1486.7	1491.8	0.34
	e	CTR6	163.8	162.8	-0.60	1486.7	1491.9	0.35
	f	CTR6	163.8	162.9	-0.56	1486.7	1492.0	0.36
	g	CTR4	163.9	162.4	-0.92	1486.7	1492.0	0.36
	h	CTR4	164.7	162.3	-1.42	1486.7	1492.1	0.36
	i	GL12	164.4	162.5	-1.14	1486.7	1492.4	0.38
	j	GL12	164.1	162.3	-1.10	1488.3	1492.2	0.26
	k	GL10	164.7	162.1	-1.59	1488.3	1492.6	0.28
	l	GL10	164.3	162.0	-1.41	1488.3	1492.0	0.25
	m	GL8	164.5	161.1	-2.05	1489.1	1492.1	0.20
	n	GL8	164.6	162.0	-1.54	1489.1	1492.2	0.20
	o	CTR20	254.5	255.9	0.59	1490.0	1491.3	0.09
	p	CTR20	254.8	256.7	0.78	1490.8	1491.7	0.06
	q	CTR8	255.7	256.6	0.36	1491.5	1491.9	0.03
	r	CTR8	254.9	256.8	0.74	1491.5	1492.1	0.04
	s	CTR6	254.9	255.6	0.28	1491.5	1491.6	0.00
	t	CTR6	255.5	255.5	0.03	1491.5	1491.6	0.00
	u	CTR4	255.9	256.4	0.18	1492.3	1491.7	-0.05
	v	CTR4	256.1	256.7	0.25	1492.3	1491.8	-0.04
	w	GL12	254.8	255.6	0.33	1493.1	1492.2	-0.06
	x	GL12	254.7	254.8	0.03	1493.9	1492.7	-0.08
	y	GL10	254.9	255.2	0.12	1494.7	1494.2	-0.03
	z	GL10	255.5	254.6	-0.35	1494.7	1493.9	-0.05
	aa	GL8	256.1	254.5	-0.62	1496.2	1495.9	-0.02
	bb	GL8	255.8	255.3	-0.17	1496.2	1497.8	0.10
1111	a	CTR20	352.6	352.2	-0.11	1490.0	1491.3	0.09
	b	CTR20	353.6	352.7	-0.27	1490.0	1491.6	0.11
	c	CTR8	352.9	353.0	0.02	1490.8	1491.8	0.07
	d	CTR8	353.5	353.1	-0.12	1491.5	1491.9	0.03
	e	CTR6	354.9	352.0	-0.83	1491.5	1492.0	0.03
	f	CTR6	354.2	352.8	-0.41	1491.5	1491.2	-0.02
	g	CTR4	354.4	353.2	-0.36	1491.5	1491.5	0.00
	h	CTR4	353.5	353.0	-0.13	1491.5	1491.4	-0.01
	i	GL12	355.1	352.3	-0.77	1493.1	1492.0	-0.07
	j	GL12	355.9	352.4	-0.98	1493.9	1492.4	-0.10
	k	GL10	354.9	351.9	-0.84	1494.7	1493.4	-0.09
	l	GL10	356.0	351.5	-1.24	1494.7	1493.6	-0.07
	m	GL8	354.5	350.5	-1.14	1495.4	1494.2	-0.08
	n	GL8	356.4	352.4	-1.12	1496.2	1497.0	0.05

DISTURBANCE 1

Summary of Results for Disturbance 1
* CTR - continuous, GL - Gauss-Legendre sampling strategies

Date	*Run*	*Sampling Strategy**	*Reference Discharge [l/s]*	*Measured Discharge [l/s]*	*Discharge Error [%]*	*Empirical Sound Spd. [m/s]*	*Measured Sound Spd. [m/s]*	*Sound Spd. Error [%]*
1113	a	CTR20	457.4	464.4	1.55	1482.5	1481.2	0.09
	b	CTR12	457.6	463.3	1.24	1483.4	1480.9	0.17
	c	CTR8	457.0	468.8	2.58	1483.4	1482.7	0.05
	d	CTR6	458.4	469.3	2.38	1483.4	1484.3	-0.06
	m	CTR4	462.7	467.5	1.04	1490.0	1491.1	-0.08
	n	CTR4	461.5	464.9	0.74	1490.8	1491.1	-0.02
	h	GL10	459.3	473.5	3.10	1486.7	1489.0	-0.16
	i	GL8	458.4	476.2	3.87	1488.3	1492.3	-0.27
	j	GL6	459.6	500.4	8.89	1488.3	1492.2	-0.26
	k	GL4	462.3	464.3	0.42	1489.1	1492.3	-0.21
	l	GL2	461.8	278.5	-39.69	1490.0	1492.5	-0.17
	o	GL12	462.8	468.7	1.27	1490.8	1486.7	0.27
1115	a	CTR20	457.5	452.6	-1.08	1479.9	1480.8	-0.06
	b	CTR20	456.9	454.7	-0.47	1481.6	1481.3	0.02
	c	CTR12	458.5	458.7	0.05	1482.5	1480.6	0.12
	d	CTR12	459.8	460.3	0.11	1486.8	1490.7	-0.26
	e	CTR8	460.7	457.4	-0.71	1487.5	1490.6	-0.21
	f	CTR8	460.3	460.3	0.01	1490.0	1490.9	-0.06
	g	CTR6	463.9	456.5	-1.59	1490.0	1490.3	-0.02
	h	CTR6	462.5	460.0	-0.53	1490.0	1490.7	-0.05
	I	CTR4	458.3	461.3	0.66	1490.8	1491.0	-0.02
	j	CTR4	460.0	462.0	0.43	1491.5	1491.0	0.03
	k	GL10	461.9	462.7	0.17	1491.5	1492.3	-0.05
	l	GL10	462.5	463.5	0.22	1491.5	1492.4	-0.06
	m	GL8	462.3	463.9	0.35	1492.3	1492.6	-0.02
	n	GL8	461.9	464.2	0.49	1493.1	1492.2	0.06
	o	GL6	463.6	476.3	2.75	1493.9	1492.4	0.10
	p	GL6	461.4	476.7	3.32	1493.9	1492.5	0.09
	s	GL2	465.9	290.2	-37.73	1494.7	1492.7	0.13
	t	GL2	465.2	290.9	-37.46	1494.7	1493.2	0.10

Summary of Results for Disturbance 1 (continued)
* CTR - continuous, GL - Gauss-Legendre sampling strategies

Date	*Run*	*Sampling Strategy**	*Reference Discharge [l/s]*	*Measured Discharge [l/s]*	*Discharge Error [%]*	*Empirical Sound Spd. [m/s]*	*Measured Sound Spd. [m/s]*	*Sound Spd. Error [%]*
1118	a	CTR20	345.6	344.1	-0.45	1485.9	1491.4	-0.37
	b	CTR20	345.1	346.8	0.50	1486.7	1491.8	-0.35
	c	CTR12	346.4	351.0	1.34	1486.7	1491.1	-0.30
	d	CTR12	345.2	351.1	1.69	1486.7	1491.4	-0.32
	e	CTR8	346.4	347.2	0.21	1487.5	1491.8	-0.29
	f	CTR8	346.2	348.4	0.65	1488.3	1492.0	-0.25
	g	CTR6	346.4	351.3	1.42	1488.3	1491.8	-0.23
	h	CTR6	345.8	349.8	1.14	1488.3	1491.3	-0.20
	I	CTR4	345.3	347.1	0.52	1488.3	1491.3	-0.20
	j	CTR4	346.3	346.2	-0.05	1489.1	1491.5	-0.16
	k	GL10	347.0	349.7	0.77	1490.0	1492.2	-0.15
	l	GL10	346.7	349.1	0.69	1490.0	1492.2	-0.15
	m	GL8	347.9	354.4	1.86	1490.8	1492.6	-0.12
	n	GL8	347.9	354.5	1.88	1491.5	1492.7	-0.08
	o	GL6	347.9	358.0	2.92	1491.5	1492.5	-0.06
	p	GL6	347.9	362.5	4.19	1494.7	1492.8	0.13
	q	GL4	349.8	317.4	-9.26	1493.1	1492.4	0.05
	r	GL4	349.0	314.6	-9.85	1493.9	1492.6	0.09
	s	CTR20	247.6	245.9	-0.70	1496.2	1497.9	-0.11
	t	CTR20	247.5	247.9	0.16	1496.2	1497.4	-0.08
	u	CTR12	246.9	247.4	0.21	1496.2	1497.3	-0.07
	v	CTR12	248.5	247.2	-0.55	1496.2	1497.3	-0.08
	w	CTR8	248.3	250.3	0.82	1497.0	1497.9	-0.06
	x	CTR8	248.1	246.7	-0.58	1497.0	1499.4	-0.16
	y	CTR6	247.6	253.2	2.27	1497.7	1500.9	-0.21
	z	CTR6	249.0	251.9	1.16	1497.7	1501.7	-0.26
	aa	CTR4	248.4	250.5	0.85	1497.7	1501.8	-0.27
	bb	CTR4	248.0	251.2	1.29	1497.7	1501.8	-0.27
	cc	GL10	248.5	251.1	1.03	1497.7	1502.5	-0.32
	dd	GL10	249.4	252.4	1.21	1498.5	1502.2	-0.25
	ee	GL8	248.5	255.0	2.62	1499.2	1502.6	-0.23
	ff	GL8	249.8	254.2	1.79	1499.2	1502.9	-0.25
	gg	GL6	248.7	259.4	4.33	1499.2	1503.0	-0.25
	hh	GL6	249.2	257.8	3.45	1499.2	1503.1	-0.26
	ii	GL4	249.1	224.7	-9.80	1499.2	1503.3	-0.27
	jj	GL4	249.3	222.3	-10.81	1499.2	1503.3	-0.27

DISTURBANCE 2

Summary of Results for Disturbance 2
* CTR - continuous, GL - Gauss-Legendre sampling strategies

Date	*Run*	*Sampling Strategy**	*Reference Discharge [l/s]*	*Measured Discharge [l/s]*	*Discharge Error [%]*	*Empirical Sound Spd. [m/s]*	*Measured Sound Spd. [m/s]*	*Sound Spd. Error [%]*
1120	a	CTR20	240.8	241.8	0.40	1486.7	1491.3	-0.31
	b	CTR4	240.8	242.6	0.77	1486.7	1491.8	-0.34
	c	CTR4	241.0	242.7	0.70	1486.7	1491.6	-0.33
	d	CTR	239.0	241.1	0.87	1486.7	1491.5	-0.33
	e	GL10	240.2	243.4	1.33	1487.5	1492.5	-0.34
	f	GL10	240.4	242.0	0.65	1488.3	1492.5	-0.28
	g	GL10	240.8	241.8	0.42	1489.1	1492.4	-0.22
	h	GL4	240.9	241.8	0.39	1490.0	1492.2	-0.15
	I	GL4	241.0	241.2	0.07	1490.0	1492.3	-0.16
	j	GL4	242.0	240.2	-0.73	1490.8	1492.6	-0.12
1121	a	CTR20	342.1	342.6	0.14	1483.4	1486.8	-0.23
	b	GL10	342.3	344.8	0.75	1484.2	1488.4	-0.28
	c	GL10	342.7	344.3	0.48	1484.2	1488.9	-0.32
	d	GL4	343.3	348.3	1.45	1485.9	1491.9	-0.41
	e	GL4	344.1	348.5	1.27	1486.7	1492.3	-0.37
	f	CTR4	343.9	343.6	-0.11	1486.7	1491.4	-0.32
	g	CTR4	346.0	344.3	-0.49	1486.7	1491.7	-0.34
	h	CTR20	453.1	452.4	-0.15	1487.5	1491.1	-0.24
	I	CTR4	457.3	453.2	-0.91	1488.3	1491.1	-0.19
	j	CTR4	451.6	453.1	0.34	1488.3	1491.4	-0.21
	k	GL4	454.1	464.0	2.18	1488.3	1492.3	-0.26
	l	GL4	454.0	450.5	-0.78	1485.9	1484.9	0.07
	m	GL4	452.7	452.3	-0.09	1486.7	1487.0	-0.02

DISTURBANCE 3

Summary of Results for Disturbance 3

* CTR - continuous, GL - Gauss-Legendre sampling strategies

Date	*Run*	*Sampling Strategy**	*Reference Discharge [l/s]*	*Measured Discharge [l/s]*	*Discharge Error [%]*	*Empirical Sound Spd. [m/s]*	*Measured Sound Spd. [m/s]*	*Sound Spd. Error [%]*
1123	a	CTR20	454.31	455.69	0.30	1477.3	1481.0	0.25
	b	CTR8	453.25	456.24	0.66	1478.1	1480.6	0.16
	c	CTR8	452.24	454.89	0.59	1478.1	1480.8	0.18
	d	CTR4	451.08	454.11	0.67	1479.0	1481.1	0.14
	e	CTR4	450.63	453.98	0.74	1479.0	1481.4	0.16
	f	GL10	451.96	456.10	0.92	1479.9	1481.9	0.14
	g	GL10	452.16	453.10	0.21	1480.8	1482.0	0.09
	h	GL8	453.74	454.16	0.09	1481.6	1481.9	0.02
	I	GL8	453.15	454.62	0.32	1482.5	1482.8	0.02
	j	GL4	452.05	467.12	3.34	1483.4	1482.9	-0.03
	k	GL4	454.79	467.88	2.88	1483.4	1482.9	-0.03
1202	a	CTR20	354.21	352.90	-0.37	1470.9	1472.8	0.13
	b	CTR8	354.29	353.38	-0.26	1472.7	1473.1	0.03
	c	CTR8	353.85	355.35	0.42	1472.7	1476.2	0.23
	d	CTR4	354.92	354.82	-0.03	1472.7	1476.7	0.27
	e	CTR4	352.83	355.41	0.73	1473.6	1476.8	0.21
	f	GL10	354.24	355.06	0.23	1474.6	1479.2	0.31
	g	GL10	354.41	357.37	0.83	1475.5	1481.9	0.44
	h	CTR8	355.05	356.18	0.32	1476.4	1482.1	0.39
	I	CTR8	356.15	356.11	-0.01	1476.4	1482.3	0.40
	j	GL4	356.31	372.32	4.49	1477.3	1482.1	0.33
	k	GL4	355.48	373.40	5.04	1478.1	1482.3	0.28
1202	m	CTR8	256.93	259.13	0.86	1481.6	1481.2	-0.03
	n	CTR8	257.73	259.97	0.87	1481.6	1481.3	-0.02
	o	CTR4	256.84	257.55	0.28	1482.5	1481.5	-0.07
	p	CTR4	257.43	259.17	0.68	1482.5	1482.3	-0.02
	q	GL10	256.62	259.01	0.93	1482.5	1483.9	0.09
	r	GL10	256.34	259.02	1.05	1483.4	1484.0	0.04
	s	GL8	258.04	260.32	0.88	1484.2	1487.5	0.22
	t	GL8	257.40	260.83	1.33	1485.0	1488.6	0.24
	u	GL4	258.42	272.85	5.58	1485.0	1488.9	0.26
	v	GL4	258.50	274.62	6.24	1485.0	1491.0	0.40

DISTURBANCE 4

Summary of Results for Disturbance 4
* CTR - continuous, GL - Gauss-Legendre sampling strategies

Date	*Run*	*Sampling Strategy**	*Reference Discharge [l/s]*	*Measured Discharge [l/s]*	*Discharge Error [%]*	*Empirical Sound Spd. [m/s]*	*Measured Sound Spd. [m/s]*	*Sound Spd. Error [%]*
1204	a	CTR20	451.99	464.45	2.76	1475.5	1480.0	0.31
	b	CTR8	452.99	465.13	2.68	1476.4	1481.2	0.33
	c	CTR8	452.15	465.50	2.95	1477.3	1480.5	0.22
	d	CTR4	452.99	464.75	2.60	1477.3	1480.8	0.24
	e	CTR4	452.20	464.18	2.65	1478.1	1481.2	0.20
	f	GL10	452.71	464.34	2.57	1478.1	1481.7	0.24
	g	GL10	452.81	466.23	2.96	1480.8	1482.1	0.09
	h	GL8	455.20	463.28	1.78	1479.9	1481.9	0.14
	I	GL8	453.35	462.83	2.09	1480.8	1482.3	0.10
	j	GL4	455.00	466.80	2.59	1481.6	1481.8	0.01
	k	GL4	454.05	469.30	3.36	1481.6	1481.7	0.01
1204	l	CTR20	346.18	353.35	2.07	1484.2	1487.0	0.19
	m	CTR8	345.95	353.78	2.26	1485.0	1486.9	0.12
	n	CTR8	346.19	353.42	2.09	1485.0	1487.0	0.13
	o	CTR4	346.88	353.65	1.95	1485.0	1487.2	0.15
	p	CTR4	347.58	350.92	0.96	1485.8	1487.3	0.10
	q	GL10	346.49	354.48	2.31	1485.8	1491.5	0.38
	r	GL10	347.35	355.85	2.45	1486.7	1492.0	0.36
	s	GL8	347.50	354.14	1.91	1487.5	1491.9	0.30
	t	GL8	348.22	353.91	1.63	1487.5	1492.5	0.33
	u	GL4	348.17	357.70	2.74	1488.3	1492.8	0.30
	v	GL4	349.30	359.00	2.78	1488.3	1492.5	0.28
1205	a	CTR20	189.07	191.48	1.27	1478.1	1481.7	0.24
	b	CTR8	188.63	192.12	1.85	1479.9	1481.6	0.12
	c	CTR8	188.34	191.12	1.48	1479.9	1481.2	0.09
	d	CTR4	187.17	190.17	1.60	1479.9	1481.3	0.09
	e	CTR4	188.74	192.02	1.74	1480.8	1481.8	0.07
	f	GL10	188.88	190.95	1.10	1481.6	1481.7	0.01
	g	GL10	189.31	189.63	0.17	1482.5	1483.5	0.07
	h	GL8	189.11	191.28	1.15	1483.4	1484.6	0.08
	I	GL8	189.41	191.93	1.33	1483.4	1485.3	0.13
	j	GL4	189.41	193.71	2.27	1485.0	1488.3	0.22
	k	GL4	189.95	195.29	2.81	1485.0	1489.4	0.29

DISTURBANCE 5

Summary of Results for Disturbance 5
* CTR - continuous, GL - Gauss-Legendre sampling strategies

Date	*Run*	*Sampling Strategy**	*Reference Discharge [l/s]*	*Measured Discharge [l/s]*	*Discharge Error [%]*	*Empirical Sound Spd. [m/s]*	*Measured Sound Spd. [m/s]*	*Sound Spd. Error [%]*
1207	a	CTR20	459.55	448.17	2.80	1476.4	1480.3	0.27
	b	CTR8	459.55	448.17	2.46	1477.3	1479.4	0.15
	c	CTR8	458.92	447.56	3.30	1478.1	1480.3	0.15
	d	CTR4	456.89	445.57	3.72	1478.1	1480.6	0.17
	e	CTR4	460.46	449.05	2.36	1478.1	1479.7	0.10
	f	GL10	460.69	449.28	2.78	1479.0	1481.6	0.17
	g	GL10	460.37	448.96	2.88	1479.9	1480.8	0.06
	h	GL8	461.73	450.29	2.26	1480.8	1482.3	0.10
	I	GL8	461.26	449.84	1.96	1481.6	1481.7	0.00
	j	GL4	461.31	449.88	3.88	1481.6	1481.9	0.02
	k	GL4	463.28	451.81	3.32	1482.5	1482.5	0.00
1208a	a	CTR20	345.21	336.66	3.35	1477.3	1481.3	0.28
	b	CTR8	345.49	336.93	3.22	1479.0	1481.3	0.15
	c	CTR8	345.08	336.53	3.29	1479.9	1481.5	0.11
	d	GL4	345.41	336.86	3.07	1479.9	1481.3	0.10
	e	GL4	348.02	339.40	2.28	1479.9	1480.1	0.02
	f	GL10	347.67	339.06	2.34	1480.8	1482.1	0.09
	g	GL10	345.68	337.12	2.95	1481.6	1481.8	0.01
	h	GL8	347.66	339.05	2.23	1483.4	1483.1	-0.02
	I	GL8	347.93	339.31	2.29	1483.4	1483.4	0.01
	j	GL4	347.71	339.10	2.30	1483.4	1483.5	0.01
	k	GL4	347.45	338.85	3.09	1484.2	1488.1	0.27
1208b	l	CTR20	173.30	169.01	0.47	1485.0	1488.3	0.22
	m	CTR8	173.31	169.01	1.03	1485.9	1491.2	0.36
	n	CTR8	173.35	169.06	0.61	1486.7	1491.4	0.32
	o	CTR4	173.21	168.92	0.39	1486.7	1491.6	0.33
	p	CTR4	173.73	169.43	0.35	1504.2	1491.8	-0.82
	q	GL10	173.57	169.27	0.36	1487.5	1492.2	0.32
	r	GL10	173.82	169.51	0.06	1488.3	1492.3	0.27
	s	GL8	172.75	168.48	-0.10	1488.3	1492.0	0.25
	t	GL8	173.73	169.43	-0.63	1489.9	1492.4	0.17
	u	GL4	174.09	169.78	-0.19	1489.9	1492.6	0.18
	v	GL4	173.47	169.17	0.23	1489.9	1492.4	0.16